



TECHNISCHE
UNIVERSITÄT
WIEN

Vienna University of Technology

DISSERTATION

HIGH-RESOLUTION SKY MODELS IN BUILDING PERFORMANCE ASSESSMENT

ausgeführt zum Zwecke der Erlangung des akademischen Grades
eines **Doktors der technischen Wissenschaften**

unter der Leitung von

Univ.-Prof. Dipl.-Ing. Dr.techn. Ardeshir Mahdavi

E 259-3 Abteilung für Bauphysik und Bauökologie

Institut für Architekturwissenschaften

eingereicht an der

Technischen Universität Wien

Fakultät für Architektur und Raumplanung

von

Ehsan Mahmoudzadehvazifeh

Matrikelnr. 1227658

Am Heumarkt 3/2/10, 1030, Wien

Wien, im Juni 2016

Kurzfassung

Eine große Anzahl von gebäudebezogenen Evaluierungswerkzeugen, beispielsweise zur Ermittlung von Energiekennzahlen, thermischer-Komfort-Evaluierung, Haustechniksimulation und Tageslichtbewertung, benötigt verlässliche Eingabedaten hinsichtlich Tageslichtparametern. Ein Beispiel für solche Eingabedaten sind Leuchtdichteverteilungsmodelle des Himmelsgewölbes („Sky Models“). Viele Wetterstationen messen zwar Strahlungsdaten, aber zumeist lediglich Horizontalstrahlung. Eine messtechnische Erfassung von Direkt- und Diffusstrahlung wird vielerorts nicht vorgenommen. Um verlässliche Sky Models zu erstellen benötigt man Information über i) direkte und indirekte Komponenten der Beleuchtungsstärke, sowie ii) Modelle der Lichtausbeute. Viele vergangene Forschungsbemühungen befassten sich mit der Ableitung von einfach zu generierenden, aber ausreichend-detaillierten Sky Models mit entsprechender Unterscheidung von diffusen und direkten Komponenten aus Horizontalstrahlungswerten. Diese Dissertation untersucht die meist verwendeten Modelle im Detail, sowie deren Potential für alternative Modellierungstechniken und Ansätze. Dabei wurden verschiedene Aspekte der Modelle untersucht:

Diffuse fraction models: Zunächst wurden verschiedene existierenden Methoden zur Ableitung des Diffusanteils ausgewählt. Danach wurden Messdaten betreffend Globalstrahlung und Diffustrahlung (7 Orte in den USA, sowie Wien, Österreich) akquiriert. Mit den verschiedenen Methoden wurden aus den Globalstrahlungswerten die Diffusstrahlungen errechnet und anschließend mit den Messdaten der Diffusstrahlung verglichen. Aufbauend darauf wurde eine neue, empirische Methode zur Errechnung des Diffusanteils anhand der Messdaten aus Wien erarbeitet. Mit dem Vergleich der errechneten und gemessenen Werte lässt sich die akkurateste Methode bestimmen. Anhand dieser Bemühungen lässt sich festhalten, dass ein Performanceranking der Modelle immer relativ ähnlich ausfiel, also weitestgehend unabhängig von dem Standort ist. Hinsichtlich der Qualität der Modelle muss festgehalten werden, dass keines der Modelle wirklich befriedigende Genauigkeiten aufweist. Die Methode nach

Skartveit und Olseth liefert die genauesten Resultate. Die Eigenentwicklung liefert lediglich standort-bezogen für Wien exzellente Genauigkeiten.

Sky luminance/radiance models: Um den Effekt des verwendeten Sky Models auf die Verlässlichkeit von Licht-Simulationsergebnisse zu untersuchen wurde die Simulationsumgebung Radiance verwendet. Hierbei wurden Beleuchtungsstärken im Innenraum eines Testraums (Dachraum *TU Wien*) verwendet, und zwar sowohl in Simulation wie auch via Messung. Szenarien in der Simulation stützten sich auf die bereits angesprochenen unterschiedlichen Himmelsmodelle. Zusätzlich wurde ein Himmelsmodell verwendet, dass Mithilfe eines Sky-Scanners am Dach der *TU Wien* erstellt wurde. Messungen und Simulationsergebnisse wurden anschließend verglichen. Die Ergebnisse liefern Rückschlüsse über die Qualität von Simulationen zur Vorhersage von Beleuchtungsstärken im Innen- und Außenraum, speziell unter verschiedenen und wechselnden Randbedingungen.

Luminous efficacy models: Vier Lichtausbeutemodelle wurden hinsichtlich ihrer Performance auf die Ableitung von Horizontalstrahlungswerten untersucht. Die Resultate weisen durch die Bank auf eine hohe Ergebnisqualität hin.

Keywords: Himmelsmodelle / Sky models, Diffusanteil, Leuchtdichtevertelung, Globalstrahlung, Direktstrahlung.

Summary

Many building performance applications (energy use, solar gains, thermal comfort, renewable energy systems, daylight, etc.) require reliable representations of boundary conditions – typically in terms of sky luminance distribution models. Nonetheless, most of the meteorological stations only monitor global horizontal irradiance and data such as direct and diffuse horizontal irradiance or illuminance is not available. However, Generation of sky luminance distribution requires information on *i)* direct and diffuse components of illuminance; *ii)* luminous efficacy models. Consequently, multiple methods have been proposed in the past to derive from measured global horizontal irradiance data the diffuse fraction (diffuse fraction models) and to derive global horizontal illuminance from global horizontal irradiance data (luminous efficacy models).

This thesis thus examines a number of such models in details and potential for alternative modelling techniques and approaches in three parts:

Diffuse fraction models: A number of existing methods for the computation of the diffuse fraction were selected. Actual measurements of global and diffuse irradiance were obtained for seven locations in USA and one location in Austria. The measured global irradiance data for these locations were fed to the aforementioned diffuse fraction models. The calculation results were then compared with the corresponding empirical data. Moreover, a new empirical diffuse fraction model based on Vienna data is developed, which performs significantly better than other 7 models for Vienna, Austria. At the end, the best performing model is selected to be used in predicting diffuse horizontal irradiance as an input in generation of sky models. The comparative assessment yielded a number of findings. The relative performance ("ranking") of the models was found to be more or less consistent across the different locations. However,

none of the models can be said to be performing wholly satisfactory. The best performing model was Skartveit and Olseth. Regarding the developed model for Vienna, it only has excellent performance for Vienna location.

Sky luminance/radiance models: To explore the implications of the sky model selection on the fidelity of simulation results, we used Radiance to compute the indoor illuminance in an existing test space on the rooftop of a university building. Thereby, the aforementioned two sky models were considered. In addition to latter two scenarios, two other scenarios is created using diffuse fraction model in generation of both sky models. A fifth scenario was a sky model generated based on measured values obtained from a sky scanner. Simultaneously, the actual illuminance levels in this room were monitored under different outdoor conditions (clear, intermediate, overcast). The comparison of the measurement results with multiple model prediction results facilitates an empirically based evaluation of the reliability of outdoor and indoor illuminance predictions in the face of different assumptions pertaining to the prevailing boundary conditions.

Luminous efficacy models: Four luminous efficacy models were selected and their performance were evaluated in generating global horizontal illuminance. Results indicated superior performance of all models in generation of global horizontal illuminance from measured global horizontal irradiance.

Keywords

Sky models, solar radiation, diffuse fraction, luminance distribution, clearness index, global horizontal irradiance.

Acknowledgments

The research presented in this work was supported within the special fund "Innovative Projekte" of *TU Wien*.

First and foremost, my deepest appreciation goes to my supervisor Professor Ardeshir Mahdavi. Years before starting my graduate studies I was truly excited to get a chance to work with him. Four years ago this chance became a reality. During his supervision, I have enhanced my skills and knowledge specially in field of computer science and data analytics, which helped me to build up my future career. Without question, he is the best in his field and I am proud that I could work under his supervision during the past four years.

I will always be grateful to Dr. Matthias Schuss for sharing his technical knowledge with me. Without doubt, his great and continuous help and support, assisted me in advancing my programming skills.

I would like to express a special word of thanks to Mr. Josef Lechleitner, for his patience and support in facilitating data collection from data repository of *Building Physics and Building Ecology Department, TU Wien*.

I am grateful to Ms. Ghazal Etminan, a Master of Science student at the *Department of Building Physics and Building Ecology, TU Wien* for her collaboration in studying simulation of indoor illuminance using different sky models in the frame of a Master's degree thesis.

I also express my sincere gratitude to our secretary Mrs. Elisabeth Finz at the *Department of Building Physics and Building Ecology, TU Wien*. She has helped me many times and in many ways. I have always been impressed with her constant kind nature towards all colleagues.

I am grateful for all the support I received from Ulrich Pont, Neda Ghiassi, Milena Vuckovic, Mahnameh Taheri, and Farhang Tahmasebi, as well as all

our other department's colleagues during the whole period of my work at *TU Wien*. Finishing my dissertation was a tough period for me, and I truly appreciate the encouragement they all gave me.

Lastly, from the bottom of my heart, I would like to thank my family, for their constant support and encourage: specially, my parents, who did everything for me and my siblings in order to facilitate our studies. I would like to thank my Brother, who always motivated me. At the end, I would like to thank my dearest Phillip Auvera and his beautiful family for their great support and kindness towards me.

Table of Contents

Kurzfassung	I
Summary	III
Acknowledgments	V
Table of Contents	VII
Chapter 1 Introduction	1
1.1 Background	3
1.1.1 Available diffuse fraction models	3
1.1.2 Available sky radiance/luminance distribution models	4
1.2 Motivations	4
1.3 Objectives	5
1.4 Outline	6
Chapter 2 Dataset	8
2.1 Data collection	8
2.1.1 USA	8
2.1.2 Vienna	10
2.2 Data quality control	11
Chapter 3 Diffuse fraction models	12
3.1 Introduction	12
3.2 Existing models	13
3.2.1 Polynomial models	13
3.2.2 Logistic function models	21
3.2.3 Exponential Models	22
3.3 BPI model	25
3.3.1 Approach	25
3.3.2 Model Description	34

3.4	Results and Discussions.....	35
3.5	Conclusion.....	40
Chapter 4	Sky radiance/luminance distribution model.....	41
4.1	Introduction	41
4.2	Prediction of vertical illuminance.....	42
4.2.1	Perez et al.	42
4.2.2	CIE	43
4.3	Prediction of vertical irradiance using RADIANCE.....	45
4.3.1	GENDAYLIT	46
4.3.2	GENSKY	47
4.3.3	Sky scanner	47
4.4	Results and Discussions.....	49
4.4.1	Vertical illuminance comparison	49
4.4.2	Vertical irradiance comparison.....	52
4.5	Conclusions	55
Chapter 5	Case Study: The Reliability of Indoor Illuminance Prediction	
	56	
5.1	Introduction	56
5.2	Methodology.....	56
5.2.1	Test Room	57
5.2.2	Measurements.....	57
5.2.3	Simulation	59
5.3	Results and Discussions.....	62
5.4	Conclusion.....	68
Chapter 6	Luminous Efficacy of Daylight	69
6.1	Introduction	69
6.2	Global Luminous Efficacy Models	69

6.3 Results and Discussions.....	70
Chapter 7 Conclusions.....	74
7.1 Contributions	74
7.1.1 Chapter 3	74
7.1.2 Chapter 4	74
7.1.3 Chapter 5	75
7.1.4 Chapter 6	75
7.2 Outlook.....	76
7.3 Publications.....	76
Chapter 8 References	78
8.1 Literature.....	78
8.2 Tables	86
8.3 Figures.....	87
Glossary.....	90
Appendix A – BPI Weather station	92
Appendix B – Perez Look-up table.....	95
Appendix C	103
Appendix D – Skyscanner.cal.....	105
Curriculum Vitae	113

Chapter 1 Introduction

Sun emits short and long wave radiation. Short wavelength is between 100 nm to 780 nm and long wave between 780 nm to about 5 μm . Meteorologically significant spectral range varies between 300 nm to 3000 nm. The maximum solar radiation intensity reaches at wavelength around 500 nm. Only a narrow bandwidth of the wavelength is visible for the human eyes. This wavelength is called 'visible light' and corresponds to the range of 400 nm to 780 nm (*Harbison et al., 2015*). The total amount of solar radiation outside the earth's atmosphere is almost constant over the course of a year and is called solar constant. This amounts to approximately 1366 W/m^2 , and can vary periodically throughout the year (*Gueymard, 2004*). The penetration of solar radiation through atmosphere is governed by several factors including absorption, scattering of radiation by particles and air molecules. Absorption of solar radiation occurs at the different wavelengths from ultraviolet to infrared. About 99% of harmful ultraviolet radiation, of wavelength less than 320 nm, is absorbed by ozone layer. Higher wavelengths are absorbed mainly by water vapors (H_2O) and Carbon dioxide (CO_2). This phenomenon reduces the electromagnetic radiation energy for certain wavelength (*Menzel, 2001*). *Figure 1-1* shows the comparison of extraterrestrial solar radiation for different spectrum with solar radiation measured at the ground surface of the earth. The scattering occurs when the electromagnetic radiation is diffused at any direction due to small atmospheric particles and clouds. The brightness and the blue color of the sky dome is due to the scattering of solar radiation by atmospheric particles. The sum of energy coming from the sky dome on a horizontal surface is called horizontal global irradiance. Information on solar radiation incident on the surface of the building envelope is beneficial for building thermal and visual simulation.

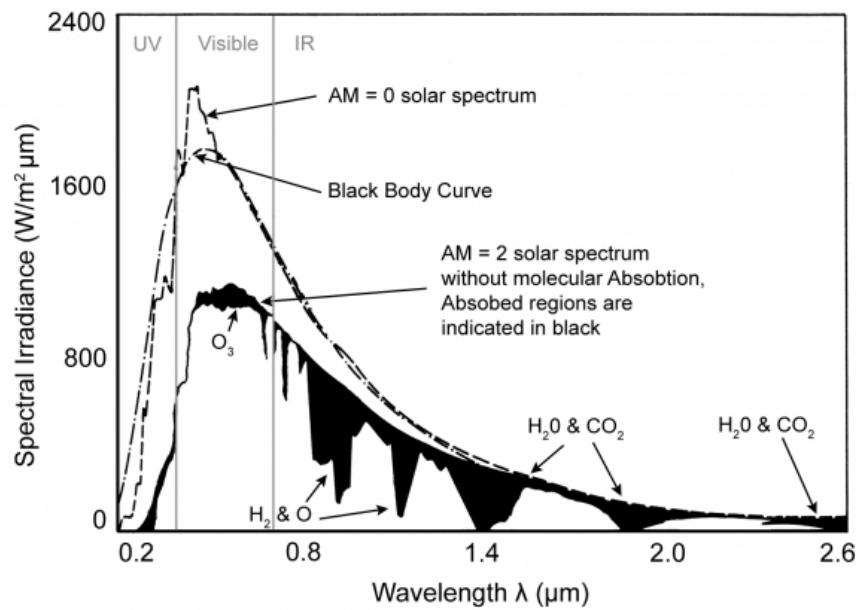


Figure 1-1. Extraterrestrial solar spectrum vs. earth surface solar spectrum (image source: <http://www.itacanet.org/the-sun-as-a-source-of-energy/part-2-solar-energy-reaching-the-earths-surface/>)

The angular diameter of sun is approximately 0.53° . Direct or Beam radiation is the radiation travelling on a straight line from the sun to the surface and includes sun disk and a circumsolar area around the disc. The respective region varies depending on the absorption and scattering effect (Blanc *et al*, 2013). The reflected radiation or Albedo is the radiation that is reflected by the terrain surface. This component extremely depends on the reflective properties of the ground surface and is negligible for low reflective terrains. In general, and due to the cost of measurement instruments, only the data on global horizontal irradiance is made freely available worldwide (Maxwell 1987). This information is not sufficient to calculate/estimate the distribution of diffuse radiance/luminance over the sky hemisphere, which is crucial for daylight, thermal, photovoltaic and solar thermal collector simulation and design purposes. Therefore, information such as: total diffuse irradiance, direct normal irradiance, diffuse and direct illuminance are needed as inputs for several engineering works. Consequently, numerous studies focus only on the prediction of the diffuse horizontal irradiance based on the global horizontal irradiance. These models are called diffuse fraction models (see section 1.1.1).

Another model which comes to support engineers is luminous efficacy models which is the ratio of illuminance over irradiance and could be deployed to convert irradiance to illuminance and vice versa (see chapter Chapter 6).

In this context, this research explores and evaluates the performance of a number of well-known hourly diffuse fraction, sky distribution and luminous efficacy models in separate chapters employing large repository of radiation data from Building physics and Building ecology department of *TU Wien* and 7 *BSRN* sites in the *USA*. In addition to evaluation of these models, a master thesis is conducted to evaluate the performance of sky models in predicting indoor illuminance values.

1.1 Background

1.1.1 Available diffuse fraction models

Initial work was done by *Parmerlee (1954)* and *Liu and Jordan (1960)*. Later several authors contributed in developing diffuse fraction models including *Choudhury (1963)*, *Stanhil (1966)*, *Boes (1975)*, *Hottel (1976)*, *Tuller (1976)*, *Orgill and Hollands (1977)*, *Bugler (1977)*, *Randall and Whitson (1977)*, *Bruno (1978)*, *Barbaro et al. (1979)*, *Iqbal (1980)*, *Bird and Hulstrom (1981)*, *Spencer (1982)*, *Erbs et al. (1982)*, *Kasten (1983)*, *Muneer et al. (1984)*, *Carrol (1985)*, *Weiss and Norman (1985)*, *Skartveit and Olseth (1987)*, *Maxwell (1987)*, *Reindl et al. (1990)*, *Bivona et al. (1991)*, *Perez et al. (1992)*, *Lam and Li (1996)*, *Boland et al. (2001)*, *Boland et al. (2008)*, *Ridley et al. (2010)*. Moreover, there are models which are adopted for specific locations such as *Ruth and Chant (1976)*, *Hawladar (1984)*, *Chendo and Maduekwe (1994)*, *Chandrasekaran and Kumar (1994)*, *de Miguel et al. (2001)*, *Oliviera et al. (2002)*, *Karatosou et al. (2003)*, *Soares et al. (2004)*, *Vazifeh et al. (2013)*.

Dervishi and Mahdavi (2011, 2012), *Vazifeh et al. (2013)* compared a number of outstanding models selected from above mentioned studies using data collected at the *Department of Building physics and Building ecology, TU Wien*. Findings indicated that none of the chosen models

shows satisfying accuracy in terms of prediction of the diffuse horizontal irradiance. Therefore, we explored in detail different meteorological variables to investigate possibility of deriving a new diffuse fraction model with higher prediction accuracy.

1.1.2 Available sky radiance/luminance distribution models

As mentioned earlier, scattering and absorbing phenomenon of radiation in the atmosphere and random distribution of the clouds, radiance/luminance distributes heterogeneously and varies for different locations and different time of the year. Solid sky radiance/luminance distribution models and daylight availability information can enhance the quality of indoor environment and building energy conservation. Several authors introduced new models to predict luminance distribution over the sky hemisphere. Early works started by *Moon and Spencer (1942)* introduced a sky luminance distribution model for overcast sky. A simplified version of their model was recommended by *CIE* as the *CIE Standard Overcast Sky (CIE, 1955)*. *Kittler (1967)* proposed a sky luminance distribution model for clear sky that was recommended by *CIE* as the *CIE Standard Clear Sky (CIE, 1973)*. *Littlefair (1981)* introduced his *BRE* average sky model for an average sky luminance distribution. *Nakamura et al. (1985, 1987)* presented the intermediate sky plus a zenith luminance equation. *Kittler (1985)* presented a homogenous sky to show absolute values of sky luminance distribution. *Perraudeau (1988)* categorized the sky into five categories and presented an equation of sky luminance distribution. *Perez et al. (1993)* proposed his All-weather sky model considering insolation condition parameters. *Kittler et al. (1997)* presented 15 sky categories, which later *CIE (2013)* recommended it as Standard General Sky.

1.2 Motivations

Engineering applications in building industry such as *i)* computational prediction of the energy demand of building designs; *ii)* placement,

configuration, and sizing of building-integrated solar energy systems (solar-thermal collectors, photovoltaic panels); *iii*) proper selection of buildings' external surfaces and their solar-thermal properties; *iv*) computational prediction of daylight levels in buildings' interior spaces; *v*) selection of location, geometry, and photometric properties of buildings' windows, apertures, and other daylighting systems require accurate information on spatial and temporal distribution of solar irradiance and illuminance on building surfaces. Performance evaluation of models that predict solar radiation data including diffuse fraction models, sky radiance/luminance distribution models, and luminance efficacy models is necessary to evaluate the validity of their applications in above mentioned engineering areas.

1.3 Objectives

Discussed models play an important role in scientific and engineering applications toward sustainability and high-energy performance building (*Igawa et al. 2004, Grigante et al. 2011, Gueymard 2008*). This thesis thus examines a number of such models in detail and explore both improvement possibilities of existing models and the potential for alternative modeling techniques and approaches. Toward this end, the current research specifically evaluates existing high-resolution sky radiance and sky luminance models for the city of Vienna. In order to generate sky radiance maps, typically the diffuse radiation component of the global horizontal irradiance must be derived based on proper diffuse fraction models (*Dervishi and Mahdavi 2012*). Consequently, the proposed research starts with evaluating existing diffuse fraction models. Once both diffuse and direct horizontal irradiance data is available, the existing models for sky radiance generation can be comprehensively evaluated. For this purpose, we deploy our existing monitoring facility and other available resources to systematically collect both typical weather station data and additional information concerning the diffuse component of the global horizontal irradiance, global horizontal illuminance, vertical irradiance, as well as detailed sky luminance and radiance distribution.

1.4 **Outline**

Some sections of this thesis are based on the notes written by my research supervisor Professor Ardeshir Mahdavi, and also publications authored by us and other colleagues. This thesis is structured in 7 chapters, alongside the Introduction as follow.

- Chapter 2:

This chapter describes data used in current work and characterization of the locations and climate conditions of employed stations.

- Chapter 3:

This chapter explores existing diffuse fraction models and their shortcomings to predict the diffuse horizontal irradiance. Moreover, a high performance empirical model for Vienna location is presented which is developed at the *Department of Building Physics and Building Ecology, TU Wien, Vienna, Austria*.

- Chapter 4:

In this chapter, two studies are discussed. First study assesses two well-known sky luminance distribution models to predict illuminance on four cardinal vertical surfaces. Second study explore the performance of mentioned sky models to predict irradiance values on four cardinal vertical surfaces in *RADIANCE rendering program*.

- Chapter 5:

This chapter which is the result of a collaborative work with Ms. Ghazal Etminan (Master of science student at *TU Wien*), evaluates the performance of sky models and our own developed sky model (based on measured data from sky scanner) in prediction of indoor illuminance of a test room compared to measured indoor illuminance values taken in Vienna for 3 defined sky conditions.

- Chapter 6:

This chapter evaluates the performance of luminous efficacy models in generating global horizontal illuminance.

– Chapter 7:

The last chapter discusses the contribution of this dissertation and possibility of future works.

Chapter 2 Dataset

2.1 *Data collection*

Due to the spherical shape of the earth, solar radiation is not equally distributed over the planet. In addition to that, meteorological conditions and site topography influences solar radiation magnitudes. Therefore, in order to examine the universality of the radiation models, having access to data from different locations is required. For this purpose, we gathered data from one location in Vienna, Austria and 7 locations in United States.

2.1.1 USA

Baseline Surface Radiation Network project is a Data and Assessment Panel from the Global energy and Water Cycle Experiment (*GEWEX*) under the umbrella of the World Climate Research Program (*WCRP*) (*König-Langlo and Sieger, 2012*).

In this study, 7 USA sites' data is accessed from Baseline Surface Radiation Network (*BSRN*) database for year 2013 (see *Figure 2-1*). *Table 2-1* shows general information on each station. 20 variables are available from each station. Data were reported 1-min averages, which during the pre-processing phase we converted to hourly averages.

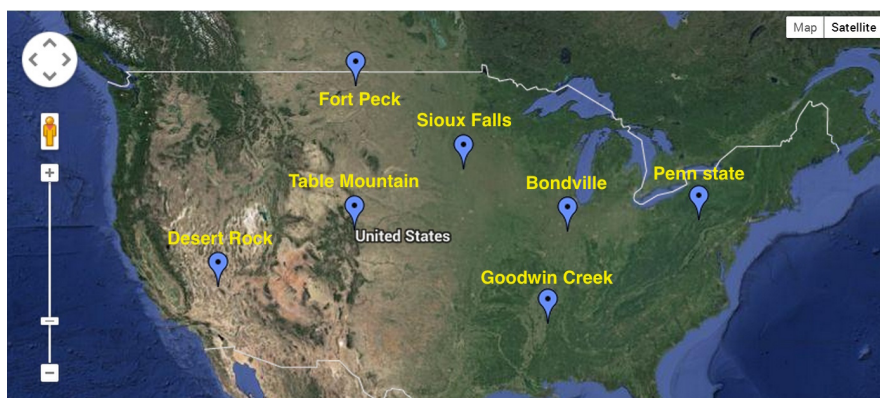


Figure 2-1. Distribution map of BSRN sites deployed in this study

Table 2-1. Characteristics of stations in the USA (BSRN)

Station	Abb.	Lat, Long (E +)	Elev.	Comment
<i>Bondville, IL</i>	bon	40.06, -88.36	213m	BSRN sta. #: 32; Surface type: grass; Topography type: flat, rural
<i>Desert Rock, NV</i>	dra	36.62, -116.01	1007m	BSRN sta. #: 35; Surface type: desert, gravel; Topography type: flat, rural
<i>Fort Peck, MT</i>	fpk	48.31, -105.10	634m	BSRN sta. #: 31; Surface type: grass; Topography type: flat, rural
<i>Goodwin Creek, MS</i>	gwn	34.25, -89.87	98m	BSRN sta. #: 33; Surface type: grass; Topography type: hilly, rural
<i>Rock Springs, PA</i>	psu	40.72, -77.93	376m	BSRN sta. #: 36; Surface type: cultivated; Topog. type: mountain valley, rural
<i>Sioux Falls, SD</i>	sxf	43.73, -96.62	473m	BSRN sta. #: 37; Surface type: grass; Topography type: hilly, rural
<i>Table Mountain, CO</i>	tbl	40.12, -105.24	1689m	BSRN sta. #: 34; Surface type: grass; Topography type: hilly, rural

2.1.2 Vienna

Vienna has a mild climate with warm summers and is classified as Cfb in *Köppen-Geiger* classification. The sky in Vienna is most of the year partly cloudy to overcast. The median cloud cover varies from 44% to 89% through the year (*Climate-Data.org*, 2016).

The weather station belongs to *Department of Building Science and Building Ecology, TU Wien* and is located near Karlsplatz, city center. The measurement devices are mounted on the rooftop of the *TU Wien's* main building. In the purpose of this work, data from a number of meteorological, solar radiation and photonic sensors are employed. A short information list of these sensors is presented in *Table 2-2* (Detailed specification of these sensors including their mounting status can be find in appendix A).

Table 2-2. List of deployed sensors for Vienna

Instrument	Measurement	Brand	Image
<i>CM3 Pyranometer</i>	irradiance	Kipp&Zonen	
<i>SPN1 Pyranometer</i>	irradiance	Delta-T Devices	
<i>Skyscanner MS321LR</i>	radiance & luminance	Eko Instruments	
<i>CM121 Shadow ring</i>	irradiance	Kipp&Zonen	
<i>CLIMA Sensor</i>	meteorological	Thies Clima	

2.2 *Data quality control*

BSRN Surfrad data are written in ASCII text and are organized in one-minute intervals after beginning of 2009. A QC flag of zero qualifies the data point. Data points with QC flag other than zero were eliminated to increase the quality of data.

Data quality plays an important role in data analysis and model development. To achieve a reliable and trustful level of data, several steps of rigorous quality control analysis is done to the BPI data, which are:

1. The comparison of global horizontal irradiance data from sunshine Pyranometer (*Delta-T SPN1*) with an accurate Pyranometer (*Kipp & Zonen CM3*) and elimination of data, with more than 5% of deviation for the whole period of the measurement
2. Discarding the data with solar altitude of less than 5 degrees, due to the possibility of obstructed sun by the surrounding hills
3. Elimination of data with global horizontal radiance less than 50 watts per square meters or clearness index of higher than unit
4. Replacement of error containing patches by average value of surrounding patches
5. Elimination of patches exceeding sensor maximum range

Chapter 3 Diffuse fraction models

3.1 *Introduction*

Clearness index (k_t , ratio of global horizontal irradiance over extraterrestrial horizontal irradiance) provides useful information on sky solar energy conditions (see equation 1). The lower the horizontal diffuse component of solar radiation is, the higher the clearness index. This index barely exceeds 0.85 for location Vienna, Austria. The reason for this phenomenon is that, even on clearest day there will be a portion of solar energy absorbed or reflected by the atmosphere back to the space before reaching the earth ground. Although, under certain circumstances, this number can nearly reach to unit, e.g. sky with bright clouds and unobstructed sun (*Skartveit & Olseth 1987*).

There has been much research about the effect of other variables on diffuse component of solar radiation, e.g. air temperature, relative humidity, water content, and solar altitude. This chapter explores some of available diffuse fraction models and evaluates their performances compared to measured data. Selection of these models was based on highly cited papers among other diffuse fraction models. The models are divided into three categories, namely, polynomials, logistic, and exponential models (see *Table 3-1*). Definition of each models and their formulas are explained in section 2 of this chapter. Moreover, the author proposes a new diffuse fraction model and its performance is compared with those models.

$$k_t = \frac{I_{gh}}{I_{ext} \times \sin \alpha} \quad (1)$$

$$k_d = \frac{I_{dh}}{I_{gh}} \quad (2)$$

$$I_{ext} = 1367 \left(1 + 0.33 \cos \frac{360n}{365} \right) \quad (3)$$

Table 3-1. Summarized description of models and their variables

Model	Function type	Variables
<i>Erbs et al. (1982)</i>	Polynomial	k_t
<i>Maxwell (1987)</i>	Exponential	k_t, m_{air}
<i>Skartveit and Olseth (1987)</i>	Polynomial	k_t, α, σ_3
<i>Reindl et al. (1990)</i>	Polynomial	$k_t, \sin \alpha, T, \phi$
<i>Perez et al. (1992)</i>	Exponential	$W, Z, k_t', \Delta k_t'$
<i>Boland et al. (2008)</i>	Logistic	k_t
<i>BRL (2010)</i>	Logistic	$k_t, AST, \alpha, K_t, \varphi$

3.2 Existing models

3.2.1 Polynomial models

Polynomial functions are of the simplest methods to derive correlations despite the fact that they are less realistic. Some of the earliest diffuse fraction models were based on polynomial function. In 1960, *Liu and Jordan* proposed a linear diffuse fraction model as a function of clearness index.

Orgill and Hollands (1997) proposed a polynomial diffuse fraction model as a function of clearness index using data from Toronto, Canada. *Iqbal (1980)* later proposed a diffuse fraction model as a function of clearness index and solar altitude, which showed a significant enhancement in the model performance. *Reindl et al. (1990)* proposed two models, a full version and a simplified model. Full version model is based on 4 variables, namely, clearness index, solar altitude, temperature, and relative humidity, and the simplified version as a function of clearness index and solar altitude. In their findings full version model gained 26% and

simplified version 23% improvement in comparison to *Erbs et al. (1982)* model.

3.2.1.1 Erbs et al. (1982)

Erbs et al. (1982) suggested a diffuse fraction model as a function of clearness index, which has different function for different bins of clearness index. They demonstrated different approaches to estimate diffuse fraction based on hourly, daily, and monthly average data. The data to obtain their model was collected from four available stations in the USA, Fort Hood (TX), Livermore (CA), Raleigh (NC), and Maynard (NM). The direct beam irradiance was measured using a Pyrheliometer and global horizontal irradiance data using a Pyranometer. In order to validate the data, they used data from Highett, Victoria, Australia that was measured with an unshaded and shaded Pyranometer. In addition to clearness index dependent model, they calculated diffuse fraction as a function of k_c , the ratio of horizontal global irradiance to clear sky horizontal global irradiance. However, results suggested no significant change in the standard deviation between measured values and predicted one.

Below *Erbs et al. (1982)* model as a function of clearness index is described:

For $k_t \leq 0.22$;

$$\frac{I_{dh}}{I_{gh}} = 1 - 0.09k_t \quad (4)$$

For $0.22 \leq k_t \leq 0.8$

$$\frac{I_{dh}}{I_{gh}} = 0.9511 - 0.1604k_t + 4.39k_t^2 - 16.64k_t^3 + 12.34k_t^4 \quad (5)$$

For $k_t > 0.8$;

$$\frac{I_{dh}}{I_{gh}} = 0.165 \quad (6)$$

For values of clearness index more than 0.8, they use a constant diffuse fraction, similar to the *Orgill and Hollands (1997)* approach. They explain the increase of diffuse fraction for the clearness index values of higher than 0.8 with the bright diffuse reflection from the clouds and unobstructed sun.

3.2.1.2 Skartveit and Olseth (1987)

In 1987, *Olseth and Hollands* presented an hourly diffuse fraction model using clearness index and solar altitude as input variables. In 1998, Authors published another article which was improved with adding 2 variables of variability index and regional surface albedo. Data sets from Bergen, Norway were used with data only for April to October due to a significant snow cover in other months of the year. In this study a snow-free case of Skartveit and Olseth has been considered for the comparison purposes.

3.2.1.2.1 The variability index

Distribution of clouds strongly affects diffuse and beam irradiance values (*Erbs et al. 1982*). Clouds can be in different colors/temperatures, different thickness, and different layers and height. Lower the temperature; lower the emission is from those clouds. Thicker clouds diffuse the solar radiation uniformly but reflect most of it back to the space. Multi-layer clouds can cause random distribution pattern of the radiance/luminance. All above-mentioned variations in the clouds will increase the complexity of sky radiance/luminance distribution. A diagnostic method to predict the cloud presence, which has a similar approach as *Perez (1992)*, an hourly variability index σ_3 was introduced by the authors. It is defined as a root mean square of deviation between clear sky index of the time step (ρ_t) and, respectively, the preceding (ρ_{t-1}) and the subsequent (ρ_{t+1}) hour:

$$\sigma_3 = \sqrt{\frac{(\rho_t - \rho_{t-1})^2 + (\rho_t - \rho_{t+1})^2}{2}} \quad (7)$$

In the case, when the preceding or subsequent hour is missing, the following formula is used:

$$\sigma_3 = |\rho_t - \rho_{t\pm 1}| \quad (8)$$

Clear sky index ρ is:

$$\rho = \frac{k_t}{k_1} \quad (9)$$

And k_1 is:

$$k_1 = 0.83 - 0.56e^{-0.06 \times \alpha} \quad (10)$$

Where α is solar altitude in degrees.

σ_3 is almost independent of solar altitude. Low σ_3 shows overcast sky, which $0.9 < \rho_t < 1.0$ represents nearly cloudless sky. It was indicated that k_t for clear sky is only related to solar elevation and rarely reaches up to 0.75; higher k_t occurs in the case of dealing with partially cloudy sky with unobstructed sun disk in snow-free areas or locations with high surface albedo. In those cases, only diffuse component will increase, while the amount of radiation coming directly from the sun remains constant. In appendix II, observation of various sky types and correlation of k_t with solar components is discussed.

If for any reason σ_3 is unknown, the following equation may be applied:

For $\rho < 1.04$:

$$\sigma_3 = 0.021 + 0.397\rho - 0.231\rho^2 - 0.13 e^{[-\{ \frac{(\rho - 0.931)}{0.134} \}]^2} \quad (11)$$

For $\rho > 1.04$:

$$\sigma_3 = 0.12 + 0.65(\rho - 1.04) \quad (12)$$

3.2.1.2.2 Invariable hours

For $\sigma_3 = 0$, the diffuse fraction model is developed applying linear least square regression to Bergen's data for each bins (I-IV) of clearness index k_t , as follows:

- i. For $k_t < 0.22$, Skartveit and Olseth considers a totally overcast sky without any direct beam irradiance:

$$k_d = 1.00 \quad (13)$$

- ii. For $0.22 \leq k_t \leq k_2$, Broken clouds and semi unobstructed sun dominates.

$$k_d = f(k_t, \alpha) = 1 - (1 - k_{d1})(0.11\sqrt{K} + 0.15K + 0.74K^2) \quad (14)$$

Where

$$K = 0.5(1 + \sin \left[\frac{k_t - 0.22}{k_1 - 0.22} \pi - 0.5\pi \right]) \quad (15)$$

$$k_2 = 0.95k_1 \quad (16)$$

$$k_{d1} = 0.07 + 0.046 \frac{90 - \alpha}{\alpha + 3} \quad (17)$$

For α less than 1.4° , k_{d1} is considered as 1.

- iii. For $k_2 \leq k_t \leq k_{max}$, an almost cloudless sky was assumed. Thus, diffuse component will be constant, and diffuse fraction will be dependent on solar elevation and turbidity. From this assumption:

$$k_d = k_{d2} k_2 \frac{(1 - k_t)}{k_t(1 - k_2)} \quad (18)$$

The upper limit k_{max} is derived from k_{bmax} :

$$k_{max} = \frac{k_{bmax} + \frac{k_{d2} k_2}{(1 - k_2)}}{1 + \frac{k_{d2} k_2}{(1 - k_2)}} \quad (19)$$

Where k_{bmax} is fitted to an extreme beam transmittance modelled by the SMARTS2 (Gueymard 1993):

$$k_{bmax} = 0.81^\omega \quad (20)$$

$$\omega = \frac{1}{\sin \alpha}^{0.6} \quad (21)$$

- iv. For $k_t \geq k_{max}$, they assumed that diffuse fraction is only influenced by clouds, due to the constant beam irradiance:

$$k_d = 1 - k_{max} \frac{1 - k_{dmax}}{k_t} \quad (22)$$

Where maximum diffuse fraction for maximum clearness index is:

$$k_{dmax} = k_{d2} k_2 \frac{(1 - k_{max})}{k_{max}(1 - k_2)} \quad (23)$$

3.2.1.2.3 Variable hours

For $\sigma_3 > 0$, the least square analysis indicated use of a term $\Delta(k_t, \alpha, \sigma_3)$, which should be added to the above invariable hours diffuse fraction for all bins (I to IV):

For $0.14 \leq k_t \leq k_x$:

$$\Delta(k_t, \alpha, \sigma_3) = -2k_L^2(1 - k_L)\sigma_3^{1.3} \quad (24)$$

For $k_x \leq k_t \leq k_x + 0.71$:

$$\Delta(k_t, \alpha, \sigma_3) = 3k_R(1 - k_R)^2\sigma_3^{0.6} \quad (25)$$

For $k_t > k_x + 0.71$ and for $k_t < 0.14$:

$$\Delta(k_t, \alpha, \sigma_3) = 0 \quad (26)$$

Where:

$$k_x = 0.56 - 0.32e^{-0.06\alpha} \quad (27)$$

$$k_L = \frac{k_t - 0.14}{k_x - 0.14} \quad (28)$$

$$k_R = \frac{k_t - k_x}{0.71} \quad (29)$$

3.2.1.3 Reindl et al. (1990)

Reindl et al. (1990) presented a polynomial diffuse fraction model. Their goal was to derive a model which is simple and uses basic microclimatic weather data such as global horizontal irradiance, temperature and humidity. They used data from 5 locations (three in Europe and two in United States) and data from Oslo, Norway for comparison purposes. All data was processed to achieve high quality data such as elimination of flagged, elimination of data which violate physical limits or conversion principles. The motivation behind their study was to investigate whether adding extra predictors to the *Liu and Jordan* type models will significantly reduce the standard errors. They also limited the model inputs to

commonly observed climatic variables such as ambient temperature, relative humidity, etc. Three piecewise correlation was presented using different number of variables. A piecewise correlation over three ranges of clearness index:

For $k_t \leq 0.3$; $\frac{I_{dh}}{I_{gh}} \leq 1.0$

$$\frac{I_{dh}}{I_{gh}} = 1.00 - 0.232k_t + 0.0239 \sin \alpha - 0.000682T_a + 0.0195\phi \quad (30)$$

For $0.3 < k_t < 0.78$

$$\frac{I_{dh}}{I_{gh}} = 1.329 - 1.716k_t + 0.267 \sin \alpha - 0.00357T_a + 0.106\phi \quad (31)$$

For $k_t \geq 0.78$ & $\frac{I_{dh}}{I_{gh}} \geq 0.1$

$$\frac{I_{dh}}{I_{gh}} = 0.426k_t - 0.256 \sin \alpha + 0.00349T_a + 0.0734\phi \quad (32)$$

Where, I_{dh} is horizontal diffuse irradiance, I_{gh} is horizontal global irradiance, T_a is outdoor temperature and ϕ is relative humidity. For the locations, where temperature and relative humidity are not available, they presented second piecewise correlation:

For $k_t \leq 0.3$; $\frac{I_{dh}}{I_{gh}} \leq 1.0$

$$\frac{I_{dh}}{I_{gh}} = 1.02 - 0.254k_t + 0.0123 \sin \alpha \quad (33)$$

For $0.3 < k_t < 0.78$

$$\frac{I_{dh}}{I_{gh}} = 1.4 - 1.749k_t + 0.177 \sin \alpha \quad (34)$$

For $k_t \geq 0.78$ & $\frac{I_{dh}}{I_{gh}} \geq 0.1$

$$\frac{I_{dh}}{I_{gh}} = 0.486k_t - 0.182 \sin \alpha \quad (35)$$

Comparison results revealed that first piecewise correlation (Four variables) reduced the residual sum of squares by 14.4% comparing to the correlation that depends only on clearness index (using the same dataset).

3.2.2 Logistic function models

3.2.2.1 Boland

Boland et al. (2001), made an attempt on finding a model for the whole range of k_t , unlike previous models such as *Erbs et al. (1982)*, *Reindl et al. (1990)*, *Olseth and Hollands (1987)*, and *Spencer (1982)*, which split data according to different ranges of k_t . Accordingly, he used logistic function that could fit the data. Using curve-fitting tool he derived two equations, Eq. 36 for 15-minutes data and Eq. 37 for hourly data:

$$\frac{I_{dh}}{I_{gh}} = \frac{1}{1 + e^{8.645(k_t - 0.613)}} \quad (36)$$

$$\frac{I_{dh}}{I_{gh}} = \frac{1}{1 + e^{7.997(k_t - 0.586)}} \quad (37)$$

Mentioned model was compared with *Reindl* model and showed slight improvement in the statistical measures such as *R-square* and Composite Residual sum of squares (CRSS). The main advantage of Boland model is the use of one single equation for the whole range of k_t . This equation predicts low diffuse fraction for high k_t , which is not the case in reality and due to the sky with visible sun and partly cloudy, k_t will reach near 0.9. Consequently, there will be a high diffuse irradiance as a result of the reflection of clouds.

3.2.2.2 Boland-Ridley-Lauret (BRL)

Employing a Bayesian framework, *Lauret et al. (2010)* derived a simple logistic hourly model by using 5 variables, which are apparent solar time

(AST), solar altitude α , clearness index k_t , daily clearness index K_t and persistence index ψ . Application of these variables enhances the performance of the predictive model due to their characteristics. The proposed model is:

$$\frac{I_{dh}}{I_{gh}} = \frac{1}{1 + e^{-5.32 + 7.28k_t - 0.03AST - 0.0047\alpha + 1.72K_t + 1.08\psi}} \quad (38)$$

$$K_t = \frac{\sum_{i=1}^{24} I_i}{\sum_{i=1}^{24} I_{0,i}} \quad (39)$$

$$\psi = \begin{cases} \frac{k_{t+1} + k_{t-1}}{2} & \text{sunrise} < t < \text{sunset} \\ k_{t+1} & t = \text{sunrise} \\ k_{t-1} & t = \text{sunset} \end{cases} \quad (40)$$

3.2.3 Exponential Models

Maxwell (1987) introduced an exponential model based on physical principles by developing a computer program, called the Direct Insolation Simulation Code (*DISC* model). Following this step, *Perez (1992)* used Maxwell beam irradiance for his first model, applying correcting coefficients to predict beam irradiance more accurately. His second model is air-mass independent.

3.2.3.1 Maxwell

Maxwell (1987) predicted normal beam irradiation I_b from hourly global irradiation values, using quasi-physical model. The amount of diffuse fraction can be calculated in order to compare it with other models. Initially, Maxwell calculated a maximum k_t for clear sky $K_{n,c}$:

$$K_{n,c} = 0.866 - 0.122m_{air} + 0.0121m_{air}^2 - 0.000653m_{air}^3 + 0.000014m_{air}^4 \quad (41)$$

In which m_{air} is air mass depending on α :

$$m_{air} = \frac{1}{\sin(\alpha) + \frac{0.50572}{(\alpha + 6.07995)^{1.6364}}} \quad (42)$$

Then a reduction ΔK_n of the maximum is considered:

$$\Delta K_n = a + be^{cm_{air}} \quad (43)$$

Where parameters of a, b and c are determined for two ranges of k_t , using two equations below:

$$\text{If } k_t \leq 0.6 \quad \begin{cases} a = 0.512 - 1.560k_t + 2.286k_t^2 - 2.222k_t^3 \\ b = 0.370 + 0.962k_t \\ c = -0.280 + 0.932k_t - 2.048k_t^2 \end{cases} \quad (44)$$

$$\text{If } k_t > 0.6 \quad \begin{cases} a = -5.743 + 21.77k_t - 27.49k_t^2 + 11.56k_t^3 \\ b = 41.4 - 118.5k_t + 66.05k_t^2 + 31.9k_t^3 \\ c = -47.01 + 184.2k_t - 222k_t^2 + 73.81k_t^3 \end{cases} \quad (45)$$

Finally, the direct normal irradiance and diffuse horizontal irradiance can be derived using:

$$I_{b, Disk} = I_0 \cdot K_n \quad (46)$$

$$I_d = I - I_{b, Disk} \sin \alpha \quad (47)$$

3.2.3.2 Perez

Perez et al. (1992) used a statistical approach from a large multi-climatic experimental database to derive two models for converting hourly global irradiance into hourly direct beam irradiance. This approach was based on the parameterization of insolation conditions (*Perez et al. 1990*), using four-dimensional space. In the current thesis the first model was used. Direct normal beam irradiance is:

$$I = I_{b,disk} \cdot X(K'_t, Z, W, \Delta K'_t) \quad (48)$$

Where I_{disk} the direct normal irradiance is estimated by the *DISC* model (Maxwell, 1987) and $X(K'_t, Z, W, \Delta K'_t)$ is a coefficient made of four insolation condition parameters, which are adjusted clearness index (K'_t) that represents meteorologically similar conditions irrespective of the position of the sun (Eq. 49). Z_s is the solar zenith angle (Eq. 50), $\Delta K'_t$ stability index (Eq. 51) and W is atmospheric precipitable water (Eq. 52). These coefficients are obtained from a look-up table consisting of a $6 \times 6 \times 5 \times 7$ matrix (See Table 3-2). As for the second model, Perez et al. used two terms of a and b , which were derived statistically from a large multi-climatic experimental data set. These coefficients are the average of 500 data points and were obtained from a four dimensional look-up table consisting of $8 \times 5 \times 4 \times 6$ matrixes (see Table 3-3). The instruction to how to use *Perez look up table* is given in Appendix.

$$K'_t = \frac{k'_t}{1.031 \left(e^{\left(\frac{-1.4}{0.9 + \frac{9.4}{m_{air}}} \right)} + 1 \right)} \quad (49)$$

$$Z = 90 - \alpha \quad (50)$$

$$\Delta K'_t = 0.5(|K'_t - K'_{t+1}| + |K'_t - K'_{t-1}|) \quad (51)$$

$$W = e^{(0.07T_d - 0.075)} \quad (52)$$

Table 3-2. Bins used in Perez function

Bins	K'_t	Z	W (cm)	$\Delta K'_t$
1	0.00-0.24	00-25	0-1	0.000-0.015
2	0.24-0.40	25-40	1-2	0.015-0.035
3	0.40-0.56	40-55	2-3	0.035-0.070
4	0.56-0.70	55-70	3- ∞	0.070-0.150
5	0.70-0.80	70-80	0- ∞	0.150-0.300
6	0.80-1.00	80-90		0.399-1.000
7				0.000-1.000

Table 3-3. Bins used for the Perez second model

Bins	K'_t	Z	W (cm)	$\Delta K'_t$
1	0.00-0.29	0.0-40.0	0-1.50	0.000-0.020
2	0.29-0.42	40.0-52.5	1.50-2.75	0.020-0.048
3	0.42-0.53	52.5-65.0	2.75- ∞	0.048-0.110
4	0.53-0.64	65.0-75.0	0.00- ∞	0.110-0.250
5	0.64-0.71	75.0-90.0		0.250-1.000
6	0.71-0.75			0.000-1.000
7	0.75-0.79			
8	0.79-1.00			

3.3 BPI model

This section describes in detail the efforts made to develop a high performance empirical diffuse fraction model for the Vienna climate. The model is the result of comprehensive research effort and data analysis at the *Department of Building Physics and Building Technology (BPI), TU Wien*.

3.3.1 Approach

In order to choose the appropriate parameters that correlate with the diffuse fraction, a number of commonly observed available climatic variables normalized and compared to the measured diffuse fraction. These variables, apart from the clearness index, are the global horizontal irradiance, solar altitude, temperature, and relative humidity.

3.3.1.1 Feature scaling

Since the range of variables varies widely, feature-scaling method is used to scale down variables between 0 and 1. This method increases the convergence speed when fitting methods are used. In order to standardize the independent variables rescaling is done. The formula is as follows:

$$X' = \frac{X - \min(X)}{\max(X) - \min(X)} \quad (53)$$

Where, X is the vector of each variable and X' is the normalized data.

3.3.1.2 Pearson moment correlation

Pearson moment correlation index was employed in order to estimate the strength of correlation of each variable with diffuse fraction. This index shows the linear dependency of two variables of X and Y . This index is defined as covariance of two variables divided by product of their standard deviation.

$$r = \frac{\text{cov}(X, Y)}{\sigma_X \sigma_Y} \quad (54)$$

Where, r is the Pearson index, and X and Y are variables. r can vary from -1 to 1 depending on the correlation between two variables. Absolute values of r higher than 0.7 show strong correlation while absolute values of r below 0.3 show weak correlation between two variables.

In this study scaled features (clearness index, horizontal global irradiance, solar altitude, temperature, relative humidity) are divided into 10 bins (0-0.1, to 0.9-1.0).

Workflow of Pearson index calculation for different variables is demonstrated in *Figure 3-1*. Pearson indexes are shown in *Table 3-4*. By looking at this table, it can be inferred that all 5 variables have moderate correlation with diffuse fraction, considering that highest to lowest correlations are global horizontal irradiance, clearness index, solar altitude, temperature and lowest relative humidity.

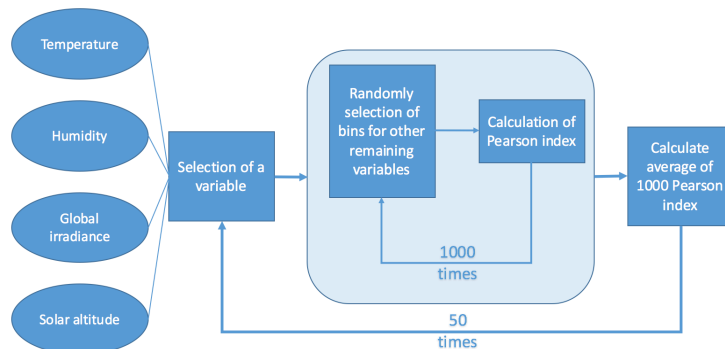


Figure 3-1. Workflow of Pearson index calculation

Table 3-4. Pearson moment correlation for different variables vs. diffuse fraction

Pearson moment number	Varying feature
0.45	Global horizontal irradiance
0.45	Global horizontal irradiance
0.44	Global horizontal irradiance
0.44	Global horizontal irradiance
0.44	Global horizontal irradiance
0.44	Global horizontal irradiance
0.44	Global horizontal irradiance
0.43	Global horizontal irradiance
0.43	Global horizontal irradiance
0.43	Global horizontal irradiance
0.42	Global horizontal irradiance
0.42	Global horizontal irradiance
0.41	Solar altitude
0.41	Temperature
0.41	Solar altitude
0.41	Global horizontal irradiance
0.41	Solar altitude
0.40	Solar altitude
0.40	Solar altitude
0.40	Temperature
0.40	Global horizontal irradiance
0.40	Solar altitude
0.40	Solar altitude
0.39	Temperature
0.38	Temperature
0.38	Temperature
0.38	Temperature
0.38	Humidity
0.38	Temperature
0.38	Temperature
0.37	Temperature
0.37	Solar altitude
0.37	Humidity
0.37	Temperature
0.37	Humidity
0.37	Solar altitude
0.36	Solar altitude
0.36	Humidity
0.36	Humidity
0.35	Humidity
0.35	Humidity
0.35	Temperature
0.35	Humidity
0.35	Humidity
0.35	Humidity
0.35	Humidity
0.35	Humidity
0.34	Humidity
0.33	Humidity

In order to better observe the correlation of each variable with diffuse fraction, each variable plus clearness index is compared with diffuse fraction in a contour and 3D plot. *Figure 3-2* shows that higher global horizontal irradiance (I_{gh}) corresponds with higher and lower clearness index and diffuse fraction respectively. Same correlation can be seen in 3D plot plus the fact that average global irradiance covers almost entire range of clearness-diffuse fraction (see *Figure 3-3*). *Figure 3-4* and *Figure 3-5* shows the correlation of temperature with diffuse fraction and clearness index. In most cases temperature doesn't impact diffuse fraction but extreme high and low temperatures slightly correlate to extreme low and high diffuse fraction respectively. Similar to temperature, extreme relative humidity correlates with extreme diffuse fraction but in a reverse correlation, which means, extreme high relative humidity values (near 100%) corresponds to diffuse fraction near 1 and extreme dry instances (relative humidity below 20%) represents low diffuse fraction (see *Figure 3-8* and *Figure 3-9*).

In general, there is no strong correlation between any of these variables and diffuse fraction. Therefore, development of a high resolution diffuse fraction model based on these data is not possible. However, we attempted and were successful to develop an empirical diffuse fraction model which is able to accurately predict diffuse fraction for Vienna.

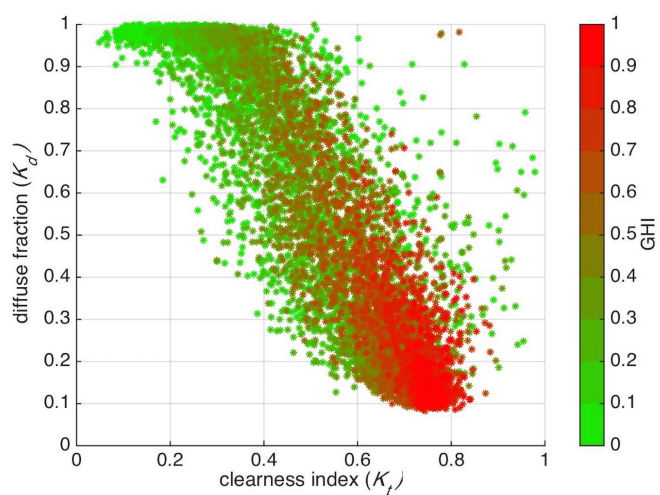


Figure 3-2. Comparison of diffuse fraction vs. clearness index for different global horizontal irradiance (I_{gh})

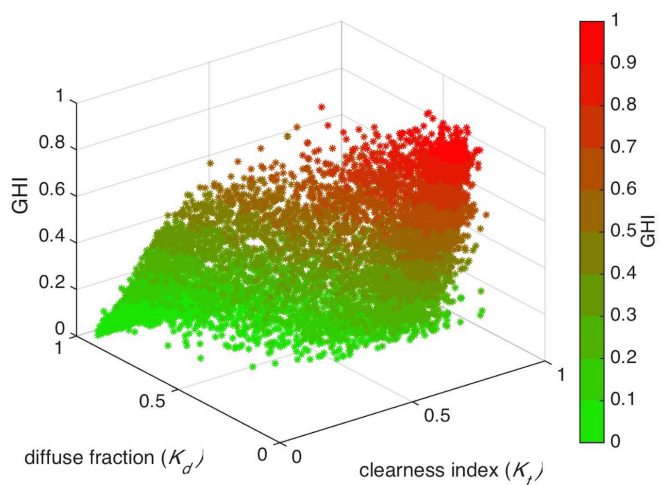


Figure 3-3. Three-dimensional comparison of diffuse fraction vs. clearness index and I_{gh}

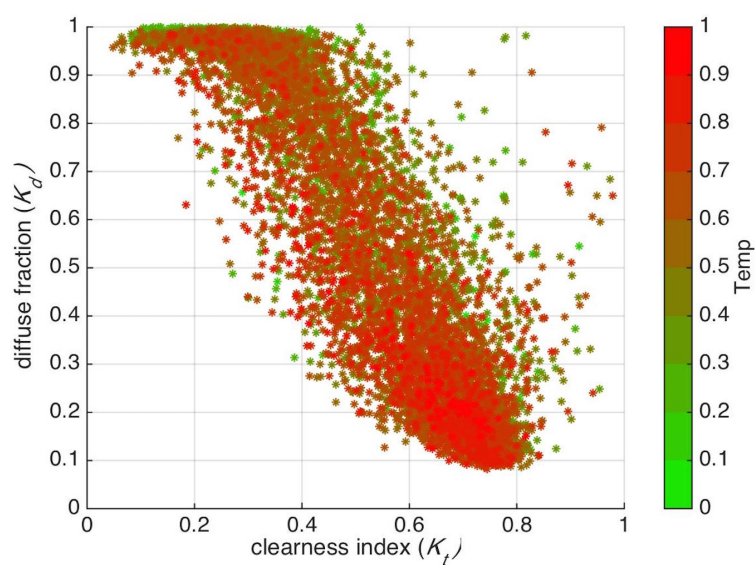


Figure 3-4. Comparison of diffuse fraction vs. clearness index for different temperatures

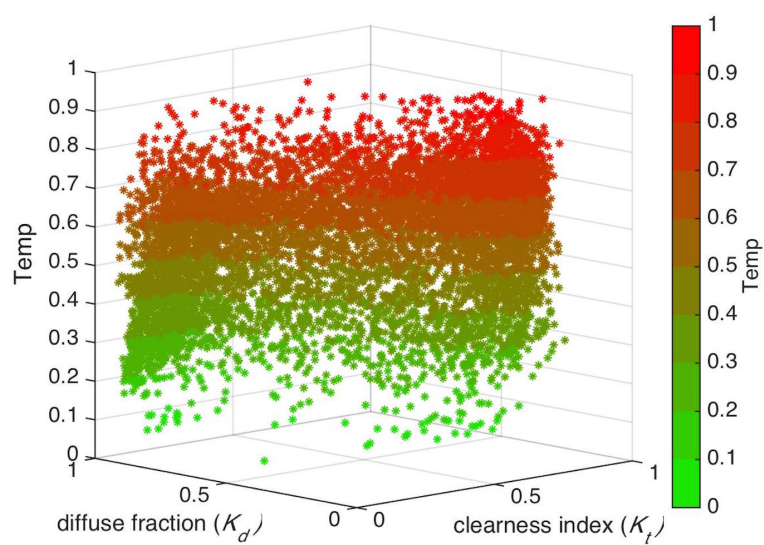


Figure 3-5. Three-dimensional comparison of diffuse fraction vs. clearness index and temperatures

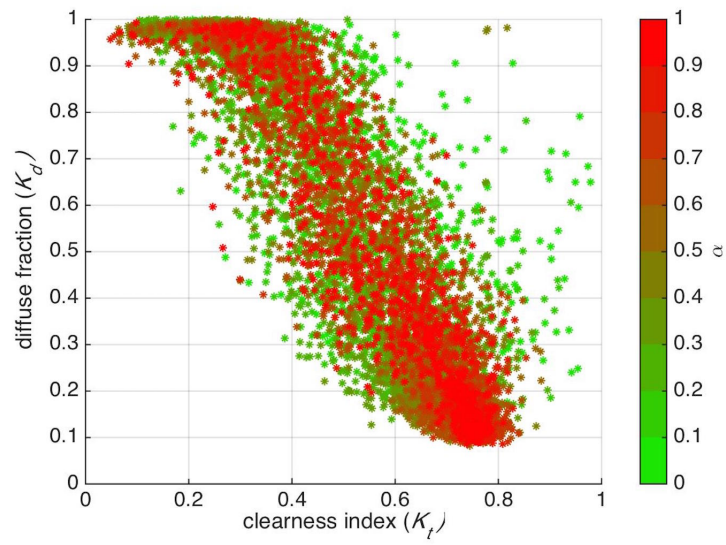


Figure 3-6. Comparison of diffuse fraction vs. clearness index for different solar altitudes

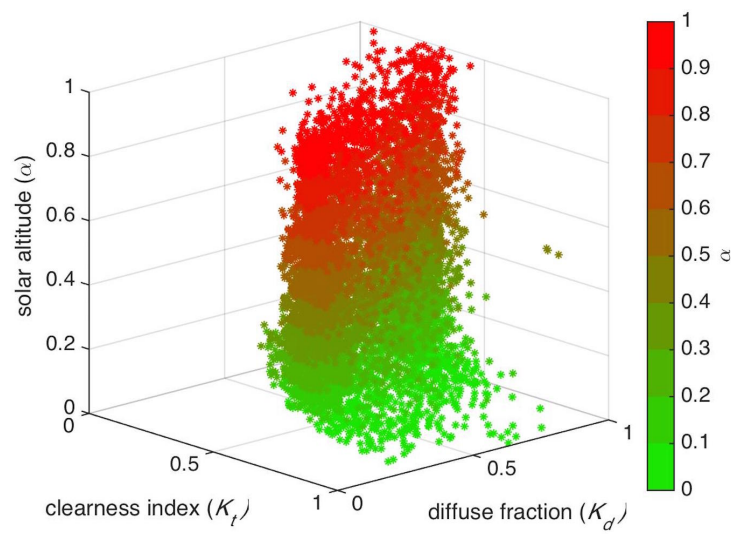


Figure 3-7. Three-dimensional comparison of diffuse fraction vs. clearness index and solar altitudes

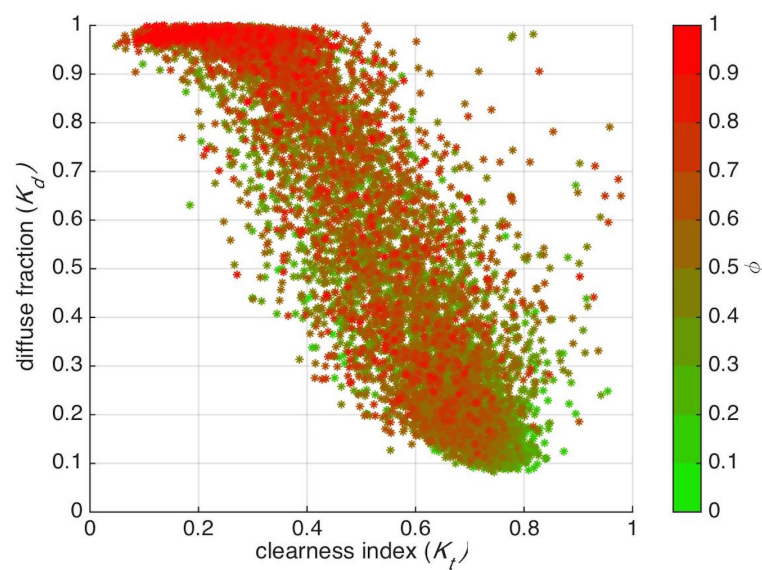


Figure 3-8. Comparison of diffuse fraction vs. clearness index for different relative humidity

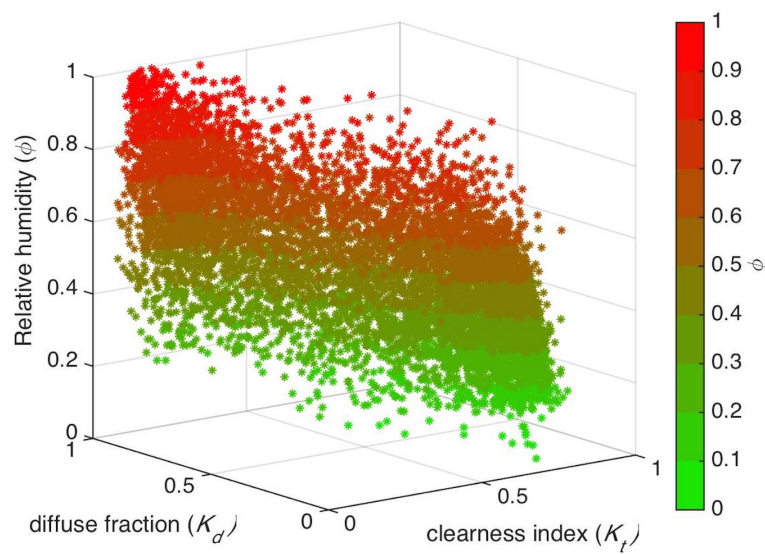


Figure 3-9. Three-dimensional comparison of diffuse fraction vs. clearness index and relative humidity

3.3.1.3 Sun state

Visibility of the sun disc influences global and diffuse values. We call this variable “*sun state*” and in order to classify it we assign a binary number system: in case of obstructed sun, we assign *sun state* to 0 and in case of visible sun 1. Figure 3-10 illustrates effect of *sun state* classifier in $k_d - k_t$ diagram; blue dots represent instances that sun is obstructed by clouds (*sun state* = 0) and red dots represent visible sun (*sun state* = 1). This figure shows that upper band of conventional $k_d - k_t$ diagram belongs to *sun state* = 1 and lower band to *sun state* = 0.

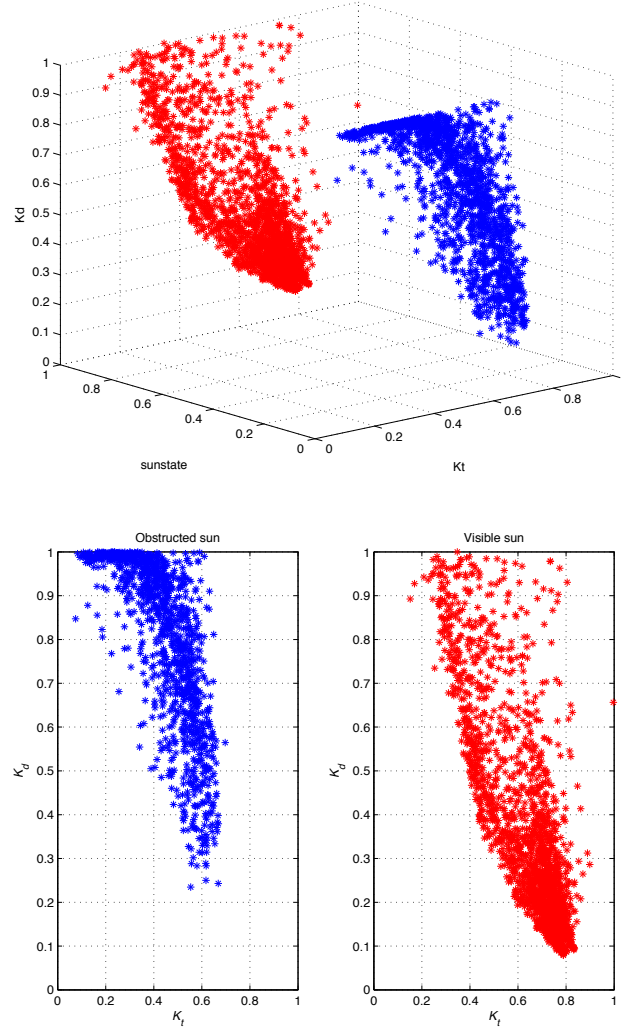


Figure 3-10. Effect of sun state (Top: 3d $k_d - k_t$ plot, Bottom: 2d $k_d - k_t$ plot)

3.3.2 Model Description

The distribution of clouds significantly affects the magnitude of solar radiation reaching the building surface. A standard weather station does not give information about cloud cover and distribution. Consequently, simple diffuse fraction models must rely on standard variables such as temperature, humidity, and global horizontal irradiance. A potential relationship between such variables and the diffuse fraction may be captured via statistical analysis of the measured data. With regard to Vienna data, we noticed that the correlation between clearness index and diffuse fraction can be improved, if multiple discrete ranges of global horizontal irradiance are differentiated. Therefore, for each bin of global horizontal irradiance, linear least square regression was employed to fit the model to the data (observed values of diffuse fraction for the Vienna location in the year 2013). From 14 initial variables, six promising ones were selected. These variables are clearness index, daily clearness index (average of hourly clearness index day), solar altitude, relative humidity, temperature, and sun state. Sun state and clearness index have the highest impact on diffuse fraction. Sun state data was imported from the Pyranometer. The selected variables and their definitions are given in *Table 3-5*.

The coefficients derived from least square regression are included in *Table 3-6*. Note that the values of temperature and relative humidity had a rather limited influence on the resulting diffuse fraction results.

Table 3-5. Variables used in BPI model

Variable	Symbol	Formulation
<i>Solar altitude</i>	α	$(\frac{\alpha}{90})^{6.7}$
<i>Clearness index</i>	k_t	$(1 - k_t)^{0.8}$
<i>Daily clearness index</i>	K_t	$(1 - K_t)^{0.5}$
<i>Temperature</i>	T	$(1 - \frac{(T + 20)}{70})^{1.8}$
<i>Relative humidity</i>	ϕ	$\phi / 100$
<i>Sun state</i>	SS	SS

Table 3-6. Coefficients for the proposed BPI model as a function of the global horizontal irradiance (I_{gh}) range

I_{gh} bins	1	SS	α	k_t	K_t	T	φ
$0 < I_{gh} < 100$	0.88	-0.39	0.33	-0.004	0.044	0.071	-0.001
$100 < I_{gh} < 200$	0.796	-0.529	0.349	-0.0890	0.231	0.0180	0.0257
$200 < I_{gh} < 300$	0.487	-0.530	-0.450	0.193	0.331	0.0750	0.0350
$300 < I_{gh} < 400$	0.535	-0.574	-0.244	0.118	0.370	0.0670	0.00180
$400 < I_{gh} < 500$	0.0980	-0.470	-0.561	0.453	0.566	0.198	0.0710
$500 < I_{gh} < 600$	0.392	-0.632	-1.27	0.287	0.387	0.220	0.115
$600 < I_{gh} < 700$	0.442	-0.644	-0.755	0.162	0.496	0.0790	0.0770
$700 < I_{gh} < 800$	0.526	-0.649	0.192	-0.174	0.451	0.0490	0.2076
$800 < I_{gh} < 900$	0.329	-0.742	-0.0110	0.502	0.610	0.136	0.0794
$900 < I_{gh} < 1000$	2.97	-2.325	-0.484	-1.365	-0.199	-0.562	0.407

3.4 Results and Discussions

2013 hourly data of 8 locations (7 in USA and 1 BPI, Vienna, Austria) were used to predict I_{dh} using above described diffuse fraction models. The predicted values are compared applying different indicators in order to evaluate the performance of the models, namely, Mean Bias Error (%), Root Mean Square Error (%), Mean Absolute Error (%), and Relative Error (%). A brief description of each indicator is given below:

1. Mean Bias Error (MBE):

$$MBE = [\sum_{i=1}^n (S_i - M_i) / M_i] / n \times 100 \quad (55)$$

2. Root Mean Square Error (RMSE):

$$RMSE = \sqrt{\{\sum_{i=1}^n [(S_i - M_i) / M_i]^2\} / n} \times 100 \quad (56)$$

3. Relative Error (RE):

$$RE_i = (S_i - M_i) / M_i \times 100 \quad (57)$$

4. Mean Absolute Error (MAE):

$$MAE = [\sum_{i=1}^n |(S_i - M_i)/M_i|] / n \times 100 \quad (58)$$

Table 3-7 to *Table 3-10* entail the comparison results of measured and calculated I_{dh} values (diffuse horizontal irradiance) in terms of typical statistics, namely Root Mean Square Error (*RMSE*) (*Table 3-7*), Mean Bias Error (*MBE*) (*Table 3-8*), Mean Absolute Error (*MAE*) (*Table 3-9*), and percentage of results with Relative Errors (*RE*) less than 20% (*Table 3-10*). In order to obtain an overview of the relative predictive performance of the models, we followed the following procedure. For each of the above four statistics and each of the locations, the models ranked numerically from 1 (best performing model) to 8 (worst performing model). The respective scores were then summed for each model and each location and displayed in *Table 3-11*. Data included in this tables suggests that the *Skartveit and Olseth*, *BRL*, and *Maxwell* models better comparatively. However, none of the models can be argued to perform satisfactorily. Assume, for instance, that we target a model performance yielding a threshold of at least 80% of the predictions with a *RE* value of less than 20%. As *Table 3-10* suggests, none of the models can come even close to meeting such a requirement.

BPI model is empirically developed using collected measured data in Vienna from year 2011. In order to validate the *BPI* model, we compared it using its driven coefficient from year 2011 with other 7 models As the *BPI* model is empirically developed based on historical data, this model performs better only for data from Vienna site and has an average

performance among other models for data from 7 locations in USA (see Figure 3-11 and Figure 3-12).

Table 3-7. Root Mean Square Error (RMSE in %) of predicted I_{dh} to SPN1 data

Model	bon	dra	fpk	gwn	psu	sxf	tbl	vie
<i>Erbs et al.</i>	37.82	66.58	50.07	39.19	38.19	48.82	51.04	46.8
<i>Maxwell</i>	30.31	48.82	40.31	29.16	33.11	42.16	44.27	37.91
<i>Reindl</i>	40.91	82.06	49.83	46.13	44.36	50.78	66.23	44.19
<i>Perez et al.</i>	32.54	53.98	42.34	35.96	33.83	40.63	55.87	40.34
<i>Skartveit</i>	27.60	49.61	38.99	29.17	30.79	38.09	51.39	40.92
<i>Boland</i>	38.10	59.97	51.9	38.42	37.6	49.94	49.02	48.33
<i>BRL</i>	29.38	37.53	39.92	28.28	29.25	39.43	40.7	36.08
<i>BPI</i>	35.32	45.86	38.67	34.45	34.70	42.92	44.68	30.98

Table 3-8. Mean Bias Error (MBE in %) of predicted I_{dh} to SPN1 data

model	bon	dra	fpk	gwn	psu	sxf	tbl	vie
<i>Erbs et al.</i>	7.38	45.28	16.09	15.68	12.41	17.54	18.14	19.21
<i>Maxwell</i>	-8.07	18.97	-3.09	3.66	1.12	1.68	5.79	9.55
<i>Reindl</i>	11.19	40.64	18.53	19.08	16.02	22.75	24.78	17.95
<i>Perez et al.</i>	-0.84	31.19	7.24	9.52	7.15	7.80	21.28	15.85
<i>Skartveit</i>	-5.55	19.10	4.38	4.82	4.81	4.00	13.97	14.76
<i>Boland</i>	6.60	34.48	15.78	13.95	11.60	18.21	10.29	19.15
<i>BRL</i>	-11.44	-0.25	-4.23	-3.01	-2.76	-1.26	-10.64	8.68
<i>BPI</i>	-2.09	-8.37	2.15	-6.28	-0.23	4.64	-5.25	6.69

Table 3-9. Mean Absolute Error (MAE in %) of predicted I_{dh} to SPN1 data

model	bon	dra	fpk	gwn	psu	sxf	tbl	vie
<i>Erbs et al.</i>	33.03	54.68	38.29	28.63	27.54	35.12	38.95	27.34
<i>Maxwell</i>	27.38	34.55	30.84	21.02	24.17	29.16	32.52	23.39
<i>Reindl</i>	33.54	57.10	36.50	30.1	29.03	35.83	44.41	26.09
<i>Perez et al.</i>	27.89	41.19	31.67	23.75	24.05	27.85	40.55	24.6
<i>Skartveit</i>	25.54	33.26	29.01	20.62	22.00	25.41	35.92	23.87
<i>Boland</i>	33.07	46.37	39.73	27.63	27.00	35.94	37.05	28.16
<i>BRL</i>	28.16	27.94	31.96	21.48	22.37	28.19	31.55	21.64
<i>BPI</i>	25.7	33.69	30.23	25.35	25.90	29.62	33.17	19.96

Table 3-10. Percentage of predicted I_{dh} data having RE less than 20% with SPN1 data

model	bon	dra	fpk	gwn	psu	sxf	tbl	vie
<i>Erbs et al.</i>	47	21	36	49	52	41	35	58
<i>Maxwell</i>	55	39	42	60	55	48	39	60
<i>Reindl</i>	50	30	39	53	52	41	38	62
<i>Perez et al.</i>	56	30	42	57	56	49	36	58
<i>Skartveit</i>	59	44	45	60	59	52	41	60
<i>Boland</i>	48	29	36	51	52	40	38	58
<i>BRL</i>	50	45	40	56	56	46	40	65
<i>BPI</i>	50	40	40	53	51	45	40	78

Table 3-11. Ranking of the performance of different models for different locations using all 4 statistical measures

model	bon	dra	fpk	gwn	psu	sxf	tbl	vie	Sum
<i>Erbs et al.</i>	25	30	29	29	28	25	25	30	221
<i>Maxwell</i>	15 ³	14	11 ³	8 ¹	13 ³	13	10 ²	13 ³	97
<i>Reindl</i>	27	29	26	30	29	29	29	23	222
<i>Perez et</i>	11 ²	20	17	17 ³	14	12 ³	28	20	139
<i>Skartveit</i>	6 ¹	12 ³	8 ¹	8 ¹	8 ¹	6 ¹	16 ³	16	80
<i>Boland</i>	25	25	29	25	24	30	18	30	206
<i>BRL</i>	20	4 ¹	15	9 ²	9 ²	10 ²	8 ¹	8 ²	83
<i>BPI</i>	15 ³	10 ²	9 ²	18	19	19	10 ²	4 ¹	104

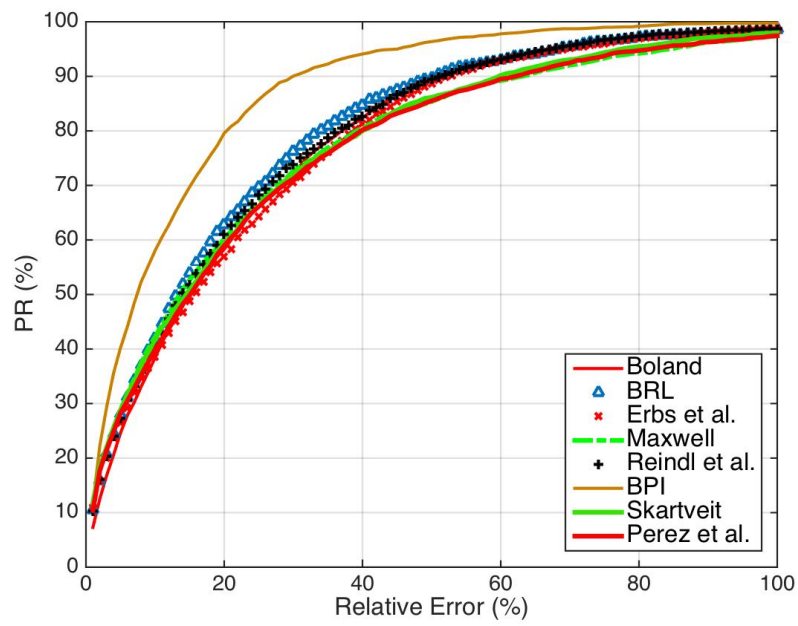


Figure 3-11. Cumulative Distribution Function of Relative Errors for percentage of results (Testing dataset – year 2011)

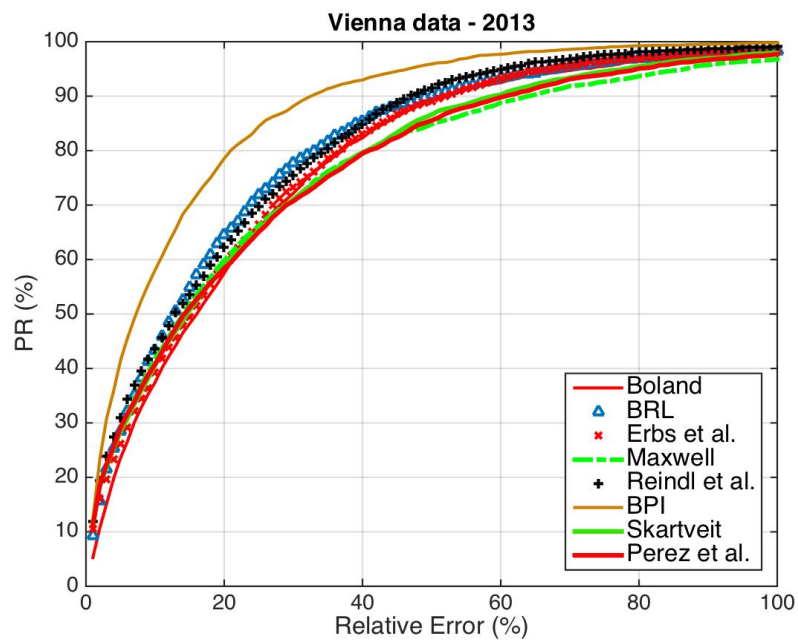


Figure 3-12. Cumulative Distribution Function of Relative Errors for percentage of results (Validation dataset)

3.5 **Conclusion**

8 models' performances including the *BPI* model were compared for 8 locations using different statistical measures. Results showed indigent performance of all models to predict diffuse fraction for overall locations. For Vienna, the *BPI* model performed significantly better than other 7 models. However, for other 7 locations, the *Skartveit and Olseth* model performed better than the other 7 models in most stations and for most statistical measures, followed by the *BRL* model.

Complexity in weather and climate models including aerosols and their specifications such as random distribution of clouds, distance, thickness, and color of clouds, significantly influence magnitude and distribution of diffuse component of solar radiation. This intricacy cannot be modeled using standard weather station data such as temperature, humidity and global horizontal irradiance. Although, in near future by increasing the number of satellites, their record intervals and image resolution, exploring this information could model this complexity and lead to high performance diffuse fraction model development which can be used for locations in which satellite data is available.

Next two chapters discuss generation of sky models and their implications in indoor illuminance, which as input they require global and diffuse irradiance. Therefore, to verify reliability of top performing diffuse fraction models in estimating indoor illuminance, we used the *Skartveit and Olseth* model in generating diffuse irradiance as input data of two sky models.

Chapter 4 Sky radiance/luminance distribution model

4.1 *Introduction*

Deployment of performance simulation in building design and control phase can enhance the buildings' performance in their life cycle. This requires reliable input data for simulation models. Specifically, obtaining high-resolution solar radiation data can represent a challenge. Several authors have proposed models to predict the distribution of radiance and luminance over the sky hemisphere based on global and diffuse horizontal irradiance and illuminance data (*Nakamura et al., 1985, Matsuura and Iwata, 1990, Perez et al., 1993, Brunger and Hooper, 1993, Igawa et al., 1997, Kittler et al., 1997, Kittler et al., 1998, Tregenza, 1999, CIE, 1955, 1973, 1994, 1996, and Mahdavi & Dervishi, 2013*). Among these models, *CIE (1955, 1973)* and *Perez et al. (1993)* are widely used and are embedded in the *RADIANCE* simulation application (*Ward, 1994*). This chapter investigates general performance of these sky models within two studies. One study reports on the comparison of predicted vertical illuminance values (obtained using the above mentioned sky models) with corresponding measurements for the location Vienna, Austria. Second study compares simulated vertical irradiance values generated by *RADIANCE* software using two embedded sky models *GENDALYIT* (*Ward, 2014*), *GENSKY* (*Ward, 2014*) with corresponding measurements. *GENDALYIT* is based on *Perez et al.* sky model (*Perez et al., 1993*) and *GENSKY* based on four literatures, mainly *CIE (CIE, 1955, 1973, 1994, and 1996)*.

4.2 Prediction of vertical illuminance

Two mentioned sky models (*Perez et al.* and *CIE*) are described below and implemented in *MATLAB* (*MATLAB, 2010*) to calculate vertical illuminances on four cardinal surfaces and to calculate luminance on 145 *Tregenza* (1999) patches over sky hemisphere.

4.2.1 Perez et al.

Combining physical principles and a large set of experimental data, *Perez et al. (1993)* introduced a model to predict the relative sky luminance for discrete sky patches (L_r). The model contains two variables and five coefficients (Eq. 59). The variables are the zenith angle of the considered sky point and the angular distance between the sky point and the sun disk. The coefficients resulted from least square fitting of the data and can be obtained from a table.

$$L_r = \left[1 + ae^{\frac{b}{\cos(Z)}} \right] \left[1 + ce^{d\xi} + e\cos^2(\xi) \right] \quad (59)$$

Here, L_r is the relative luminance, which is the ratio of sky luminance over zenith luminance (L_z), ξ is the angular distance between the sky element and the sun disk, Z is the zenith angle of considered sky element and a , b , c , d , and e are insolation conditions and are function of sky brightness (Δ) and sky clearness (ϵ) and Zenith angle. In order to choose the five coefficients of each instance from the table, two variables, namely, sky brightness (Δ) and sky clearness (ϵ) must be calculated (Eq. 60, 61).

$$\epsilon = \frac{\left[\frac{I_{dh} + I_{dn}}{I_{dh}} + 1.041Z_s^3 \right]}{1 + 1.041Z_s^3} \quad (60)$$

$$\Delta = \frac{m_{air}I_{h.dif}}{I_{ext}} \quad (61)$$

Here, I_{dh} is the horizontal diffuse irradiance, I_{dn} the normal direct irradiance, Z_s the solar zenith angle, m_{air} the optical air mass, and I_{ext} the

extraterrestrial normal irradiance. I_{dn} is generated based on a diffuse fraction model (Perez et al. 1992). Zenith luminance (L_z) was calculated according to Perez et al. (1990).

A short description of the effect of each coefficient is as follows:

- **Coefficient a:** positive a denotes that relative luminance is darkening from zenith to the horizon. While negative a denotes brightening of sky from the zenith to the horizon
- **Coefficient b:** b modulates luminance gradient near the horizon. Smaller b represents narrower bright band near horizon
- **Coefficient c:** magnitude of c represents relative intensity of circumsolar region. Higher the c, higher the magnitude of relative luminance of circumsolar region
- **Coefficient d:** represents width of circumsolar region. Higher the absolute of d, sharper the circumsolar region (less width)
- **Coefficient e:** shows the backscattered effect of light from the ground on counterpart to the sun.

4.2.2 CIE

International Commission on Illumination (CIE, 2003) distinguishes 15 sky types. For each sky type, CIE offers a specific formula to calculate the Luminance values. To deploy this version of the CIE model, for each instance, we calculated 15 types of sky luminance and chose the best fitting sky type based on RMSE with sky scanner data. The ratio of the patch luminance L_i to zenith luminance L_z is expressed as follows:

$$\frac{L_i}{L_z} = \frac{f(X)\phi(Z)}{f(Z_s)\phi(0^\circ)} \quad (62)$$

X is calculated using the following equation:

$$\mathcal{X} = \arccos(\cos(Z_s) \cos(Z) + \sin(Z_s) \sin(Z) \cos(A_z)) \quad (63)$$

Here, A_z is azimuth angle difference between sun disk and patch element. In this case, zenith luminance (L_z) was derived based on *Darula and Kittler (2002)*.

None of the models estimates the direct luminance. In fact, they calculate the diffuse luminance distribution. In order to estimate the direct luminance value for each instance, direct normal illuminance measured data was converted to direct luminance:

$$L_{sun} = \frac{E_n}{\pi(\sin^2(\eta/2))} \quad (64)$$

Here, L_{sun} is direct luminance, E_n is direct normal illuminance, and η is angular diameter of the sun (assumed 0.53°).

After adding the direct luminance, all patch values were normalized to the horizontal global illuminance:

$$L_i^{norm} = \frac{E_{gh}}{\sum_{i=1}^{145} [\Omega_i \cos(Z_i)]} L_i \quad (65)$$

Here, L_i^{norm} is the normalized patch luminance and $E_{h,g}$ is the horizontal global illuminance.

Note that it is not possible to differentiate between the 15 *CIE* skies solely on the basis of weather station data. Therefore, for each instance we selected the sky category that yielded the closest results to the measured patch luminance data.

We implemented both models in *MATLAB* (*MATLAB, 2010*). For comparison purposes, vertical illuminance values were derived from patch luminance values of the two sky models:

$$\psi_i = \Omega_i \cos(\varphi_i) \cos(\lambda_i - \beta) \quad (66)$$

$$E_{ver,\beta} = \sum_{i=1}^{145} L_i \vartheta_i \quad (67)$$

Here, ϑ_i is i^{th} patch vertical transformation function, Ω_i is i^{th} patch solid angle, λ_i is the i^{th} patch azimuth angle, β is the vertical plane normal angle, L_i is i^{th} patch luminance values and $E_{ver,\beta}$ is vertical illuminance value in the direction of β .

Model-based predictions of vertical illuminance values were compared with corresponding measured vertical illuminance for the aforementioned 8 months' period. Moreover, to evaluate the accuracy of the sky luminance distribution predicted by the two models, we also utilized the sky scanner luminance measurements for 145 discrete *Tregenza* sky patches (*Tregenza, 1999*). Thus, a patch-to-patch comparison of calculated and measured luminance values could be facilitated for data obtained for the same period.

4.3 **Prediction of vertical irradiance using RADIANCE**

In order to calculate radiance on 145 patches of *Tregenza* over hemisphere and irradiance values of four cardinal vertical surfaces, we deployed *RADIANCE* rendering program. Both embedded sky models (*GENDAYLIT* and *GENSKY*, see *Figure 4-1* for an overview of sky generation) and own developed sky model for sky scanner data are deployed. A brief description of each model is provided in the following sections.

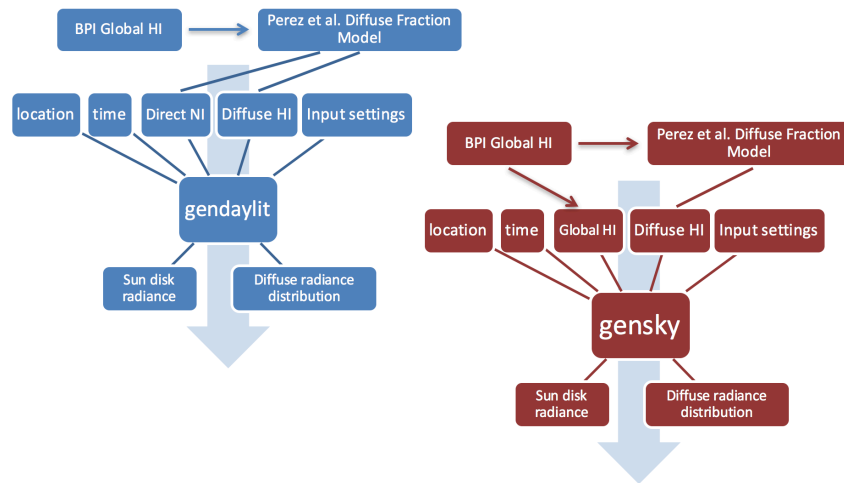


Figure 4-1. Flowchart of sky generation in RADIANCE (GENDAYLIT on the left – GENSKY on the right)

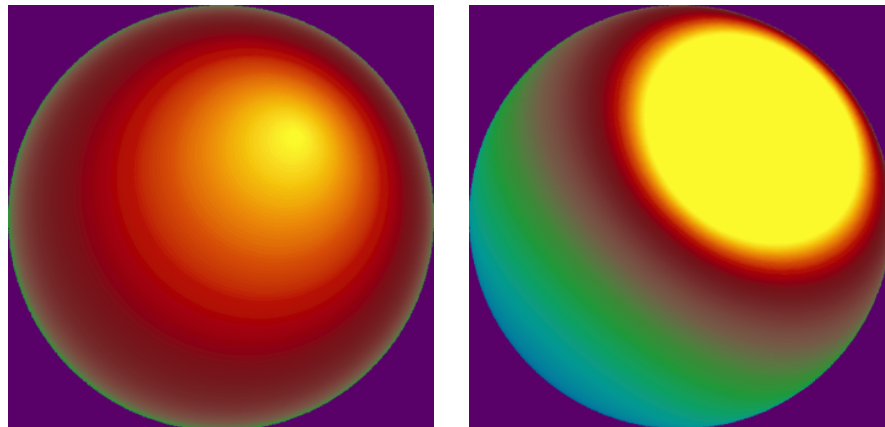


Figure 4-2. Sky fisheye high dynamic range images for GENDAYLIT (on the left) and GENSKY (on the right) – 10:45 a.m. local time, 10 July 2014, Vienna

4.3.1 GENDAYLIT

GENDAYLIT generates a *RADIANCE* scene description based on the Perez sky distribution model (Perez et al., 1993) for the given atmospheric inputs (direct and diffuse component of the solar irradiance/illuminance), date, and local standard time. The default output is the radiance of the sun (direct) and the sky distribution (diffuse) integrated over the visible spectrum. In cases, where illuminance data are given as input, luminous efficacy factor is used to convert illuminance values to irradiance. In order to assure having the correct input for each instance, sun zenith and

altitude are given instead of local time data. An important input parameter to consider using *GENDAYLIT* model is $-O$ parameter, which defines the output to be in visible range or full spectrum of radiance or luminance (0, 1, and 2 respectively).

4.3.2 GENSKY

GENSKY generates a *RADIANCE* scene description based on *CIE* sky distribution model. Similar to *GENDAYLIT*, sun azimuth and altitude are given for each instance as input data instead of local time. With regard to *GENSKY*, it is important to consider that four types of sky conditions are distinguished, namely: sunny, cloudy, uniform, and intermediate. Each sky category must be defined by the user as input for *RADIANCE GENSKY* program. To deploy the implemented *GENSKY* model in *RADIANCE*, we made use of the option to assign specific values to the tool's pertinent parameter in accordance with the relevant sky category. Toward this end, we considered the following categories: clear (sunny in terms of *GENSKY*), overcast (cloudy in terms of *GENSKY*), and intermediate (intermediate in terms of *GENSKY*). In order to map our weather station data into these four categories, we used a simple assignment rule based on the magnitude of the direct normal and diffuse horizontal irradiance components (see *Table 4-1*). The output of both *GENDAYLIT* and *GENSKY* sky models in *RADIANCE* consists of sky patch radiance values in $W.sr^{-1}.m^{-2}$ (see *Figure 4-2* for example of sky generation using both skies).

Table 4-1. *GENSKY* categorization in the present study

$I_{n,d}$	K_t	K_d	Category
$\geq 200 W.m^{-2}$	-	$<1/3$	Clear sky
$< 200 W.m^{-2}$	$<1/3$	$\geq 1/3$	Overcast sky
else			Intermediate sky

4.3.3 Sky scanner

Sky scanner MS321-LR (*EKO Instruments, 2014*) measures distribution of radiance and luminance of 145 sky patches using its 11° aperture sensors.

It takes around 4.5 minutes to track 145 patches having two axis control. Luminance values are measured per kcd/m^2 and radiance values per $W/m^2/sr$. Radiance and luminance sensors of sky scanner are not able to measure direct irradiance and luminance values respectively. Maximum measuring capacity of sensors are $300 W/m^2/sr$ for radiance and $50 kcd/m^2$ for luminance. Therefore, sky scanner is measuring diffuse distribution of radiance and luminance over sky hemisphere (see *Figure 4-3*).

In order to generate sky scanner sky within *RADIANCE program* several steps are involved including:

- Normalization of 145 patches radiance values using total diffuse horizontal irradiance
- Generation of patches with creating *skybright.cal* function for sky scanner (see Appendix E for source code)
- Creation of a text “rad file” to define sky glow to include generated *skybright.cal* for sky scanner
- Defining angular diameter of the sun equals to 0.533° as a light source giving its x, y, and z unit orientation

It should be noted that sun light intensity is defined from calculating direct radiance from direct irradiance deploying Equation 64. Direct irradiance is calculated from the difference between global horizontal irradiance and diffuse horizontal irradiance.

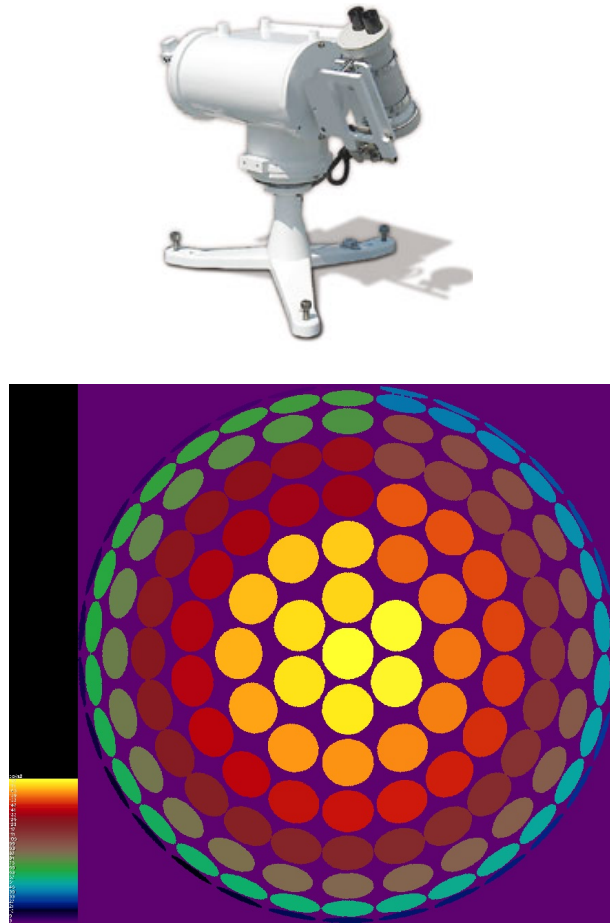


Figure 4-3. Top: Sky scanner MS-321LR, Bottom: Fisheye image of sky generated via sky scanner

4.4 Results and Discussions

4.4.1 Vertical illuminance comparison

Table 4-2 provides an overview of the main results. Thereby, measured and predicted vertical illuminance and patch luminance values were compared. Note that the *RMSE* and *MBE* values for vertical illuminance values are given in units of klx , whereas those for patch luminance values are given in $kcd.m^{-2}$. The distributions of the relative errors of the illuminance predictions for the four surface orientations are depicted in Figure 4-4. Figure 4-5 shows, for both sky models, the cumulative distribution function of percentage of results with Relative Errors *RE* (%) of calculated vertical illuminance values. Likewise, Figure 4-6 illustrates

relative errors in calculation of patch luminance values in terms of cumulative distribution functions.

To evaluate the performance of data we can look at the percentages of results with relative errors less than 20% (*Figure 4-5*). This yields for the best performing model (*CIE*) 82% (North), 80% (East), 74% (South), and 75% (West) and for *Perez et al.* 72% (North), 77% (East), 71% (South), and 70% (West). Patch comparison similarly suggests a rather modest performance level (*CIE*: 51%; *Perez et al.*: 46%). The slightly better performance of the *CIE* model may be due to the fact that in this case, for each instance we used the best possible sky category, as mentioned in introduction.

Table 4-2. Statistical evaluation of CIE and Perez models based on vertical illuminance predictions

Orient.	Model	R²	RMSE	CV_{RMSE}	MBE
<i>Illuminance North</i>	CIE	0.90	2.05	18.41	-0.05
	Perez	0.87	2.34	21.00	-0.13
<i>Illuminance East</i>	CIE	0.97	6.29	23.66	-1.56
	Perez	0.97	6.55	24.64	-0.60
<i>Illuminance South</i>	CIE	0.95	8.77	25.52	-3.56
	Perez	0.94	8.94	26.00	-1.76
<i>Illuminance West</i>	CIE	0.96	7.20	26.40	-1.11
	Perez	0.95	7.64	28.03	0.08
<i>Patch luminance</i>	CIE	0.88	3.54	43.13	-0.05
	Perez	0.82	4.32	52.65	0.32

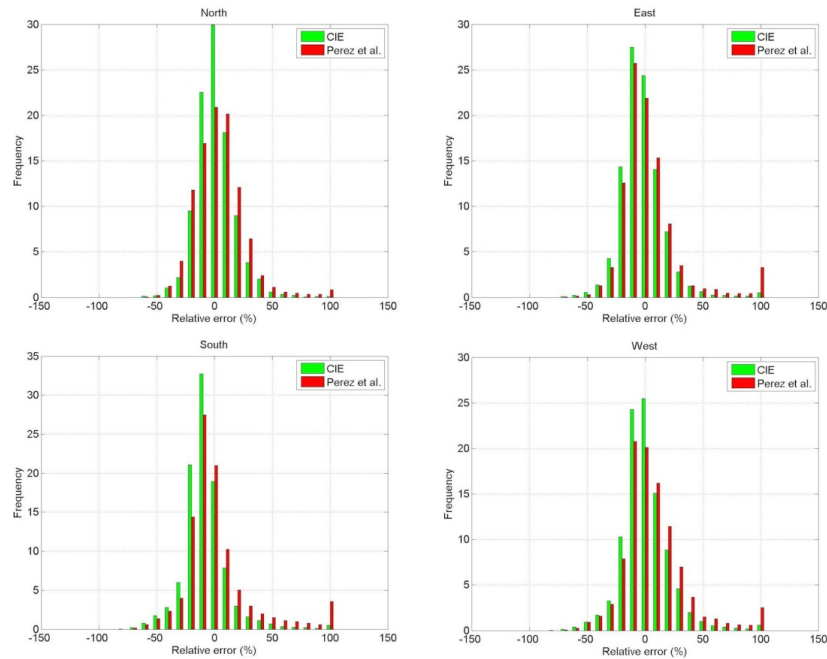


Figure 4-4. Comparison of the CIE and Perez sky models in terms of relative error distributions of predicted vertical illuminance values (Relative errors over 100% are merged into the 100% error bin)

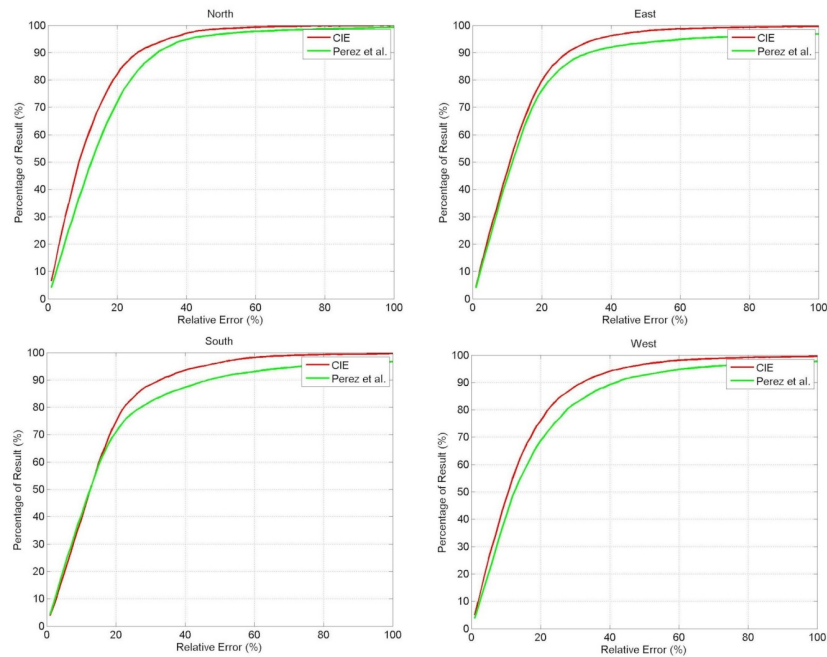


Figure 4-5. Comparison of CIE and Perez et al. sky models' relative errors (%) for vertical surfaces facing the four cardinal directions in terms of cumulative distribution functions

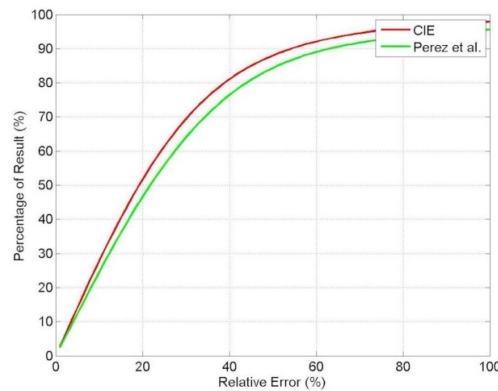


Figure 4-6. Cumulative distribution functions of the relative errors (%) of the two models' patch luminance predictions with respect to sky scanner data

4.4.2 Vertical irradiance comparison

Table 4-3 provides a comparison of the measured and predicted vertical irradiance and patch radiance values. Note that *RMSE* and *MBE* values for vertical irradiance are given in units of $W.m^{-2}$ whereas, those for radiance are given in $W.m^{-2}.sr^{-1}$. The distributions of the relative errors of the irradiance predictions for the four surface orientations are depicted in Figure 4-7. Figure 4-8 shows a comparison of measured patch radiances with the respective predictions of the two sky models. Figure 4-6 shows the cumulative distribution function of the relative errors of the calculated vertical irradiance for both sky models. Figure 4-9 shows the cumulative distribution function of the relative errors of the patch radiance values for both models.

Table 4-3. Statistical evaluation of vertical irradiance (incident on surfaces facing four cardinal directions) and sky patch radiance as predicted via GENDAYLIT and GENSKY

Orient.	Model	R2	RMSE	CV_RMSE	MBE
Irradiance North	GENDAYLIT	0.74	27.0	27.4	-1.49
	GENSKY	0.69	28.8	29.0	-3.00
Irradiance East	GENDAYLIT	0.97	64.8	22.5	8.11
	GENSKY	0.95	73.5	25.4	13.91
Irradiance South	GENDAYLIT	0.97	44.4	17.0	-0.69
	GENSKY	0.96	46.6	17.8	-2.97
Irradiance West	GENDAYLIT	0.96	64.9	22.8	2.53
	GENSKY	0.96	68.6	23.5	7.57
Patch radiance	GENDAYLIT	0.86	37.6	49.4	-1.13
	GENSKY	0.85	38.5	50.5	0.89

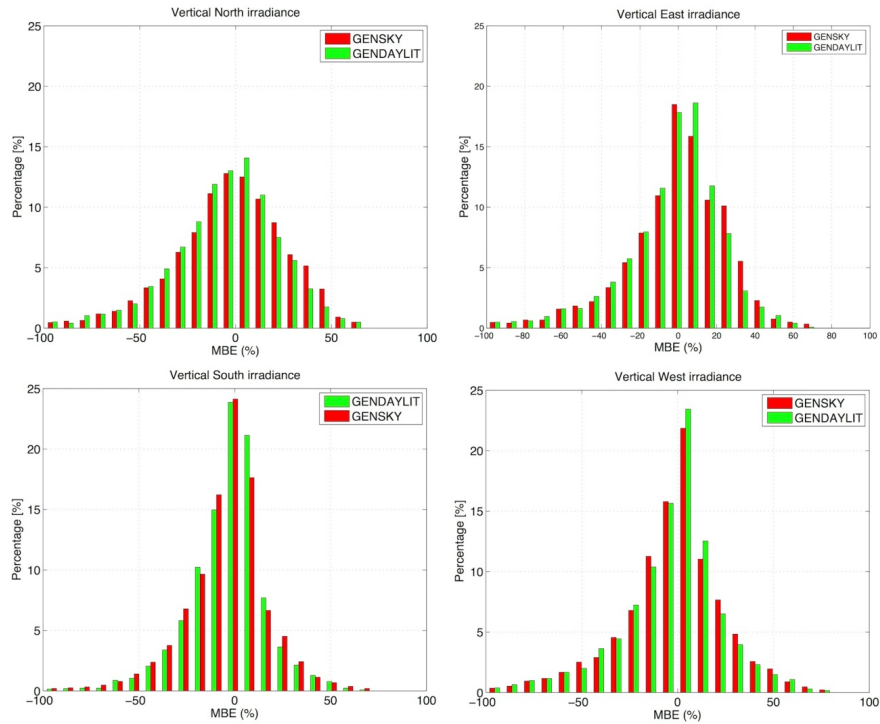


Figure 4-7. Comparison of the GENSKY and GENDAYLIT sky models in terms of distributions of the relative errors of predicted vertical irradiance values

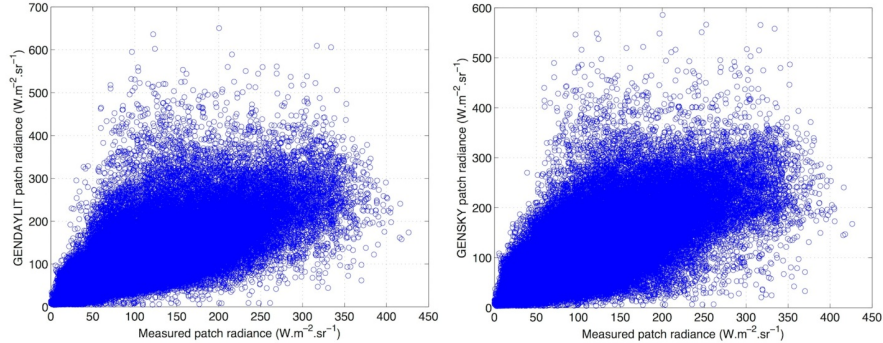


Figure 4-8. Comparison of measured and computed patch radiance values (Left: GENDAYLIT; Right: GENSKY)

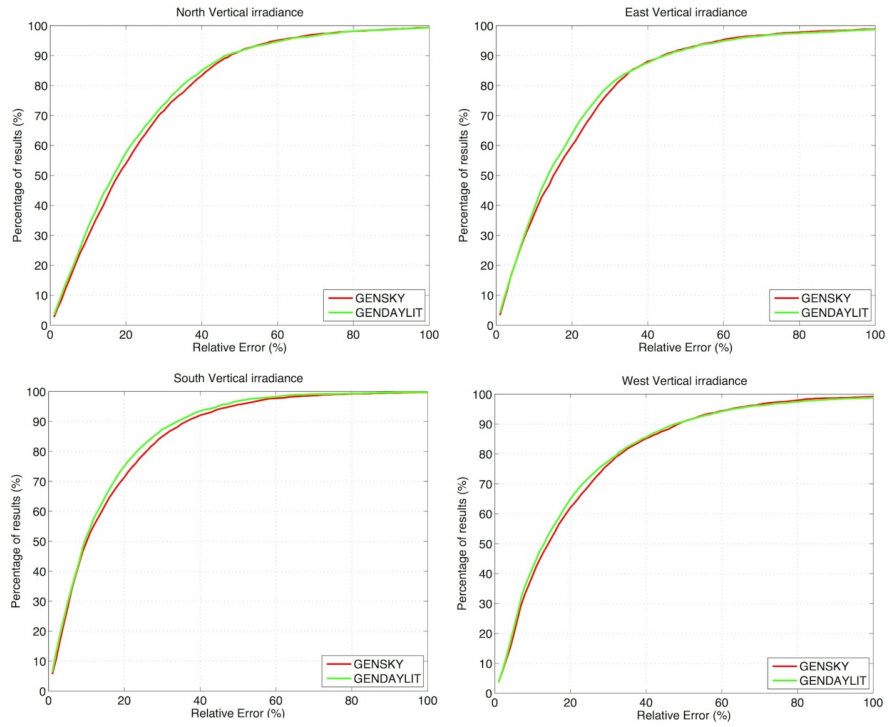


Figure 4-9. Comparison of GENSKY and GENDAYLIT sky models' relative errors (%) for vertical surfaces facing the four cardinal directions in terms of cumulative distribution functions

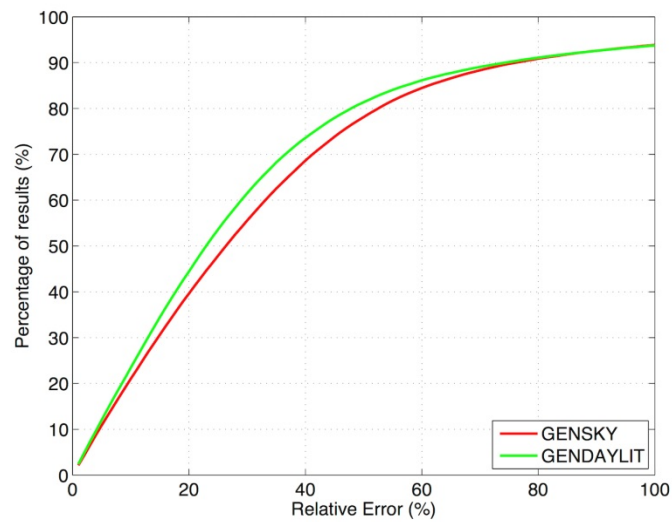


Figure 4-10. Comparison of patch radiance values of two models with sky scanner data using cumulative distribution of percentage of the results for different relative errors (%)

4.5 *Conclusions*

Illuminance on four vertical surfaces as well as luminance values of 145 sky patches were estimated using two sky models (*Perez et al., CIE*). The comparison of the computational results with corresponding high-resolution measurements conducted in Vienna points to a rather limited predictive potential. Hence, these sky models would have to be substantially improved – or at least calibrated – to reproduce the measured data with sufficient accuracy. Future research will pursue a collaborative multi-location model comparison using larger data sets and more detailed statistical analyses.

Irradiance on four vertical surfaces as well as radiance values of 145 sky patches were estimated using two sky models (*GENDAYLIT, GENSKY*) embedded in the *RADIANCE rendering program*. While the *GENDAYLIT* appears to perform slightly better, the comparison of the computational results with corresponding measurements conducted in Vienna points to a rather limited predictive potential of both models studied. In the case of a patch-to-patch comparison of measured and computed radiance values, large errors may be expected, given the chaotic nature of cloud distribution and corresponding radiance variance across the sky dome. In our study, only about 42% of patch radiance predictions display a relative error less than 20%. But the errors are quite large even in case of vertical irradiance calculations. For instance, the slightly better performing *GENDAYLIT* model yields the following percentages of results with relative errors less than 20%: 60% (North), 65% (East), 73% (South), and 64% (West). Hence these sky models would have to be improved – or calibrated – to more reliably reproduce the measured data.

Chapter 5 **Case Study: The Reliability of Indoor Illuminance Prediction**

5.1 *Introduction*

Recent advancements in ITC enables us to process huge amount of data in real-time resolution. Building predictive control systems can benefit from ITC. There are different aspects in building predictive control. One of these aspects is indoor lighting and daylight. In addition to building predictive control, indoor daylighting design plays an important role in design phase of a building. Different factors are limiting general accuracy of daylighting simulation, e.g. boundary conditions, modelling enclosure, simulation engine (e.g. radiosity, raytracing). In this case, boundary conditions are sky luminance distribution data and outdoor obstructions. The latter chapter we evaluated performance of sky models in predicting sky luminance/radiance distribution. Current chapter which is partly a master thesis, evaluates the performance of diffuse fractions and sky models in estimating indoor illuminances in a test room located at rooftop of *TU Wien*.

5.2 *Methodology*

This study has two main part, *i)* measuring indoor horizontal illuminances of 6 points on work-plane and 2 vertical points of the test room, *ii)* simulating indoor horizontal illuminances of same points. In order to simulate indoor illuminances, we deployed *RADIANCE rendering program*. Description of the test room, measurement, and simulation parts are explained in details.

5.2.1 Test Room

The test room is located on the rooftop of the main building of *TU Wien* (48.1986° N, 16.3694° E, see *Figure 5-1*). The room has about 8 meters' length, 2.3 meters' width, and 2.6 meters' height and has two windows which are facing the south-west (each has 1.16 m height and 0.9 m width) and are double glazed. As the room is located on the rooftop there aren't any significant obstruction to block the direct sun shine from sunrise to sunset through the whole year long. The room is painted in white and had only three tables and a TV hanging on the west wall during the measurements were taken.



Figure 5-1. Location of the test room, TU Wien, Vienna, Austria

5.2.2 Measurements

Three set of measurements were taken in this study, *i)* illuminance measurements, *ii)* indoor surfaces reflectance, and *iii)* transmissivity of the glazing. To measure illuminance, lux meters were deployed. 8 sensors were installed, two vertically oriented at the height of 1 meters on the walls and 6 horizontally on the tables at the height of 74 cm from the floor (see *Figure 5-3*). For measuring the approximate reflectance of the opaque

interior surfaces, illuminance (lux) and luminance (cd/m²) at the specific point of each surface were measured deploying *Minolta* luminance meter (*LS-100*) and illuminance meter (*T10-A series*) (See Figure 5-2). A list of all reflectance of surfaces is presented in *Table 5-1*. The transmissivity of windows was measured using two illuminance meter, one installed in the outer surface of glazing and other one inside. Both sensors measured simultaneously illuminance values. The fraction of illuminance which passes through glazing is transmissivity of the glazing. After several recording of transmissivity, 0.73 were assumed as an average value for transmissivity of windows.

Measurements were taken under three different sky conditions, clear, overcast, and intermediate, the 3rd of July, the 5th of September, and the 7th of September 2015 respectively to represent almost all weather conditions. All measurements were logged in 1-minute intervals.



Figure 5-2. Minolta luminance meter (*LS-100*) (on the left) and illuminance meter (*T10-A series*) (on the right)

Table 5-1. The reflectance of the test room surfaces

Surface	R	G	B	Specularity	Roughness
Table	0.51	0.51	0.51	0.083	0.08
Wall	0.88	0.88	0.88	0.02	0.08
Floor	0.43	0.43	0.43	0.03	0.43
Radiator	0.58	0.58	0.58	0.02	0.08
Entrance door	0.81	0.81	0.81	0.02	0.08
Door (Staircase)	0.88	0.88	0.88	0.02	0.08
Ceiling	0.88	0.88	0.88	0.02	0.08
Window frame	0.85	0.85	0.85	0.08	0.02



Figure 5-3. Arrangement of illuminance meters in the test room (Photo credit: Ghazal Etminan)

5.2.3 Simulation

A 3D model of the test room was created in *Google SketchUp* program (see Figure 5-4) and then with the help of the “*su2ds*” plug-in we exported

the geometric data from *Google SketchUp* to *RADIANCE*. All sensors in the test room were included in a separate file in the model, positioned in the same points as the actual sensors in the room.

In order to simulate indoor illuminances several steps were followed:

1. Drawing the test room's geometry using *Google Sketchup*
2. Deploying *Su2ds* plug-in to convert test room's geometry from *Google Sketchup* to *RADIANCE* rad file (geometry.rad)
3. Preparing material file using surface reflectance and transmissivity of windows (material.rad)
4. Preparing sensor position and orientation file (sensor.pts)
5. Collecting weather data (Global and diffuse horizontal irradiance)
6. Generation of sky models (sky.rad)
7. Adding sky and ground source to the sky.rad file
8. Creation of octree file from geometry.rad, material.rad, and sky.rad using *oconv RADIANCE* command
9. Calculation of illuminances for sensor points using *rtrace RADIANCE* command

A schema of all these steps are demonstrated in *Figure 5-5*. The simulation interval is chosen to be 15-minutes. Therefore, a *MATLAB* code is written to loop through item 5 to 9 from above list and calculate illuminance values for each instance.

As we discussed in chapter 3, in order to evaluate the impact of diffuse fraction models in prediction of indoor illuminance, we have created both sky models using Skartveit and Olseth model to predict diffuse horizontal irradiance as sky models' input. Therefore in total 5 scenarios of simulation were generated (see *Figure 5-6*).

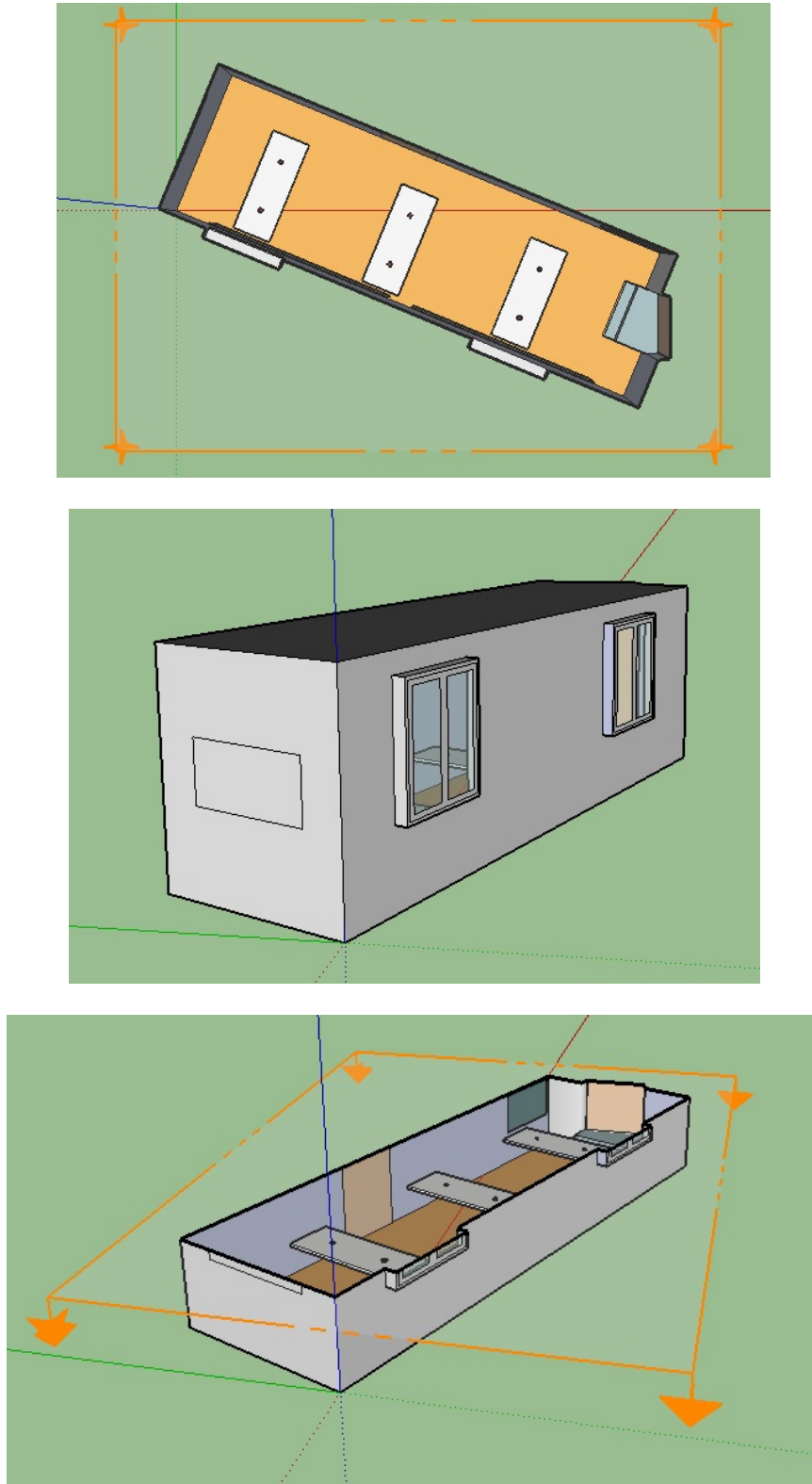


Figure 5-4. Different view from test room geometry in Sketchup (from top to bottom: Top view, North-East view, North-East view section)

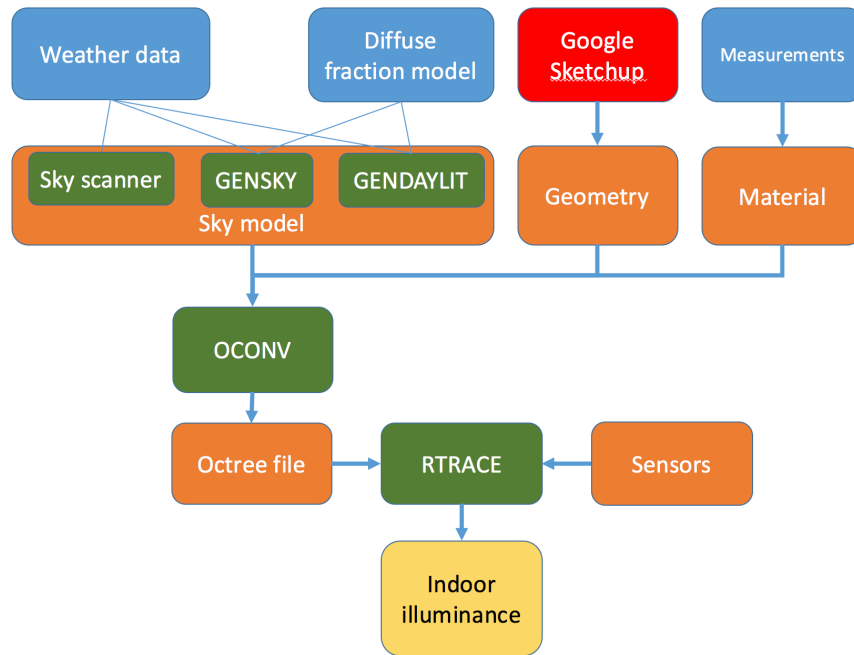


Figure 5-5. An overview of simulation steps to calculate indoor illuminances

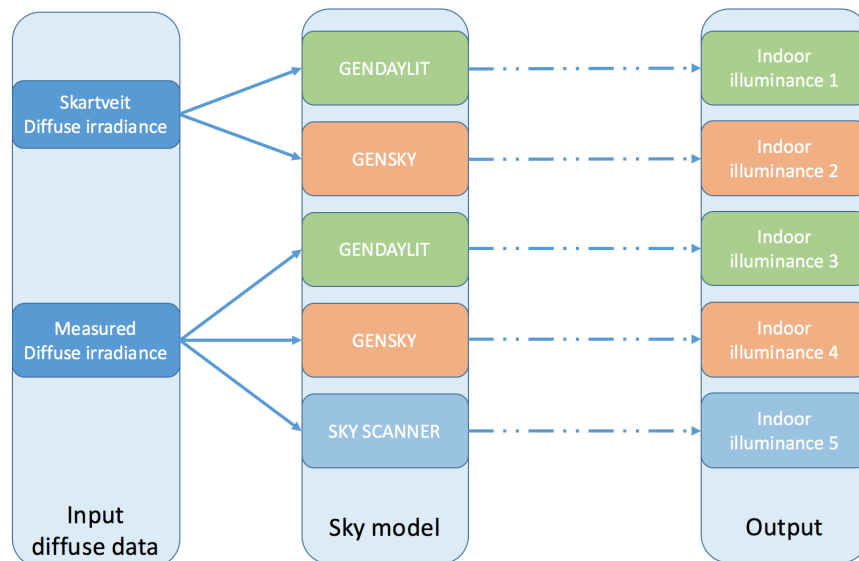


Figure 5-6. Five simulation scenarios deploying different diffuse irradiance and different sky models

5.3 Results and Discussions

Figure 5-8 to Figure 5-15 illustrates the cumulative distribution function of Relative Errors (RE) for 8 indoor virtual sensors. In order to better

understand and compare all sensors, we plotted the percentages of data having less than 20% *RE* for all sensors in *Figure 5-7*. Moreover, a numerical table compares different scenarios for all 8 sensors (see *Table 5-2*). In addition to *RE*, Root Mean Square Errors (*RMSE*) of each scenario for all 8 sensors is presented in *Table 5-3*. In order to shorten sky model terms in figures, we used following abbreviations, *GENDAYLIT* as *GDY*, *GENSKY* as *GSK*. For both statistical measures (*RE* and *RMSE*) Sky scanner scenario shows significant better performance, which was expected as sky scanner scenario is based on measured sky radiance values. All four scenarios other than sky scanner scenario have *RMSE* more than 30% in all 8 sensors. In the 6 out of the 8 sensors, the sky scanner scenario displays about 80% of the cases *RE* less than 20%. All other 4 datasets barely reach the criteria of having 60% of the cases with relative error *RE* less than 20%. On average the sky scanner scenario has 40% less *RMSE* than other 4 scenarios (about 30% *RMSE*). In sensors 3 and 7 which are close to the windows, all scenarios including sky scanner fail to reach even 50% of the cases with less than 20% *RE*. The only explanation for this could be due to the errors in indoor illuminance meters to measure high illuminance values near the windows.

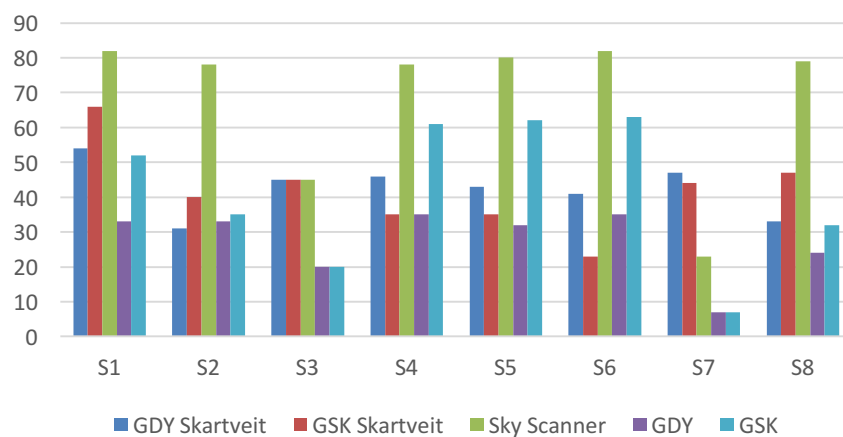


Figure 5-7. Percentage of results with less than 20% RE for different sensors (Overview)

Table 5-2. Percentage of results having less than 20% RE for different sensors and different scenarios

Scenario	S1	S2	S3	S4	S5	S6	S7	S8
<i>GDY_{Skartveit}</i>	54	31	45	46	43	41	47	33
<i>GSK_{Skartveit}</i>	66	40	45	35	35	23	44	47
<i>SkyScanner</i>	82	78	45	78	80	82	23	79
<i>GDY</i>	33	33	20	35	32	35	7	24
<i>GSK</i>	52	35	20	61	62	63	7	32

Table 5-3. Root Mean Square Errors (RMSE in %) of 5 scenarios for all sensors

Scenario	S1	S2	S3	S4	S5	S6	S7	S8
<i>GDY_{Skartveit}</i>	46.9	43.8	55.9	39.9	111.9	213.2	63.6	39.2
<i>GSK_{Skartveit}</i>	46.6	51.5	67.0	39.1	106.3	212.8	76.9	48.5
<i>SkyScanner</i>	13.7	18.3	39.7	18.9	81.5	16.6	49.0	15.1
<i>GDY</i>	93.0	72.5	85.7	70.2	133.1	66.7	101.5	72.9
<i>GSK</i>	42.1	46.4	61.9	30.8	51.1	28.6	75.1	50.0

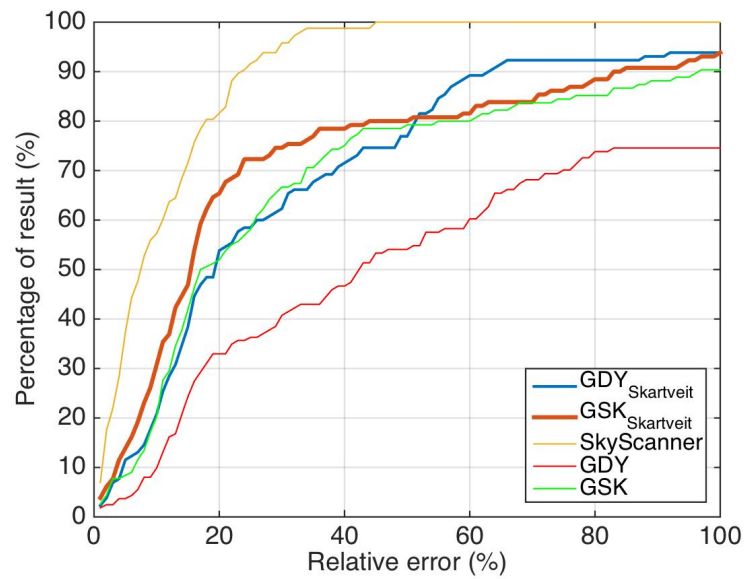


Figure 5-8. Cumulative Distribution Function of Relative Errors (Sensor 1)

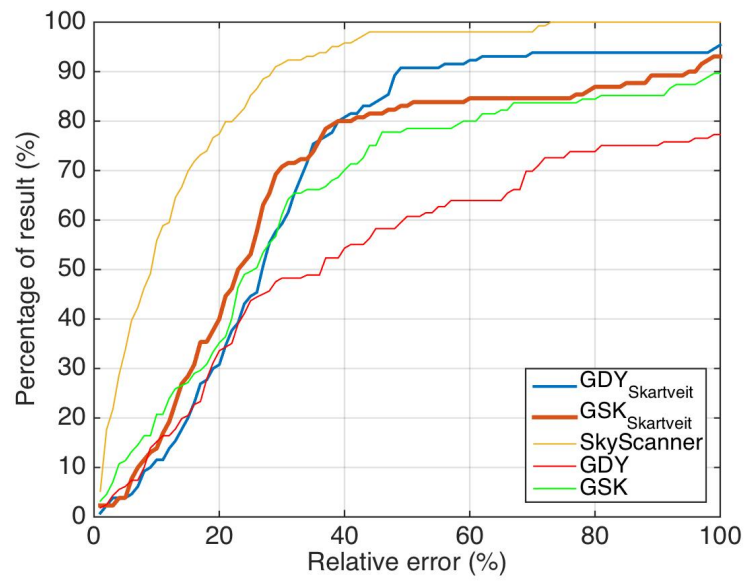


Figure 5-9. Cumulative Distribution Function of Relative Errors (Sensor 2)

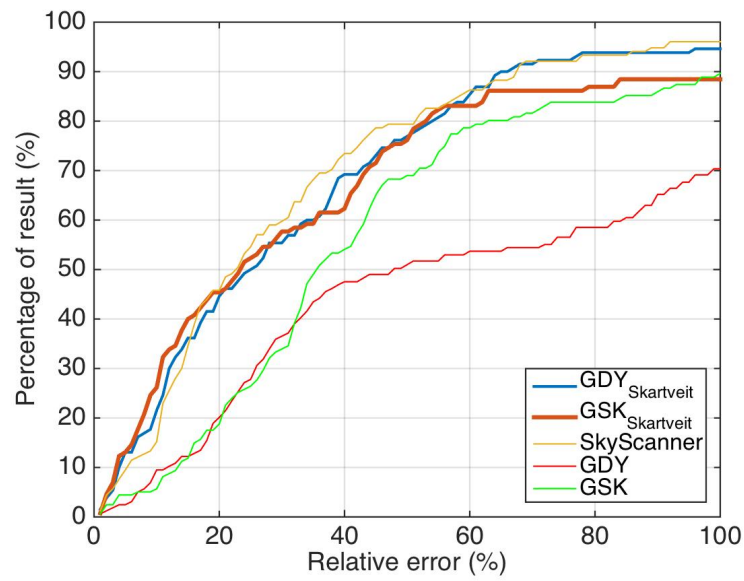


Figure 5-10. Cumulative Distribution Function of Relative Errors (Sensor 3)

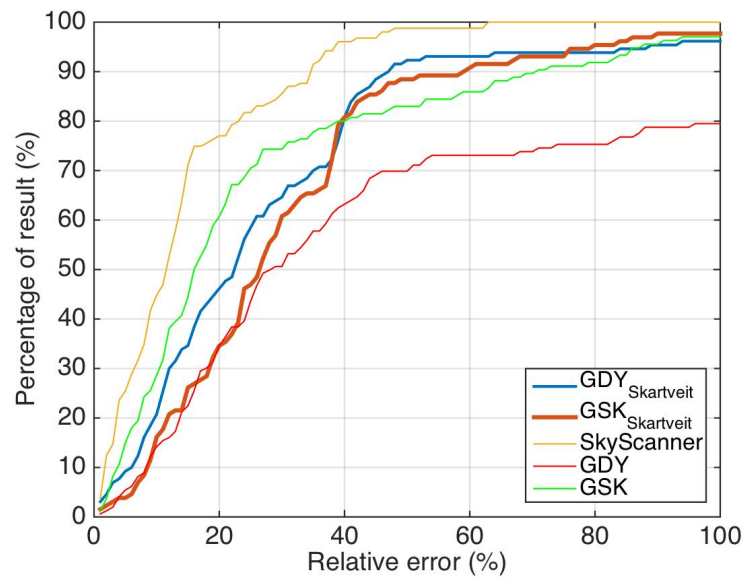


Figure 5-11. Cumulative Distribution Function of Relative Errors of (Sensor 4)

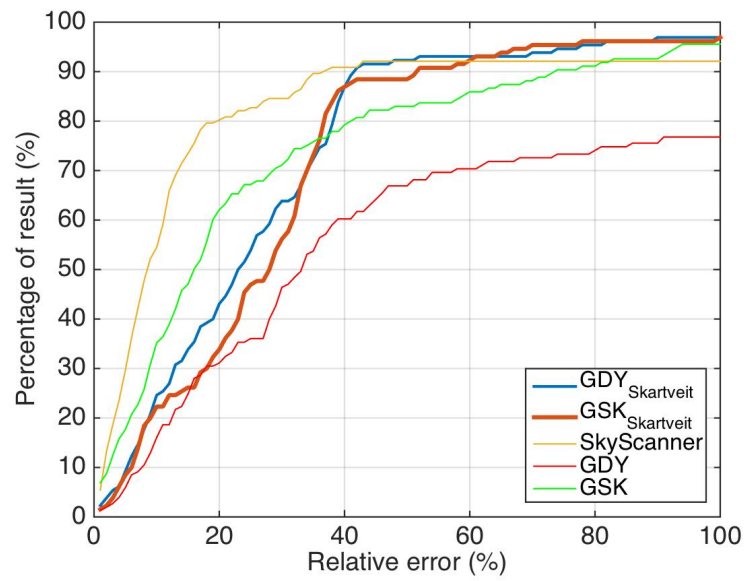


Figure 5-12. Cumulative Distribution Function of Relative Errors of (Sensor 5)

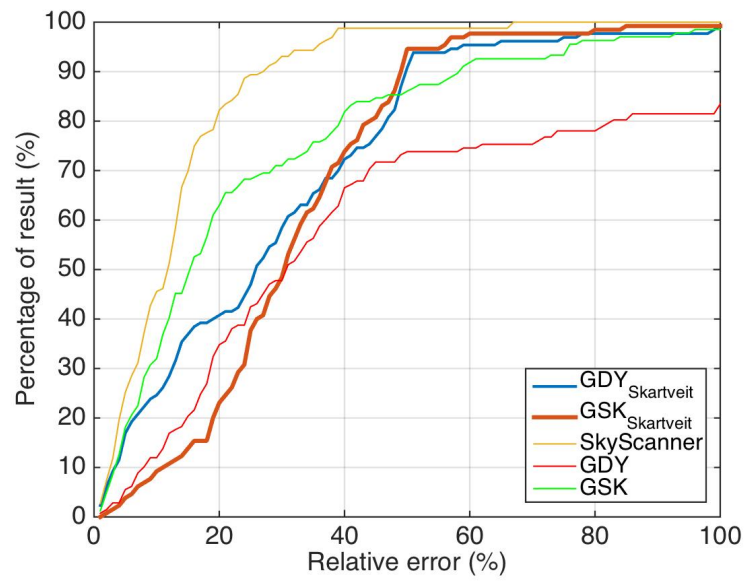


Figure 5-13. Cumulative Distribution Function of Relative Errors of (Sensor 6)

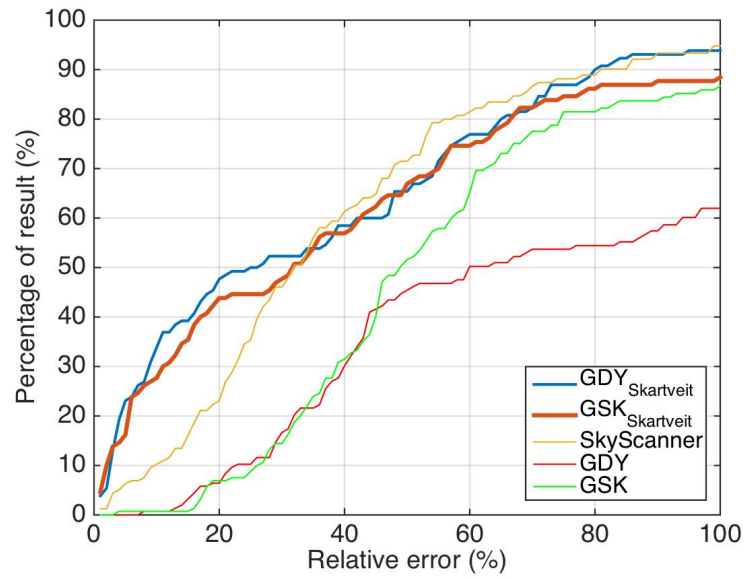


Figure 5-14. Cumulative Distribution Function of Relative Errors of (Sensor 7)

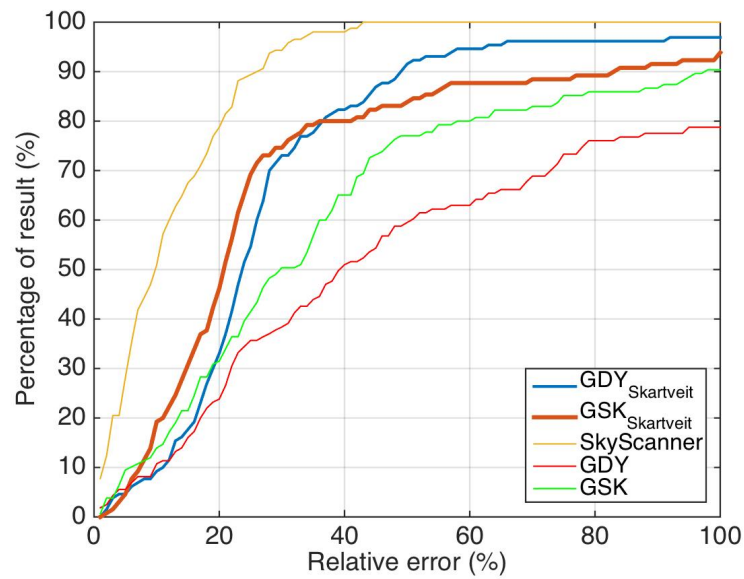


Figure 5-15. Cumulative Distribution Function of Relative Errors of (Sensor 8)

5.4 Conclusion

5 different scenarios simulated indoor illuminance in a modelled test room in Vienna, Austria (see Figure 5-6). Simulation results compared with measured values taken from test room at the rooftop of *TU Wien*. Results suggest that Sky scanner simulation scenario performs significantly better than other 4 scenarios in predicting indoor illuminances.

No significant performance difference was found between following scenarios: i) *GENSKY* generated via measured diffuse horizontal irradiance & *GENSKY* generated via diffuse fraction model of Skartveit, ii) *GENDAYLIT* generated via measured diffuse horizontal irradiance & *GENDAYLIT* generated via diffuse fraction model of Skartveit and Olseth. It can be inferred that deploying predicted diffuse irradiance in generation of sky models had no significant impact in prediction of indoor illuminance. As it was shown, errors of using sky models for indoor illuminance prediction are enough high that employment of diffuse fraction models may not necessarily increase the errors.

Chapter 6 Luminous Efficacy of Daylight

6.1 *Introduction*

When it comes to simulation of indoor illuminance, it is essential to have knowledge on sky luminance. As we discussed earlier high resolution daylight data is mostly unavailable or is in other forms such as irradiation data. Luminous efficacy let us generate daylight data where measured illuminances are not available (*Littlefair, 1985*). Luminous efficacy of daylight is the ratio of illuminance over irradiance with the unit of lumen per Watt which is not a constant. There are different luminous efficacy measures for different components of daylight, e.g., global horizontal luminous efficacy, diffuse luminous efficacy, direct luminous efficacy. Various research is done in order to calculate luminous efficacy or develop a model to predict luminous efficacy. One of earliest works was in Scandinavia (*Pleijel, 1954*), Kew, England (*Blackwell, 1954*), Uccle, Belgium (*Dogniaux, 1960*), South Africa (*Drummond, 1960*). Many of those proposed a constant value for luminous efficacy of between 105 to 128 lm/W. Thought later works developed prediction models manly function of clearness index (e.g., *Perez et al., 1990, Muneer et al., 2000, Ruiz et al., 2001, Dervishi and Mahdavi, 2013*). Part of “*Innovativ Projekte*” was dedicated to compare different luminous efficacy on a horizontal surface.

6.2 *Global Luminous Efficacy Models*

We have compared performance of four luminous efficacy K_g models in estimating hourly luminous efficacy for Vienna for year 2013. An overview of each model is as follow:

- *Muneer et al. (2000)* first model

$$K_g = 136.6 - 74.541k_t + 57.342k_t^2 \quad (68)$$

- *Muneer-Robledo second model (Ruiz et al., 2001):*

$$K_g = 138.45 - 91.641k_t + 67.08k_t^2 \quad (69)$$

Where, k_t is clearness index

- *Ruiz, Soler, and Robledo model:*

$$K_g = 104.83(\sin \alpha)^{0.026}k_t^{-0.108} \quad (70)$$

Where, k_t is clearness index and α is altitude of the sun in radian

- *Perez et al. model (1990):*

$$K_g = a_i + b_i W + c_i \cos Z + d_i \ln \Delta \quad (71)$$

Where a_i , b_i , c_i , and d_i are coefficients and are chosen from a table knowing *Perez ε*. W is water vapor, Z_s is solar zenith angle, and Δ is *Perez sky's* brightness.

6.3 Results and Discussions

Figure 6-1 illustrates global horizontal irradiance measured values versus global horizontal illuminance values from *TU Wien* station 2013. In order to better understand the correlation between global horizontal irradiance measured values versus global horizontal illuminance values, luminous efficacy of data is calculated and plotted in a box plot format. The median luminous efficacy for 2013 was 121.16 *lumen/Watt* (see *Figure 6-2*). Luminous efficacy models that we discussed in this chapter mainly are function of clearness index and solar altitude. Therefore, we plotted luminous efficacy against these two variables in *Figure 6-3* and *Figure 6-4*. It can be inferred that by increasing solar altitude luminous efficacy is also

increased. Conversely, by increasing in clearness index luminous efficacy decreased.

In order to examine the performance of luminous efficacy models, Mean Bias Errors (*MBE*), Mean Absolute Errors (*MAE*), and Root Mean Square Errors (*RMSE*) (see *Table 6-1*). Moreover, to better evaluate the models, Cumulative Distribution Function of Relative Errors (*RE*) for different models are displayed in *Figure 6-5*.

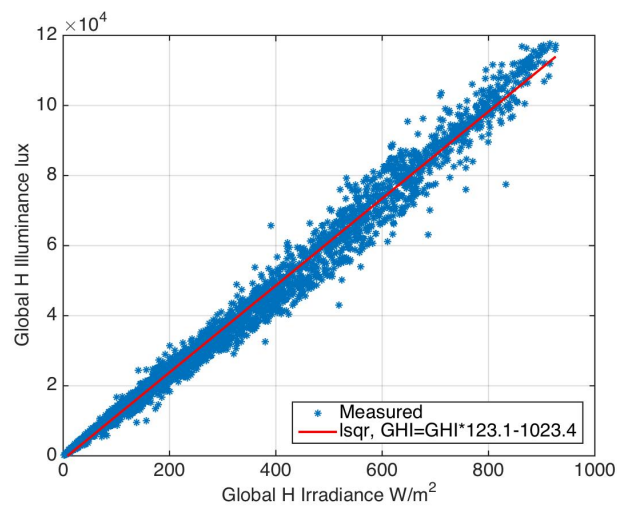


Figure 6-1. Global horizontal irradiance vs. global horizontal illuminance for Vienna – 2013

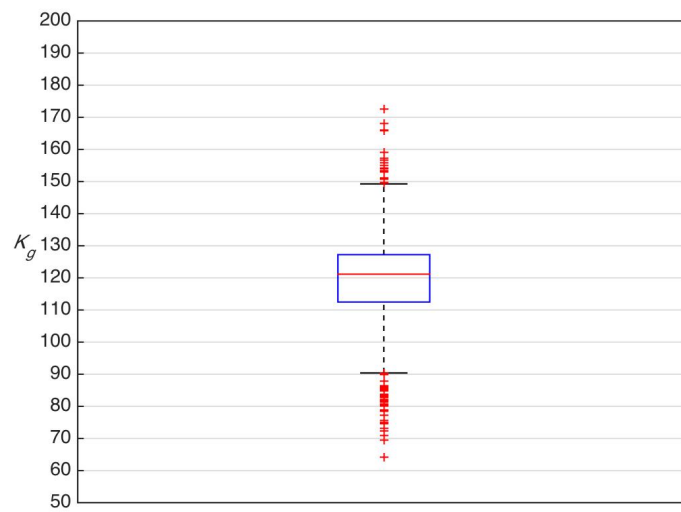


Figure 6-2. Global luminous efficacy for Vienna – 2013

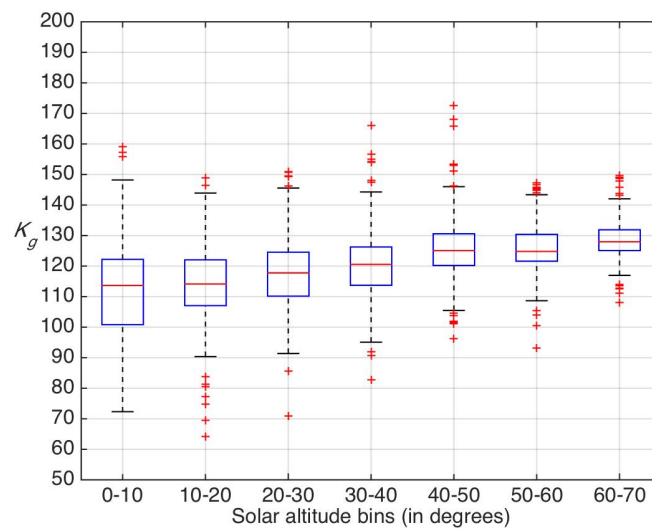


Figure 6-3. Global luminous efficacy as a function of solar altitude for Vienna – 2013

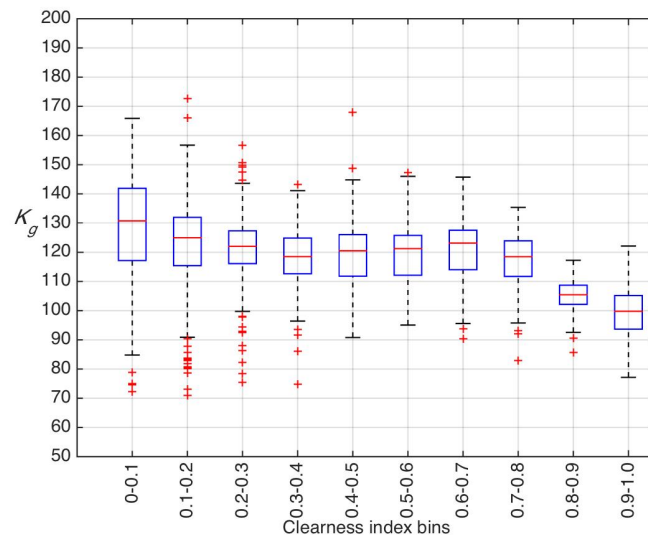


Figure 6-4. Global luminous efficacy as a function of clearness index for Vienna
– 2013

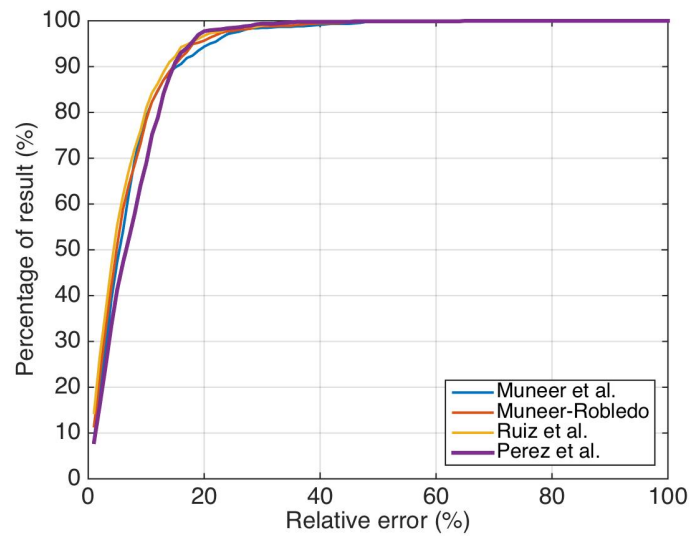


Figure 6-5. Cumulative Distribution Function of Relative Errors (RE) for 4 luminous efficacy models

Table 6-1. Global luminous efficacy model performance comparison

Model	PR>20%RE	MBE	MAE	RMSE
Muneer et al.	+5	+3.8	+7.2	+10.3
Muneer-Robledo	+4	+1.2	+6.8	+9.7
Ruiz et al.	+3	+0.8	+6.2	+8.9
Perez et al.	+2	-4.5	+7.6	+9.7

Chapter 7 **Conclusions**

7.1 *Contributions*

7.1.1 Chapter 3

We compared 7 well-known diffuse fraction models with 1 locally developed model for Vienna (*BPI*). The comparison made based on data from multiple locations with different climates. The *Skartveit and Olseth* model performed slightly better than the other 7 models in most stations and for most statistical measures, followed by *BRL* model. However, none of the models can be said to be performing wholly satisfactory.

We developed a high resolution local diffuse fraction model for Vienna. Results suggest that Vienna model performs significantly better than other models just for Vienna data and has an average performance on other locations. The followings are a number of reasons that we think it is not possible to develop a global high resolution diffuse fraction model using basic weather data. The complexity in weather and climate models including aerosols as well as the nature and distribution of clouds, significantly influence the magnitude and distribution of the diffuse component of solar radiation. This intricacy is not reflected in the data typically provided by standard weather stations (e.g., temperature, humidity and global horizontal irradiance).

7.1.2 Chapter 4

We compared two widely used sky models with corresponding measurements in generation of sky luminance and radiance description from their original article and deploying *RADIANCE rendering program* respectively. Results suggest that both sky models failed to predict satisfactorily vertical illuminance or irradiance values on cardinal surfaces.

Principles behind the subpar performance of these models lies in the fact that distribution of luminance or radiance over sky hemisphere is highly a function of cloud distribution and characteristics. Therefore, employing basic weather data from a standard weather station does not provide adequate information to accurately predict radiance and luminance distributions.

7.1.3 Chapter 5

We had 5 different simulation scenarios in *RADIANCE rendering program*. Indoor illuminance values based on each scenario compared with measured indoor illuminance from a test room located in Vienna, Austria. Results suggest that Sky scanner simulation scenario performs significantly better than other 4 scenarios as it was expected.

No significant performance difference was found between following scenarios: *i) GENSKY* generated via measured diffuse horizontal irradiance & *GENSKY* generated via diffuse fraction model of Skartveit, *ii) GENDAYLIT* generated via measured diffuse horizontal irradiance & *GENDAYLIT* generated via diffuse fraction model of Skartveit and Olseth.

Given the limited scope of our study (a single room, relatively short measurement period), the generalization of the results might not be warranted. However, the presented case study does imply the need for careful characterization of the daylight simulation process in general and the reliability of sky luminance models in particular. Qualification of related accuracy statements and claims must be carefully approached lest providing the users with overtly simplistic expectations regarding models' fidelity and applicability.

7.1.4 Chapter 6

We compared 4 luminous efficacy models with measured luminous efficacy from data in Vienna. Results indicated adequate performance of all models in prediction of global horizontal illuminance for Vienna data. Thus, these models can reliably be implicated in engineering practices

7.2 Outlook

Intensified future efforts toward combination of terrestrial measurements (via standard weather stations) with satellite-based imaging may not only lead to the formulation of more sophisticated modelling techniques and a higher quality level in prediction of the diffuse fraction of the global solar radiation but also a high resolution sky luminance distribution model using advanced machine learning techniques.

Recent achievements in ITC enable us to monitor, control, and predict building performances with real-time data. Therefore, integration of real-time high resolution sky models with other building systems (heating, cooling, and ventilation) can lead to high performance building predictive-control models (*Mahdavi, 2006, Mahdavi, 2008, Mahdavi et al., 2009*).

7.3 Publications

Vazifeh, E., Schuss, M., Mahdavi, A. (2016). A Comparative Assessment of Diffuse Fraction Models. Under proceeding of the 11th International Conference on Building & Environment, enviBUILD 2016, Brno, Czech Republic.

Etminan, G., Vazifeh, E., Mahdavi, A. (2016). The Implications of Assumed Boundary Conditions for The Reliability of Indoor Illuminance Predictions: A Case Study. Under proceeding of the 11th International Conference on Building & Environment, enviBUILD 2016, Brno, Czech Republic.

Vazifeh, E., Schuss, M., Mahdavi, A. (2015). Radiometric boundary condition models for building performance simulation: an empirical assessment. Energy Procedia, Proceedings of 6th International Building Physics Conference, IBPC, p188.

Vazifeh, E., Schuss, M., Mahdavi, A. (2015). An Empirically-Based Assessment of Computational Sky Luminance Distribution Models. Proceedings of the 14 IBPSA Conference, Hyderabad, India, Paper ID 2224, p5.

Vazifeh, E., Schuss, M., Mahdavi, A. (2015). Sky luminance patterns Distribution Patterns: Empirical Assessment and Computational Models. LpS2015 - LED Lighting Technologies - Trends & Technologies for Future Lighting Solutions, ISBN: 9783950320961. 64 - 73.

Vazifeh, E., Schuss, M., Mahdavi, A. (2015). Radiometric boundary condition models for building performance simulation: an empirical assessment. 6th International Building Physics Conference 2015, IBPC 2015.

- Vazifeh, E., Schuss, M., Mahdavi, A. (2015). Prediction of vertical irradiance on building surfaces: an empirical comparison of two models. Building Simulation Applications 2015 - 2nd IBPSA-Italy Conference. Paper ID 110, p6.
- Vazifeh, E., Schuss, M., Mahdavi, A. (2014). Development and evaluation of models for the computation of sky radiance and luminance distribution. ECPPM2014, Vienna, Austria, ISBN: 978-1-138-02710-7. 237 - 242.
- Vazifeh, E., Mahdavi, A. (2014). A Comparative Performance Study of Diffuse Fraction Models Based on Data from Vienna, Austria. 2nd ICAUD – Proceedings, EPOKA-University. p7.

Chapter 8 **References**

8.1 *Literature*

- Barbaro, S., Coppolino, S., Leone, C., & Sinagra, E. (1979). An atmospheric model for computing direct and diffuse solar radiation. *Solar Energy*, 22(3), 225-228.
- Bivona, S., Burlon, R., & Leone, C. (1991). Instantaneous distribution of global and diffuse radiation on horizontal surfaces. *Solar Energy*, 46(4), 249-254.
- Bird, R. & Hulstrom, R. (1981). A simplified clear sky model for direct and diffuse insolation on horizontal surfaces. Golden, Colo.: Solar Energy Research Institute.
- Blackwell, M.J. (1954). Five-year continuous recordings of total and diffuse solar irradiance at Kew Observatory. Meteorological Resource Publication 895, Meteorological Office, London.
- Blanc, P., Espinar, B., Wald, L. (2013). Report on Direct Normal Irradiance Standards. MACC-II, Technical Report D121.1.
- Boes, E. C. (1975). Estimating the direct component of solar radiation. Sandia Report SAND75-0565.
- Boland, J., Scott, L., & Luther, M. (2001). Modelling the diffuse fraction of global solar radiation on a horizontal surface. *Environmetrics*, 12(2), 103-116.
- Boland, J., Ridley, B., & Brown, B. (2008). Models of diffuse solar radiation. *Renewable Energy*, 33(4), 575-584.
- Brunger, A. & Hooper, F. (1993). Anisotropic sky radiance model based on narrow field of view measurements of shortwave radiance. *Solar Energy*, 51(1), 53-64.
- Bruno, R. (1978). A correction procedure for separating direct and diffuse insolation on a horizontal surface. *Solar Energy*, 20(1), 97-100.

- Bugler, J. (1977). The determination of hourly insolation on an inclined plane using a diffuse irradiance model based on hourly measured global horizontal insolation. *Solar Energy*, 19(5), 477-491.
- Carroll, J. (1985). Global transmissivity and diffuse fraction of solar radiation for clear and cloudy skies as measured and as predicted by bulk transmissivity models. *Solar Energy*, 35(2), 105-118.
- Chendo, M. & Maduekwe, A. (1994). Hourly global and diffuse radiation of Lagos, Nigeria—Correlation with some atmospheric parameters. *Solar Energy*, 52(3), 247-251.
- Chandrasekaran, J. & Kumar, S. (1994). Daily utilizability from hourly cumulative frequency curves. *Renewable Energy*, 4(8), 891-895.
- Choudhury, N. (1963). Solar radiation at New Delhi. *Solar Energy*, 7(2), 44-52.
- CIE. (1955). Natural Daylight. *Compte Rendu CIE 13 Session*. Official Recommendation, 2, part 3.2, II-IV & 35-37.
- CIE. (1973). Standardization of luminance distribution on clear skies. Paris.
- CIE. (1995). Spatial distribution of daylight. Vienna.
- CIE. (2003). Spatial distribution of daylight. Vienna, Austria.
- Climate-Data.org. 2015. <http://en.climate-data.org/region/1461/> (Last accessed, June, 2016)
- Darula, S. and Kittler, R. (2002). CIE general sky standard defining luminance distributions. eSim, Montreal, Canada.
- De Miguel, A., Bilbao, J., Aguiar, R., Kambezidis, H., & Negro, E. (2001). Diffuse solar irradiation model evaluation in the North Mediterranean Belt area. *Solar Energy*, 70(2), 143-153.
- Dervishi, S. & Mahdavi, A. (2011). A comparison of luminous efficacy models based on data from Vienna, Austria. *Building Simulation*, 4, 4; 183 - 188.
- Dervishi, S. & Mahdavi, A. (2012). Computing diffuse fraction of global horizontal solar radiation: A model comparison. *Solar Energy*, 86(6), 1796-1802.

- Dervishi, S. & Mahdavi, A. (2013). A simple model for the derivation of illuminance values from global radiation data. *Building Simulation*, 6, 4; 379 - 383.
- Dogniaux, R. (1960). Données météorologiques concernant l'ensoleillement et l'éclairage naturel. *Cahiers du Centre Scientifique du Bâtiment*, 44:1-24.
- Drummond A. J. (1960). Note on the measurement of natural illumination II. Daylight and skylight at Pretoria: The luminous efficacy of daylight. *Architectural Meteorology Vienna; Series B*, 9:1-149.
- EKO instruments CO. (2014). Instruction manual for Sky scanner MS-321LR.
- Erbs, D., Klein, S., & Duffie, J. (1982). Estimation of the diffuse radiation fraction for hourly, daily and monthly-average global radiation. *Solar Energy*, 28(4), 293-302.
- Gueymard, C. (1993). Critical analysis and performance assessment of clear sky solar irradiance models using theoretical and measured data. *Solar Energy*, 51(2):121–138
- Gueymard, C. (2004). The sun's total and spectral irradiance for solar energy applications and solar radiation models. *Solar Energy*, 76(4), 423-453.
- Gueymard, C. (2008). REST2: High-performance solar radiation model for cloudless-sky irradiance, illuminance, and photosynthetically active radiation – Validation with a benchmark dataset. *Solar Energy*, 82(3), 272-285.
- Grigianti, M., Mottes, F., Zardi, D., De Franceschi, M. (2011). Experimental solar radiation measurements and their effectiveness in setting up a real-sky irradiance model. *Renewable Energy*, (36), 1–8
- Harbison, R., Lee, R., & Stedeford, T. (2015). *Hamilton Hardy's Industrial Toxicology*. John Wiley & Sons.
- Hawklader, M.N.A. (1984). Solar diffuse, global and extraterrestrial solar radiation for Singapore. *International Journal of Ambient Energy*, 5(1):31-37.
- Hottel, H. (1976). A simple model for estimating the transmittance of direct solar radiation through clear atmospheres. *Solar Energy*, 18(2), 129-134.

- Igawa, N., Nakamura, H., Matsuzawa, T., Koga, Y., Goto, K., Kojo, S. (1997). Sky luminance distribution between two CIE standard skies. *Proc. Lux Pacifica*, E7-E18.
- Igawa, N., Koga, Y., Matsuzawa, T., & Nakamura, H. (2004). Models of sky radiance distribution and sky luminance distribution. *Solar Energy*, 77(2), 137-157.
- Iqbal, M. (1980). Prediction of hourly diffuse solar radiation from measured hourly global radiation on a horizontal surface. *Solar Energy*, 24(5), 491-503.
- Karatasou, S., Santamouris, M., & Geros, V. (2003). Analysis of experimental data on diffuse solar radiation in Athens, Greece, for building applications. *International Journal Of Sustainable Energy*, 23(1-2), 1-11.
- Kasten, F. (1983). Parametrisierung der globalstrahlung durch bedeckungsgrad und trubungsfaktor, *Ann. Met.* 20, 49- 50.
- Kittler, R., (1967). Standardization of outdoor conditions for the calculation of daylight factor with clear skies. In: *Proceedings of the CIE International Conference on Sunlight in Buildings*, Bouwcentrum International, Rotterdam, pp. 273–285.
- Kittler, R. (1985). Luminance distribution characteristics of homogeneous skies: a measurement and prediction strategy. *Light. Res. and Technol.*, 17, 4, 183-188
- Kittler, R., Perez, R., and Darula, S. (1997). A new generation of sky standards. In: *proceedings of the Lux Europa 1997*. 359-373.
- Kittler R., Perez R., and Darula S. (1998). A set of standard skies characterizing daylight conditions for computer and energy conscious design. *US SK 92 052 Final Report*, ICA SAS Bratislava, Polygrafia Bratislava.
- König-Langlo, G. and Sieger, R. (2012). BSRN-Archive Overview and Status, Twelfth BSRN Scientific Review and Workshop, AWI Potsdam, Germany.
- Lam, J. & Li, D. (1996). Correlation between global solar radiation and its direct and diffuse components. *Building And Environment*, 31(6), 527-535.

- Lauret, P., Boland, J. Ridley, B. (2010). Derivation of a solar diffuse fraction model in a Bayesian framework, *Case Studies in Business, Industry and Government Statistics* 1, 3:108-122.
- Littlefair, P. (1981). The luminance distribution of an average sky. *Lighting Research And Technology*, 13(4), 192-198.
- Littlefair, P. (1985). The luminous efficacy of daylight: a review. *Lighting Research And Technology*, 17(4), 162-182.
- Liu, B. & Jordan, R. (1960). The interrelationship and characteristic distribution of direct, diffuse and total solar radiation. *Solar Energy*, 4(3), 1-19.
- Mahdavi, A. (2006). The technology of sentient buildings. *ITU A|Z*. 3 (1/2), 24:36.
- Mahdavi, A. (2008). Predictive simulation-based lighting and shading systems control in buildings. *Build. Simul.*, 1(1), 25-35.
- Mahdavi, A., M. Schuss, G. Suter. (2009). Recent advances in simulation powered building systems control. Eleventh International IBPSA Conference. Glasgow, Scotland.
- Mahdavi, A. and Dervishi, S. (2013). A simple all-weather sky radiance model. *IBPSA, Chambéry*. 916-921.
- MATLAB (2010). MATLAB Statistics Toolbox Release 2010a. The MathWorks, Inc., Natick, Massachusetts, United States.
- Matsuura, K., Iwata, T. (1990). A model of daylight source for the daylight illuminance calculations on the all weather conditions. *Proceeding of 3rd international daylighting conference*. Moscow, USSR.
- Maxwell, E.L. (1987). A quasi-physical model for converting hourly global horizontal to direct normal insolation, Report SERI/TR-215-3087, Solar Energy Institute, Golden, CO.
- Menzel, W. (2001). Applications with meteorological satellites. World Meteorological Organization.
- Moon, P., Spencer, D.E., (1942). Illumination from a non- uniform sky. *Trans. Illum. Engng. Soc.* 37, 707–726.

- Muneer, T., Hawas, M., & Sahili, K. (1984). Correlation between hourly diffuse and global radiation for New Delhi. *Energy Conversion And Management*, 24(4), 265-267.
- Muneer, T., Gul, M., & Kubie, J. (2000). Models for Estimating Solar Radiation and Illuminance From Meteorological Parameters. *Journal Of Solar Energy Engineering*, 122(3), 146.
- Nakamura, H., Oki, M., & Hayashi, Y. (1985). Luminance distribution of intermediate sky. *J. Light & Vis. Env.*, 9(1), 6-13.
- Nakamura, H., Oki, M., and Iwata, T. (1987). Mathematical Description of the Intermediate Sky. *Proc. of 21st CIE Session*, CIE, Venice, Italy, pp. 230–231.
- Oliveira, A., Escobedo, J., Machado, A., & Soares, J. (2002). Correlation models of diffuse solar-radiation applied to the city of São Paulo, Brazil. *Applied Energy*, 71(1), 59-73.
- Orgill, J. & Hollands, K. (1977). Correlation equation for hourly diffuse radiation on a horizontal surface. *Solar Energy*, 19(4), 357-359.
- Parmerlee G.V. (1954). Irradiation of Vertical and horizontal surfaces by diffuse solar radiation from cloudless skies, *ASHVE transaction* 341-358.
- Perez, R., Ineichen, P., Seals, R., Michalsky, J., & Stewart, R. (1990). Modeling daylight availability and irradiance components from direct and global irradiance. *Solar Energy*, 44(5), 271-289.
- Perez, R., Ineichen, P., Maxwell, E., Seals, R., Zelenka, A., (1992). Dynamic global to direct irradiance conversion models. *ASHRAE Trans. Res. Series*, 354–369.
- Perez, R., Seals, R., Michalsky, J., Steward, R. (1993). All-weather model for sky luminance distribution-preliminary configuration and validation. *Solar energy*, Vol: 50 (3). 235-245.
- Perradeau, M. (1988). Luminance models. *National Lighting Conference 1988*, Cambridge. 291-292.
- Pleijel, G. (1954). The computation of natural irradiance in architecture and town planning. *Meddelande Bull., Statens Namnd for Byggnadsforskning*. Stokholm, 25:1-30.

- Randall, C. M. and Whitson, M. E. (1977). Final report--hourly insolation and meteorological data bases including improved direct insolation estimates. Aerospace Report No. ATR-78 (7592)-1.
- Reindl, D.T., Beckman, W.A., Duffie, J.A. (1990). Diffuse fraction correlations, *Solar Energy*, 45(1):1-7.
- Ridley, B., Boland, J., & Lauret, P. (2010). Modelling of diffuse solar fraction with multiple predictors. *Renewable Energy*, 35(2), 478-483.
- Ruiz, E., Soler, A., & Robledo, L. (2001). Assessment of Muneer's Luminous Efficacy Models in Madrid and a Proposal for New Models Based on His Approach. *Journal Of Solar Energy Engineering*, 123(3), 220.
- Ruth, D. & Chant, R. (1976). The relationship of diffuse radiation to total radiation in Canada. *Solar Energy*, 18(2), 153-154.
- Skartveit, A. Olseth, J.A. 1987. A model for the diffuse fraction of hourly global radiation, *Solar Energy*, 38:271-274.
- Skartveit, A., Olseth, J., & Tuft, M. (1998). An hourly diffuse fraction model with correction for variability and surface albedo. *Solar Energy*, 63(3), 173-183.
- Soares, J., Oliveira, A. Boznar, M., Mlakar, P., Escobedo, J.F. and Machado, J.A. (2004). Modeling hourly diffuse solar radiation in the city of Sao Paulo using a neural-network technique. *Applied Energy*, 79(2):201-214.
- Spencer, JW. (1982). A comparison of methods for estimating hourly diffuse solar radiation from global solar radiation, *Solar Energy*, 29:19-32.
- Stanhill, G. (1966). Diffuse sky and cloud radiation in Israel. *Solar Energy*, 10(2), 96-101.
- Stephens, G., O'Brien, D., Webster, P., Pilewski, P., Kato, S., & Li, J. (2015). The albedo of Earth. *Rev. Geophys.*, 53(1), 141-163.
- Tregenza, P.R. (1999). Standard skies for maritime climates. *Lighting Res. & Technol.* 31 (3), 97-106.
- Tuller, S. (1976). The relationship between diffuse, total and extraterrestrial solar radiation. *Solar Energy*, 18(3), 259-263.

- Vazifeh, E., Dervishi, S., Mahdavi, A. (2013). Calculation models for the diffuse fraction of global solar radiation. CESBP, Vienna, Austria. 587 - 590.
- Ward, G.J. (1994). The radiance lighting simulation and rendering system. In Proceedings of the 21st annual conference on Computer graphics and interactive techniques, pages 459–472. ACM Press.
- Ward, GJ. (2014a). http://radsite.lbl.gov/radiance/man_html/gendaylit.1.html. (Accessed May 2015).
- Ward GJ. (2014b). http://radsite.lbl.gov/radiance/man_html/gensky.1.html. (Accessed May 2015.)
- Weiss, A. & Norman, J. (1985). Partitioning solar radiation into direct and diffuse, visible and near-infrared components. *Agricultural And Forest Meteorology*, 34(2-3), 205-213.

8.2 Tables

<i>Table 2-1. Characteristics of stations in the USA (BSRN).....</i>	<i>9</i>
<i>Table 2-2. List of deployed sensors for Vienna.....</i>	<i>10</i>
<i>Table 3-1. Summarized description of models and their variables</i>	<i>13</i>
<i>Table 3-2. Bins used in Perez function</i>	<i>24</i>
<i>Table 3-3. Bins used for the Perez second model</i>	<i>25</i>
<i>Table 3-4. Pearson moment correlation for different variables vs. diffuse fraction.....</i>	<i>27</i>
<i>Table 3-5. Variables used in BPI model</i>	<i>34</i>
<i>Table 3-6. Coefficients for the proposed BPI model as a function of the global horizontal irradiance (I_{gh}) range.....</i>	<i>35</i>
<i>Table 3-7. Root Mean Square Error (RMSE in %) of predicted I_{dh} to SPN1 data</i>	<i>37</i>
<i>Table 3-8. Mean Bias Error (MBE in %) of predicted I_{dh} to SPN1 data.....</i>	<i>37</i>
<i>Table 3-9. Mean Absolute Error (MAE in %) of predicted I_{dh} to SPN1 data.....</i>	<i>37</i>
<i>Table 3-10. Percentage of predicted I_{dh} data having RE less than 20% with SPN1 data</i>	<i>38</i>
<i>Table 3-11. Ranking of the performance of different models for different locations using all 4 statistical measures</i>	<i>38</i>
<i>Table 4-1. GENSKY categorization in the present study</i>	<i>47</i>
<i>Table 4-2. Statistical evaluation of CIE and Perez models based on vertical illuminance predictions</i>	<i>50</i>
<i>Table 4-3. Statistical evaluation of vertical irradiance (incident on surfaces facing four cardinal directions) and sky patch radiance as predicted via GENDAYLIT and GENSKY</i>	<i>52</i>
<i>Table 5-1. The reflectance of the test room surfaces.....</i>	<i>59</i>
<i>Table 5-2. Percentage of results having less than 20% RE for different sensors and different scenarios</i>	<i>64</i>
<i>Table 5-3. Root Mean Square Errors (RMSE in %) of 5 scenarios for all sensors</i>	<i>64</i>
<i>Table 6-1. Global luminous efficacy model performance comparison</i>	<i>73</i>
<i>Table 0-1. Instruments specifications.....</i>	<i>92</i>
<i>Table 0-2. Recorded climate data for Vienna city from 1971 to 2000</i>	<i>93</i>
<i>Table 0-1. Perez Look-up Table</i>	<i>95</i>

8.3 Figures

Figure 1-1. Extraterrestrial solar spectrum vs. earth surface solar spectrum (image source: http://www.itacanet.org/the-sun-as-a-source-of-energy/part-2-solar-energy-reaching-the-earths-surface/)	2
Figure 2-1. Distribution map of BSRN sites deployed in this study	8
Figure 3-1. Workflow of Pearson index calculation	26
Figure 3-2. Comparison of diffuse fraction vs. clearness index for different global horizontal irradiance (I _{gh}).....	29
Figure 3-3. Three-dimensional comparison of diffuse fraction vs. clearness index and I _{gh}	29
Figure 3-4. Comparison of diffuse fraction vs. clearness index for different temperatures	30
Figure 3-5. Three-dimensional comparison of diffuse fraction vs. clearness index and temperatures.....	30
Figure 3-6. Comparison of diffuse fraction vs. clearness index for different solar altitudes	31
Figure 3-7. Three-dimensional comparison of diffuse fraction vs. clearness index and solar altitudes.....	31
Figure 3-8. Comparison of diffuse fraction vs. clearness index for different relative humidity.....	32
Figure 3-9. Three-dimensional comparison of diffuse fraction vs. clearness index and relative humidity.....	32
Figure 3-10. Effect of sun state (Top: 3d kd-kt plot, Bottom: 2d kd-kt plot).....	33
Figure 3-11. Cumulative Distribution Function of Relative Errors for percentage of results (Testing dataset – year 2011).....	39
Figure 3-12. Cumulative Distribution Function of Relative Errors for percentage of results (Validation dataset)	39
Figure 4-1. Flowchart of sky generation in RADIANCE (GENDAYLIT on the left – GENSKY on the right)	46
Figure 4-2. Sky fisheye high dynamic range images for GENDAYLIT (on the left) and GENSKY (on the right) – 10:45 a.m. local time, 10 July 2014, Vienna.....	46
Figure 4-3. Top: Sky scanner MS-321LR, Bottom: Fisheye image of sky generated via sky scanner	49
Figure 4-4. Comparison of the CIE and Perez sky models in terms of relative error distributions of predicted vertical illuminance values (Relative errors over 100% are merged into the 100% error bin)	51
Figure 4-5. Comparison of CIE and Perez et al. sky models' relative errors (%) for vertical surfaces facing the four cardinal directions in terms of cumulative distribution functions	51

Figure 4-6. Cumulative distribution functions of the relative errors (%) of the two models' patch luminance predictions with respect to sky scanner data	52
Figure 4-7. Comparison of the GENSKY and GENDAYLIT sky models in terms of distributions of the relative errors of predicted vertical irradiance values	53
Figure 4-8. Comparison of measured and computed patch radiance values (Left: GENDAYLIT; Right: GENSKY)	53
Figure 4-9. Comparison of GENSKY and GENDAYLIT sky models' relative errors (%) for vertical surfaces facing the four cardinal directions in terms of cumulative distribution functions	54
Figure 4-10. Comparison of patch radiance values of two models with sky scanner data using cumulative distribution of percentage of the results for different relative errors (%)	54
Figure 5-1. Location of the test room, TU Wien, Vienna, Austria	57
Figure 5-2. Minolta luminance meter (LS-100) (on the left) and illuminance meter (T10-A series) (on the right)	58
Figure 5-3. Arrangement of illuminance meters in the test room (Photo credit: Ghazal Etminan)	59
Figure 5-4. Different view from test room geometry in Sketchup (from top to bottom: Top view, North-East view, North-East view section) ...	61
Figure 5-5. An overview of simulation steps to calculate indoor illuminances	62
Figure 5-6. Five simulation scenarios deploying different diffuse irradiance and different sky models	62
Figure 5-7. Percentage of results with less than 20% RE for different sensors (Overview)	63
Figure 5-8. Cumulative Distribution Function of Relative Errors (Sensor 1)	64
Figure 5-9. Cumulative Distribution Function of Relative Errors (Sensor 2)	65
Figure 5-10. Cumulative Distribution Function of Relative Errors (Sensor 3)	65
Figure 5-11. Cumulative Distribution Function of Relative Errors of (Sensor 4)	66
Figure 5-12. Cumulative Distribution Function of Relative Errors of (Sensor 5)	66
Figure 5-13. Cumulative Distribution Function of Relative Errors of (Sensor 6)	67
Figure 5-14. Cumulative Distribution Function of Relative Errors of (Sensor 7)	67
Figure 5-15. Cumulative Distribution Function of Relative Errors of (Sensor 8)	68
Figure 6-1. Global horizontal irradiance vs. global horizontal illuminance for Vienna – 2013	71
Figure 6-2. Global luminous efficacy for Vienna – 2013	72
Figure 6-3. Global luminous efficacy as a function of solar altitude for Vienna – 2013	72
Figure 6-4. Global luminous efficacy as a function of clearness index for Vienna – 2013	73
Figure 6-5. Cumulative Distribution Function of Relative Errors (RE) for 4 luminous efficacy models	73

Figure 0-1. North side of the observatory station of BPI, TU Wien 92

Glossary

k_t	clearness index, ratio of global horizontal irradiance over extraterrestrial horizontal irradiance
I_{gh}	global horizontal irradiance (W/m ²)
I_{ext}	extraterrestrial irradiance (W/m ²)
α	solar altitude (degrees)
I_{dh}	diffuse horizontal irradiance (W/m ²)
I_{dn}	direct normal irradiance (W/m ²)
E_n	direct normal illuminance
k_d	diffuse fraction, ratio of diffuse horizontal irradiance over global horizontal irradiance
T_a	ambient temperature
ϕ	relative humidity
T_d	dew point temperature
σ_3	variability index
ρ	clear sky index
ψ	persistence index
AST	apparent solar time
m_{air}	air mass
K'_t	adjusted clearness index
Z_s	solar zenith angle

$\Delta K'_t$	stability index
W	atmospheric precipitable water
r	pearson moment correlation index
SS	sun state
M_i	measurement instance
S_i	simulation instance
L_r	relative sky luminance
ξ	angular distance between the sky element and the sun disk
Z	zenith angle of considered sky element
Δ	brightness index
ϵ	sky clearness
L_z	zenith luminance (cd/m ² .sr)
η	sun disc diameter angle
E_{gh}	global horizontal illuminance (lux)
Ω_i	patch solid angle
β	vertical plane normal angle
ϑ	patch vertical transformation function
λ_i	patch azimuth angle
K_g	global luminous efficacy


Appendix A – BPI Weather station

The microclimatic observatory weather station of Building physics and building ecology department is located on the rooftop of Technical university of Vienna, at the heart of Vienna city, Austria (see *Figure 0-1*). Some of the specifications of the equipment have been demonstrated in *Table 0-1*.



Figure 0-1. North side of the observatory station of BPI, TU Wien

Table 0-1. Instruments specifications

Weather station	Specifications
	<p>Outdoor air temperature: Absolute Error: < 0.3 K; Temperature range: -30 to +70 ° C; Response time < 20 s (≥ 1.5 m/s)</p> <p>Outdoor relative humidity: Absolute Error < $\pm 2\%$; Humidity range 0 to 100 %; Response time < 10 s (≥ 1.5 m/s)</p> <p>Wind speed: Absolute Error: <1%; Wind speed range 0 - 75 m.s⁻¹</p>
Sunshine Pyranometer (SPN1)	Specifications





	Global and Diffuse irradiance (Sunshine Pyranometer SPN1): Overall accuracy $\pm 5\%$; Daily integrals $\pm 5\%$ $\pm 10 \text{ W.m}^{-2}$; Hourly averages $\pm 8\%$ $\pm 10 \text{ W.m}^{-2}$; Resolution $0.6 \text{ W.m}^{-2}=0.6 \text{ mV}$; Range 0 to $> 2000 \text{ W.m}^{-2}$; Analogue output sensitivity $1\text{mv}= 1 \text{ W.m}^{-2}$; Analogue output range: 0-2500 mV; Temperature range -20 to $+70^\circ \text{ C}$; Accuracy Cosine Correction $\pm 2\%$ of incoming radiation over $0-90^\circ$ zenith angle.
Ahlborn FLA 613-GS & VLM	Specifications
	<p>GS: range 0-1200 W.m^{-2}; spectral sensitivity 400nm to 1100nm; signal output 0V to 2V; absolute error $<10\%$; operating temperature -20° to $+60^\circ$</p> <p>VLM: range: 0-170 klux; spectral sensitivity 360nm to 760nm; signal output 0V to 2V; absolute error $<10\%$; operating temperature -20° to $+60^\circ$</p>
Sky scanner (MS321LR)	Specifications
 <p>http://eko-usa.com/</p>	<p>Luminance: Sensitivity 50 kcd.m^{-2}; Resolution 15 cd.m^{-2}; Entire sky scanning time: 4 min/145 points, resolution (angle): 0.0036°, accuracy (angle): 0.2°</p> <p>Radiance: sensitivity: $300 \text{ W.m}^{-2}.\text{sr}^{-1}$, resolution: $1.0 \text{ W.m}^{-2}.\text{sr}^{-1}$, entire sky scanning time: 4 min/145 points, resolution (angle): 0.0036°, accuracy (angle): 0.2°</p>
Fisheye camera (LMK 98-4)	Specifications
	<p>Luminance: Standard resolution $1380 \times 1030 \text{ Pixel}$; Higher resolution $2448 \times 2050 \text{ Pixel}$, $4008 \times 2672 \text{ Pixel}$, $4008 \times 4008 \text{ Pixel}$; Resolution (dynamic) Single picture measurement: 1:1100 ($\sim 61 \text{ dB}$); Multi picture measurement: 1:3600 ($\sim 71 \text{ dB}$); High Dynamic measurement 1:10000000 ($\sim 140 \text{ dB}$); A/D conversion 12/14 Bit; Measurement time from 1 to 15 sec for different luminance values depending on adjusted exposure time; Accuracy: $\text{DL} < 3 \%$ (for standard illuminant A); $\text{D}_{x,y} < 0.0020$ (for standard illuminant A)</p>

Table 0-2. Recorded climate data for Vienna city from 1971 to 2000

	Jan	Feb	Mar	Apr	May	Jun	Jul	Aug	Sep	Oct	Nov	Dec	Year
Rec. Hi °C	16.7	19.1	25.5	27.8	30.7	35.9	36	37	31.1	26.4	20.8	16.1	37
Avg. Hi °C	2.9	5.1	10.3	15.2	20.5	23.4	25.6	25.4	20.3	14.2	7.5	4	14.5
Daily Avg. °C	0.1	1.6	5.7	10	15.2	18.2	20.2	19.8	15.3	9.9	4.6	1.5	10.2
Avg. L °C	-2.0	-0.9	2.4	5.8	10.5	13.5	15.4	15.3	11.7	7	2.4	-0.5	6.7
Rec. L °C	-19.6	-17.2	-15.3	-2.7	1	4.8	8.4	7	3.1	-4.5	-9.6	-18.1	-19.6
PP. mm	37.2	39.4	46.1	51.7	61.8	70.2	68.2	57.8	53.5	40	50	44.4	620.3
SF cm	18.6	15.6	8.3	1.5	0	0	0	0	0	0	7.9	16.4	68.3
APD ¹	7.3	7.6	8.3	7.5	8.5	9.1	9	8	7	6	8.3	8.2	94.8
ASD ²	13.9	10	4	0.4	0	0	0	0	0	0	2.7	8.3	39.3
MSSH ³	60.9	90.1	131.5	173.8	228	222.8	241.8	239.2	167.6	131.2	65.5	52	1804.4

¹ Average precipitation days

² Average snowy days

³ Monthly sunshine hours

Appendix B – Perez Look-up table

Perez look-up table consists of 252 rows and 6 columns, where each array is a coefficient to be multiplied by Maxwell DISC beam irradiance. In order to derive the coefficient for each time step, four insolation condition parameters must be calculated, which are adjusted Clearness index (K'_t) that represents meteorologically similar conditions irrespective of the position of the sun. Z is the solar zenith angle, $\Delta K'_t$ stability index and W as atmospheric precipitable water (See *Table 3-2*).

With all these information, the index of Perez coefficient within the matrix can be calculated with the suggested formula:

$Bin_K'_t$ = number of bin in the *Table 3-2* for the range of K'_t

Bin_Z = number of bin in the *Table 3-2* for the range of Z

$Bin_ \Delta K'_t$ = number of bin in the *Table 3-2* for the range of $\Delta K'_t$

Bin_W = number of bin in the *Table 3-2* for the range of W

Finally:

Row's number = $((Bin_Z - 1) * 6 + Bin_K'_t) * 6 + Bin_ \Delta K'_t$

Column's number = Bin_W

Table 0-1. Perez Look-up Table

Row number ↓	Column number→	1	2	3	4	5
1	1	0.38523	0.38523	0.38523	0.46288	0.31744
2	2	0.33839	0.33839	0.22127	0.31673	0.50365
3	3	0.23568	0.23568	0.24128	0.15783	0.26944
4	4	0.83013	0.83013	0.17197	0.84107	0.45737
5	5	0.54801	0.54801	0.478	0.96688	1.03637
6	6	0.54801	0.54801	1	3.01237	1.97654

7	7	0.58269	0.58269	0.22972	0.89271	0.56995
8	1	0.13128	0.13128	0.38546	0.51107	0.12794
9	2	0.22371	0.22371	0.19356	0.30456	0.19394
10	3	0.22997	0.22997	0.27502	0.31273	0.24461
11	4	0.0901	0.18458	0.2605	0.68748	0.57944
12	5	0.13153	0.13153	0.37019	1.38035	1.05227
13	6	1.11625	1.11625	0.92803	3.52549	2.31692
14	7	0.0901	0.237	0.30004	0.81247	0.66497
15	1	0.58751	0.13	0.4	0.53721	0.83249
16	2	0.30621	0.12983	0.20446	0.5	0.68164
17	3	0.22402	0.26062	0.33408	0.50104	0.35047
18	4	0.42154	0.75397	0.75066	3.70684	0.98379
19	5	0.70668	0.37353	1.24567	0.86486	1.99263
20	6	4.8644	0.11739	0.26518	0.35918	3.31082
21	7	0.39208	0.49329	0.65156	1.93278	0.89873
22	1	0.12697	0.12697	0.12697	0.12697	0.12697
23	2	0.81082	0.81082	0.81082	0.81082	0.81082
24	3	3.24168	2.5	2.29144	2.29144	2.29144
25	4	4	3	2	0.97543	1.96557
26	5	12.49417	12.49417	8	5.08352	8.79239
27	6	21.74424	21.74424	21.74424	21.74424	21.74424
28	7	3.24168	12.49417	1.62076	1.37525	2.33162
29	1	0.12697	0.12697	0.12697	0.12697	0.12697
30	2	0.81082	0.81082	0.81082	0.81082	0.81082
31	3	3.24168	2.5	2.29144	2.29144	2.29144
32	4	4	3	2	0.97543	1.96557
33	5	12.49417	12.49417	8	5.08352	8.79239
34	6	21.74424	21.74424	21.74424	21.74424	21.74424
35	7	3.24168	12.49417	1.62076	1.37525	2.33162
36	1	0.12697	0.12697	0.12697	0.12697	0.12697
37	2	0.81082	0.81082	0.81082	0.81082	0.81082
38	3	3.24168	2.5	2.29144	2.29144	2.29144
39	4	4	3	2	0.97543	1.96557
40	5	12.49417	12.49417	8	5.08352	8.79239
41	6	21.74424	21.74424	21.74424	21.74424	21.74424
42	7	3.24168	12.49417	1.62076	1.37525	2.33162
43	1	0.33744	0.33744	0.96911	1.09719	1.11608
44	2	0.33744	0.33744	0.96911	1.11603	0.6239
45	3	0.33744	0.33744	1.53059	1.02442	0.90848
46	4	0.58404	0.58404	0.84725	0.91494	1.2893

47	5	0.33744	0.33744	0.31024	1.43502	1.85283
48	6	0.33744	0.33744	1.01501	1.09719	2.11723
49	7	0.33744	0.33744	0.96911	1.14573	1.4764
50	1	0.3	0.3	0.7	1.1	0.79694
51	2	0.21987	0.21987	0.52653	0.80961	0.6493
52	3	0.38665	0.38665	0.11932	0.57612	0.68546
53	4	0.74673	0.39983	0.47097	0.98653	0.78537
54	5	0.57542	0.9367	1.6492	1.49584	1.33559
55	6	1.31967	4.00257	1.27639	2.64455	2.51867
56	7	0.66519	0.67891	1.01236	1.19994	0.98658
57	1	0.37887	0.97406	0.5	0.49188	0.66529
58	2	0.10521	0.26347	0.40704	0.55346	0.58259
59	3	0.3129	0.34524	1.14418	0.85479	0.61228
60	4	0.11907	0.36512	0.56052	0.79372	0.8026
61	5	0.78161	0.83739	1.27042	1.53798	1.29295
62	6	1.15229	1.15229	1.49208	1.24537	2.1771
63	7	0.42466	0.52955	0.96691	1.03346	0.95873
64	1	0.31059	0.71441	0.25245	0.5	0.6076
65	2	0.97519	0.36342	0.5	0.4	0.5028
66	3	0.17558	0.19625	0.47636	1.07247	0.49051
67	4	0.71928	0.69862	0.65777	1.19084	0.68111
68	5	0.42624	1.46484	0.67855	1.15773	0.97843
69	6	2.50112	1.78913	1.38709	2.39418	2.39418
70	7	0.49164	0.67761	0.68561	1.0824	0.73541
71	1	0.597	0.5	0.3	0.31005	0.41351
72	2	0.31479	0.33631	0.4	0.4	0.44246
73	3	0.16651	0.46044	0.55257	1	0.46161
74	4	0.40102	0.55911	0.40363	1.01671	0.67149
75	5	0.40036	0.75083	0.84264	1.8026	1.02383
76	6	3.3153	1.51038	2.44365	1.63882	2.13399
77	7	0.53079	0.74585	0.69305	1.45804	0.8045
78	1	0.597	0.5	0.3	0.31005	0.80092
79	2	0.31479	0.33631	0.4	0.4	0.23704
80	3	0.16651	0.46044	0.55257	1	0.58199
81	4	0.40102	0.55911	0.40363	1.01671	0.89857
82	5	0.40036	0.75083	0.84264	1.8026	3.40039
83	6	3.3153	1.51038	2.44365	1.63882	2.50878
84	7	0.20434	1.15774	2.00308	2.62208	1.40938
85	1	1.24221	1.24221	1.24221	1.24221	1.24221
86	2	0.05698	0.05698	0.65699	0.65699	0.92516

87	3	0.08909	0.08909	1.04043	1.23248	1.2053
88	4	1.05385	1.05385	1.39969	1.08464	1.23334
89	5	1.15154	1.15154	1.11829	1.53164	1.41184
90	6	1.49498	1.49498	1.7	1.80081	1.6716
91	7	1.01845	1.01845	1.1536	1.32189	1.29467
92	1	0.7	0.7	1.02346	0.7	0.94583
93	2	0.8863	0.8863	1.33362	0.8	1.06662
94	3	0.90218	0.90218	0.95433	1.12669	1.09731
95	4	1.0953	1.07506	1.17649	1.13947	1.09611
96	5	1.20166	1.20166	1.4382	1.25628	1.19806
97	6	1.52585	1.52585	1.86916	1.98541	1.91159
98	7	1.28822	1.08281	1.28637	1.16617	1.11933
99	1	0.6	1.02991	0.85989	0.55	0.8136
100	2	0.60445	1.02991	0.85989	0.6567	0.92884
101	3	0.45585	0.75058	0.80493	0.823	0.911
102	4	0.52658	0.93231	0.90862	0.98352	0.98809
103	5	1.03611	1.10069	0.84838	1.03527	1.04238
104	6	1.04844	1.65272	0.9	2.35041	1.08295
105	7	0.81741	0.97616	0.8613	0.97478	1.00458
106	1	0.78211	0.56428	0.6	0.6	0.66574
107	2	0.89448	0.68073	0.54199	0.8	0.66914
108	3	0.48746	0.81895	0.84183	0.87254	0.70904
109	4	0.70931	0.87278	0.90848	0.95329	0.84435
110	5	0.86392	0.94777	0.87622	1.07875	0.93691
111	6	1.28035	0.86672	0.76979	1.07875	0.97513
112	7	0.72542	0.86997	0.86881	0.95119	0.82922
113	1	0.79175	0.65404	0.48317	0.409	0.59718
114	2	0.56614	0.94899	0.97182	0.65357	0.71855
115	3	0.64871	0.63773	0.87051	0.8606	0.6943
116	4	0.63763	0.76761	0.92567	0.99031	0.84767
117	5	0.73638	0.94606	1.11759	1.02934	0.94702
118	6	1.18097	0.85	1.05	0.95	0.88858
119	7	0.70056	0.80144	0.96197	0.90614	0.82388
120	1	0.5	0.5	0.58677	0.47055	0.62979
121	2	0.5	0.5	1.05622	1.26014	0.65814
122	3	0.5	0.5	0.63183	0.84262	0.58278
123	4	0.55471	0.73473	0.98582	0.91564	0.89826
124	5	0.71251	1.20599	0.90951	1.07826	0.88561
125	6	1.89926	1.55971	1	1.15	1.12039
126	7	0.65388	0.79312	0.90332	0.94407	0.79613

127	1	1	1	1.05	1.17038	1.17809
128	2	0.96058	0.96058	1.05953	1.17903	1.13169
129	3	0.87147	0.87147	0.99586	1.14191	1.1146
130	4	1.20159	1.20159	0.99361	1.10938	1.12632
131	5	1.06501	1.06501	0.82866	0.93997	1.01793
132	6	1.06501	1.06501	0.62369	1.11962	1.13226
133	7	1.07157	1.07157	0.95807	1.11413	1.12711
134	1	0.95	0.97339	0.85252	1.0922	1.09659
135	2	0.80412	0.91387	0.98099	1.09458	1.04242
136	3	0.73754	0.93597	0.99994	1.05649	1.05006
137	4	1.03298	1.03454	0.96846	1.03208	1.01578
138	5	0.9	0.97721	0.94596	1.00884	0.96996
139	6	0.6	0.75	0.75	0.84471	0.8991
140	7	0.9268	0.96503	0.96852	1.04491	1.03231
141	1	0.85	1.02971	0.9611	1.05567	1.0097
142	2	0.81853	0.96001	0.99645	1.08197	1.03647
143	3	0.76538	0.9535	0.94826	1.05211	1.00014
144	4	0.77561	0.90961	0.9278	0.9878	0.9521
145	5	1.00099	0.88188	0.87595	0.9491	0.89369
146	6	0.90237	0.87596	0.80799	0.94241	0.91792
147	7	0.85658	0.92827	0.94682	1.03226	0.97299
148	1	0.75	0.85793	0.9838	1.05654	0.98024
149	2	0.75	0.98701	1.01373	1.13378	1.03825
150	3	0.8	0.94738	1.01238	1.09127	0.99984
151	4	0.8	0.91455	0.90857	0.99919	0.91523
152	5	0.77854	0.80059	0.79907	0.90218	0.85156
153	6	0.68019	0.31741	0.50768	0.38891	0.64671
154	7	0.79492	0.91278	0.96083	1.05711	0.94795
155	1	0.75	0.83389	0.86753	1.05989	0.93284
156	2	0.9797	0.97147	0.99551	1.06849	1.03015
157	3	0.85885	0.98792	1.04322	1.1087	1.0449
158	4	0.8024	0.95511	0.91166	1.04507	0.94447
159	5	0.88489	0.76621	0.88539	0.85907	0.81819
160	6	0.61568	0.7	0.85	0.62462	0.6693
161	7	0.83557	0.94615	0.97709	1.04935	0.97997
162	1	0.68922	0.8096	0.9	0.7895	0.85399
163	2	0.85466	0.85284	0.9382	0.92311	0.95501
164	3	0.9386	0.93298	1.01039	1.04395	1.04164
165	4	0.84362	0.9813	0.95159	0.9461	0.96633
166	5	0.69474	0.81469	0.57265	0.4	0.72683

167	6	0.21137	0.67178	0.41634	0.29729	0.49805
168	7	0.84354	0.88233	0.91176	0.89842	0.96021
169	1	1.05488	1.07521	1.06846	1.15337	1.06922
170	2	1	1.06222	1.01347	1.08817	1.0462
171	3	0.88509	0.99353	0.94259	1.05499	1.01274
172	4	0.92	0.95	0.97872	1.02028	0.98444
173	5	0.85	0.9085	0.83994	0.98557	0.96218
174	6	0.8	0.8	0.81008	0.95	0.96155
175	7	1.03859	1.0632	1.03444	1.11278	1.0378
176	1	1.01761	1.02836	1.05896	1.13318	1.04562
177	2	0.92	0.99897	1.03359	1.08903	1.02206
178	3	0.91237	0.94993	0.97977	1.02042	0.98177
179	4	0.84716	0.9353	0.93054	0.95505	0.94656
180	5	0.88026	0.86711	0.87413	0.97265	0.88342
181	6	0.62715	0.62715	0.7	0.77407	0.84513
182	7	0.9737	1.00624	1.02619	1.07196	1.01724
183	1	1.02871	1.01757	1.0259	1.08179	1.02424
184	2	0.92498	0.9855	1.0141	1.09221	0.99961
185	3	0.82857	0.93492	0.99495	1.02459	0.94971
186	4	0.90081	0.90133	0.92883	0.97957	0.9131
187	5	0.76103	0.84515	0.80536	0.93679	0.85346
188	6	0.6264	0.54675	0.7305	0.85	0.68905
189	7	0.95763	0.98548	0.99179	1.05022	0.9879
190	1	0.99273	0.99388	1.01715	1.05912	1.01745
191	2	0.97561	0.98716	1.02682	1.07544	1.00725
192	3	0.87109	0.93319	0.97469	0.97984	0.95273
193	4	0.82875	0.86809	0.83492	0.90551	0.87153
194	5	0.78154	0.78247	0.76791	0.76414	0.79589
195	6	0.74346	0.69339	0.51487	0.63015	0.71566
196	7	0.93476	0.95787	0.95964	0.97251	0.98164
197	1	0.96584	0.94124	0.9871	1.02254	1.01116
198	2	0.98863	0.99477	0.97659	0.95	1.03484
199	3	0.9582	1.01808	0.97448	0.92	0.98987
200	4	0.81172	0.86909	0.81202	0.85	0.82105
201	5	0.68203	0.67948	0.63245	0.74658	0.73855
202	6	0.66829	0.44586	0.5	0.67892	0.69651
203	7	0.92694	0.95335	0.95905	0.87621	0.99149
204	1	0.94894	0.99776	0.85	0.82652	0.99847
205	2	1.01786	0.97	0.85	0.7	0.98856
206	3	1	0.95	0.85	0.60624	0.94726

207	4	1	0.74614	0.75174	0.59839	0.72523
208	5	0.92221	0.5	0.3768	0.51711	0.54863
209	6	0.5	0.45	0.42997	0.40449	0.53994
210	7	0.96043	0.88163	0.77564	0.59635	0.93768
211	1	1.03	1.04	1	1	1.04951
212	2	1.05	0.99	0.99	0.95	0.99653
213	3	1.05	0.99	0.99	0.82	0.97194
214	4	1.05	0.79	0.88	0.82	0.95184
215	5	1	0.53	0.44	0.71	0.92873
216	6	0.54	0.47	0.5	0.55	0.77395
217	7	1.03827	0.92018	0.91093	0.82114	1.03456
218	1	1.04102	0.99752	0.9616	1	1.03578
219	2	0.94803	0.98	0.9	0.95036	0.97746
220	3	0.95	0.97725	0.86927	0.8	0.95168
221	4	0.95187	0.85	0.74877	0.7	0.88385
222	5	0.9	0.82319	0.72745	0.6	0.83987
223	6	0.85	0.80502	0.69231	0.5	0.78841
224	7	1.01009	0.89527	0.77303	0.81628	1.01168
225	1	1.02245	1.0046	0.98365	1	1.03294
226	2	0.94396	0.99924	0.98392	0.90599	0.97815
227	3	0.93624	0.94648	0.85	0.85	0.93032
228	4	0.81642	0.885	0.64495	0.81765	0.86531
229	5	0.74296	0.76569	0.56152	0.7	0.82714
230	6	0.64387	0.59671	0.47446	0.6	0.6512
231	7	0.97174	0.94056	0.71488	0.86438	1.00165
232	1	0.99526	0.97701	1	1	1.03525
233	2	0.93981	0.97525	0.93998	0.95	0.98255
234	3	0.87687	0.87944	0.85	0.9	0.91781
235	4	0.87348	0.87345	0.75147	0.85	0.86304
236	5	0.76147	0.70236	0.63877	0.75	0.78312
237	6	0.73408	0.65	0.6	0.65	0.71566
238	7	0.94216	0.9191	0.77034	0.73117	0.99518
239	1	0.95256	0.91678	0.92	0.9	1.00588
240	2	0.92862	0.99442	0.9	0.9	0.98372
241	3	0.91307	0.85	0.85	0.8	0.92428
242	4	0.86809	0.80717	0.82355	0.6	0.84452
243	5	0.76957	0.71987	0.65	0.55	0.7335
244	6	0.58025	0.65	0.6	0.5	0.62885
245	7	0.90477	0.85265	0.70837	0.49373	0.94903
246	1	0.91197	0.8	0.8	0.8	0.95632

247	2	0.91262	0.68261	0.75	0.7	0.95011
248	3	0.65345	0.65933	0.7	0.6	0.85611
249	4	0.64844	0.6	0.64112	0.5	0.69578
250	5	0.57	0.55	0.5988	0.4	0.56015
251	6	0.47523	0.5	0.51864	0.33997	0.52023
252	7	0.74344	0.59219	0.60306	0.31693	0.79439

Appendix C

Periodic interval

```
% calculate the average of data based on the intervals
%
% function [values_periodic]=periodic_interval(values,time,Interval,status,mode,Startdate,Enddate)
%
% DESCRIPTION
%
% periodic_interval function calculates the average of data base on
% given interval. Three methods are available for dealing with intervals
% with no measurement:
%
% 1) Interpolation between previous and next valid measurement
% 2) repeating previous measurement
% 3) removing empty intervals
%
% Moreover there are two modes for averaging between the intervals:
% 1) mid-time of last interval to mid-time of next interval
% 2) start-time of last interval to start-time of next interval
%
% INPUT ARGUMENTS
%
% values          Input data (Can be several columns)
% time            MATLAB time serial number of the input data
% Interval        Desired interval to be used in data
% status          Type of the averaging ('Interpolate','LastValue','RemoveGaps')
% mode            Modes for averaging between the intervals ('MiddleToMiddle','StartToStart')
% Startdate       Start date of the measurement (optional)
% Enddate         End date of the measurement (optional)
%
% OUTPUT ARGUMENTS
%
% values_periodic nxm dimension matrix which n is number of measurements
% and m is MATLAB time serial number plus number of datasets
%
function [values_periodic]=periodic_interval(values,time,Interval,status,mode,varargin)
if nargin==7
    Startdate=varargin{1};
    Enddate=varargin{2};
elseif nargin==5
    Startdate=floor(time(1,1));
    Enddate=ceil(time(end,1));
else
    error('Wrong number of Arguments for Start or End date!');
end
[i,j]=size(values);
if i==1
    values=values';
    time=time';
end
if strcmpi(mode,'StartToStart')
    Interv_mode=Interval/2;
else
    Interv_mode=0;
end
looptime=Startdate;
last_value=NaN*ones(1,j);
counter=0;
while looptime<Enddate
    counter=counter+1;
    ind=(time>looptime-Interval/2+Interv_mode)&(time<=looptime+Interval/2+Interv_mode);
    if sum(ind)>0
        last_value=values(ind,:);
        values_periodic(counter,2:j+1)=mean(last_value,1);
        values_periodic(counter,1)=looptime;
        looptime=looptime+Interval;
    elseif strcmpi(status,'interpolate')
        ind1=0;
        ii=0;
        looptime1=looptime;
        while sum(ind1)==0&looptime1<Enddate
            looptime1=looptime1+Interval;
            ind1=(time>looptime1-Interval/2+Interv_mode)&(time<=looptime1+Interval/2+Interv_mode);
            ii=ii+1;
        end
        for i=ii:-1:1
            values_periodic(counter+ii-i,2:j+1)=(last_value(end,:)*(i)+(ii-i+1)*(mean(values(ind1,:),1)))/(ii+1);
            values_periodic(counter+ii-i,1)=looptime;
            looptime=looptime+Interval;
        end
        counter=counter+ii-i;
    elseif strcmpi(status,'LastValue')
        values_periodic(counter,2:j+1)=last_value(end,:);
        looptime=looptime+Interval;
        values_periodic(counter,1)=looptime;
    elseif strcmpi(status,'RemoveGaps')
        values_periodic(counter,2:j+1)=NaN;
        values_periodic(counter,1)=looptime;
        looptime=looptime+Interval;
    end
end
values_periodic(isnan(values_periodic(:,2)),:)=[];
end
```

NREL sun altitude

```
% function solar_altitude_angle=nrel_solar_alt(longitude,latitude,time)
%
% This function is to calculate solar altitude
%
% Source:          http://www.nrel.gov/docs/fy08osti/34302.pdf
%
% inputs:
% 1) longitude      double    in degree    east positive
% 2) latitude       double    in degree    north positive
% 3) time           double    date number  (UTC time)
%
% output:
% 1) solar_altitude_angle  double    in radian
% Example:
% [0.2822]=nrel_solar_alt(48,16,datenum('21-06-2013 13:00:00'))
%
function solar_altitude_angle=nrel_solar_alt(longitude,latitude,time)
if nargin~=3
    error('Wrong number of Arguments!');
end

if latitude<=-90 | latitude>90
    warning('Latitude value exceeds limits (-90°, +90°)!');
end

time_zone=0;
base=datenum('1899-12-30','yyyy-mm-dd');
date=floor(time)-base;
time_local=time-floor(time);
julian_day=date+2415018.5+time_local-time_zone/24;
Julian_Century=(julian_day-2451545)/36525;
Geom_mean_long_sun=mod((280.46646+Julian_Century.*(36000.76983 + Julian_Century*0.0003032)),360);
Geom_mean_anom_sun=357.52911+Julian_Century.*(35999.05029 - 0.0001537*Julian_Century);
Eccent_earth_orbit=0.016708634-Julian_Century.*(0.000042037+0.0000001267*Julian_Century);
sun_eq_ctr=sin(Geom_mean_anom_sun*pi/180).*(1.914602-Julian_Century.*(0.004817+0.000014*Julian_Century))+...
    sin(2*Geom_mean_anom_sun*pi/180).*(0.019993-0.000101*Julian_Century)+sin(3*Geom_mean_anom_sun*pi/180)*0.000289;
sun_true_long=sun_eq_ctr+Geom_mean_long_sun;
sun_true_anom=sun_eq_ctr+Geom_mean_anom_sun;
sun_rad_vector=(1.000001018*(1-Eccent_earth_orbit).*(1+Eccent_earth_orbit))./(1+Eccent_earth_orbit.*cos(sun_true_anom*pi/180));
sun_app_long=sun_true_long-0.00569-0.00478*sin((125.04-1934.136*Julian_Century)*pi/180);
mean_obliq_ecliptic=23+(26+((21.448-Julian_Century.*(46.815+Julian_Century.*(0.00059-Julian_Century*0.001813)))))/60)/60;
obliq_corr=mean_obliq_ecliptic+0.00256*cos((125.04-1934.136*Julian_Century)*pi/180);
sun_rt_ascen=180/pi*(atan2(cos(obliq_corr*pi/180).*sin(sun_app_long*pi/180),cos(sun_app_long*pi/180)));
sun_decl=180/pi*(asin(sin(obliq_corr*pi/180).*sin(sun_app_long*pi/180)));
var_y=tan(obliq_corr/2*pi/180).*tan(obliq_corr/2*pi/180);
equation_time=4*180/pi*(var_y.*sin(2*Geom_mean_long_sun*pi/180)-2*Eccent_earth_orbit.*sin(Geom_mean_anom_sun*pi/180)+...
    4*Eccent_earth_orbit.*var_y.*sin(Geom_mean_anom_sun*pi/180).*cos(2*Geom_mean_long_sun*pi/180)-...
    0.5*var_y.*var_y.*sin(4*Geom_mean_long_sun*pi/180)-1.25*Eccent_earth_orbit.*Eccent_earth_orbit.*sin(
    2*Geom_mean_anom_sun*pi/180));
HA_sunrise=180/pi*(acos(cos(90.833*pi/180)./(cos(latitude*pi/180).*cos(sun_decl*pi/180)))-...
    tan(latitude*pi/180).*tan(sun_decl*pi/180));
solar_noon_LST=(720-4*longitude-equation_time+time_zone*60)/1440;
sunrise_time_LST=solar_noon_LST-HA_sunrise*4/1440;
sunset_time_LST=solar_noon_LST+HA_sunrise*4/1440;
true_solar_time=mode(time_local*1440+equation_time+4*longitude-60*time_zone,1440);
if true_solar_time/4<0
    hour_angle=true_solar_time/4+180;
else
    hour_angle=true_solar_time/4-180;
end
solar_zenith_angle=180/pi*(acos(sin(latitude*pi/180).*sin(sun_decl*pi/180)+...
    cos(latitude*pi/180)*cos(sun_decl*pi/180).*cos(hour_angle*pi/180)));
solar_altitude_angle=(90-solar_zenith_angle)*pi/180;
solar_altitude_angle(solar_altitude_angle<0)=0;
```

Appendix D – Skyscanner.cal

```
{RCSid $Id: Skyscanner.cal,v 1.1 2014/07/25 12:30:00 Vazifeh, E. & Mahdavi, A.
}

{
Clear Sky Radiance Distribution.

Additional arguments required for calculation of skybright:
    A1 till A145 - Radiance of the Patch
    A146, A147, A148      - sun direction
}

{skybright = wmean((Dz+1.01)^10, intersky, (Dz+1.01)^-10, A1 );
wmean(a, x, b, y) = (a*x+b*y)/(a+b);}

skybright          =          1.5708*if(5.500-acos((Dx*-0.0000+Dy*-
0.9945+Dz*0.1045)/(sqrt((Dx)^2+(Dy)^2+(Dz)^2))*
sqrt((-0.0000)^2+(-0.9945)^2+(0.1045)^2))*180/PI,19.1116,if(5.500-acos((Dx*-
0.2068+Dy*-0.9728+Dz*0.1045)
/(sqrt((Dx)^2+(Dy)^2+(Dz)^2))*sqrt((-0.2068)^2+(-
0.9728)^2+(0.1045)^2))*180/PI,14.8160,
if(5.500-acos((Dx*-0.4045+Dy*-0.9085+Dz*0.1045)/(sqrt((Dx)^2+(Dy)^2+(Dz)^2)
*sqrt((-0.4045)^2+(-0.9085)^2+(0.1045)^2))*180/PI,15.7091,
if(5.500-acos((Dx*-0.5846+Dy*-0.8046+Dz*0.1045)/(sqrt((Dx)^2+(Dy)^2+(Dz)^2)
*sqrt((-0.5846)^2+(-0.8046)^2+(0.1045)^2))*180/PI,17.7006,
if(5.500-acos((Dx*-0.7391+Dy*-0.6655+Dz*0.1045)/(sqrt((Dx)^2+(Dy)^2+(Dz)^2)
*sqrt((-0.7391)^2+(-0.6655)^2+(0.1045)^2))*180/PI,21.5319,
if(5.500-acos((Dx*-0.8613+Dy*-0.4973+Dz*0.1045)/(sqrt((Dx)^2+(Dy)^2+(Dz)^2)
*sqrt((-0.8613)^2+(-0.4973)^2+(0.1045)^2))*180/PI,28.2388,
if(5.500-acos((Dx*-0.9458+Dy*-0.3073+Dz*0.1045)/(sqrt((Dx)^2+(Dy)^2+(Dz)^2)
*sqrt((-0.9458)^2+(-0.3073)^2+(0.1045)^2))*180/PI,27.4350,
if(5.500-acos((Dx*-0.9891+Dy*-0.1040+Dz*0.1045)/(sqrt((Dx)^2+(Dy)^2+(Dz)^2)
*sqrt((-0.9891)^2+(-0.1040)^2+(0.1045)^2))*180/PI,50.1279,
if(5.500-acos((Dx*-0.9891+Dy*0.1040+Dz*0.1045)/(sqrt((Dx)^2+(Dy)^2+(Dz)^2)
*sqrt((-0.9891)^2+(0.1040)^2+(0.1045)^2))*180/PI,73.1154,
if(5.500-acos((Dx*-0.9458+Dy*0.3073+Dz*0.1045)/(sqrt((Dx)^2+(Dy)^2+(Dz)^2)
*sqrt((-0.9458)^2+(0.3073)^2+(0.1045)^2))*180/PI,234.6089,
if(5.500-acos((Dx*-0.8613+Dy*0.4973+Dz*0.1045)/(sqrt((Dx)^2+(Dy)^2+(Dz)^2)
*sqrt((-0.8613)^2+(0.4973)^2+(0.1045)^2))*180/PI,0.0000
,if(5.500-acos((Dx*-0.7391+Dy*0.6655+Dz*0.1045)/(sqrt((Dx)^2+(Dy)^2+(Dz)^2)
*sqrt((-0.7391)^2+(0.6655)^2+(0.1045)^2))*180/PI,117.4473
,if(5.500-acos((Dx*-0.5846+Dy*0.8046+Dz*0.1045)/(sqrt((Dx)^2+(Dy)^2+(Dz)^2)
*sqrt((-0.5846)^2+(0.8046)^2+(0.1045)^2))*180/PI,44.5730
```

```
,if(5.500-acos((Dx*-0.4045+Dy*0.9085+Dz*0.1045)/(sqrt((Dx)^2+(Dy)^2+(Dz)^2)
*sqrt((-0.4045)^2+(0.9085)^2+(0.1045)^2)))*180/PI,38.3126
,if(5.500-acos((Dx*-0.2068+Dy*0.9728+Dz*0.1045)/(sqrt((Dx)^2+(Dy)^2+(Dz)^2)
*sqrt((-0.2068)^2+(0.9728)^2+(0.1045)^2)))*180/PI,30.9627
,if(5.500-acos((Dx*-0.0000+Dy*0.9945+Dz*0.1045)/(sqrt((Dx)^2+(Dy)^2+(Dz)^2)
*sqrt((-0.0000)^2+(0.9945)^2+(0.1045)^2)))*180/PI,25.1488
,if(5.500-acos((Dx*0.2068+Dy*0.9728+Dz*0.1045)/(sqrt((Dx)^2+(Dy)^2+(Dz)^2)
*sqrt((0.2068)^2+(0.9728)^2+(0.1045)^2)))*180/PI,19.9690
,if(5.500-acos((Dx*0.4045+Dy*0.9085+Dz*0.1045)/(sqrt((Dx)^2+(Dy)^2+(Dz)^2)
*sqrt((0.4045)^2+(0.9085)^2+(0.1045)^2)))*180/PI,17.1737
,if(5.500-acos((Dx*0.5846+Dy*0.8046+Dz*0.1045)/(sqrt((Dx)^2+(Dy)^2+(Dz)^2)
*sqrt((0.5846)^2+(0.8046)^2+(0.1045)^2)))*180/PI,15.6912
,if(5.500-acos((Dx*0.7391+Dy*0.6655+Dz*0.1045)/(sqrt((Dx)^2+(Dy)^2+(Dz)^2)
*sqrt((0.7391)^2+(0.6655)^2+(0.1045)^2)))*180/PI,15.4322
,if(5.500-acos((Dx*0.8613+Dy*0.4973+Dz*0.1045)/(sqrt((Dx)^2+(Dy)^2+(Dz)^2)
*sqrt((0.8613)^2+(0.4973)^2+(0.1045)^2)))*180/PI,15.7269
,if(5.500-acos((Dx*0.9458+Dy*0.3073+Dz*0.1045)/(sqrt((Dx)^2+(Dy)^2+(Dz)^2)
*sqrt((0.9458)^2+(0.3073)^2+(0.1045)^2)))*180/PI,17.8614
,if(5.500-acos((Dx*0.9891+Dy*0.1040+Dz*0.1045)/(sqrt((Dx)^2+(Dy)^2+(Dz)^2)
*sqrt((0.9891)^2+(0.1040)^2+(0.1045)^2)))*180/PI,18.1382
,if(5.500-acos((Dx*0.9891+Dy*-0.1040+Dz*0.1045)/(sqrt((Dx)^2+(Dy)^2+(Dz)^2)
*sqrt((0.9891)^2+(-0.1040)^2+(0.1045)^2)))*180/PI,20.0583
,if(5.500-acos((Dx*0.9458+Dy*-0.3073+Dz*0.1045)/(sqrt((Dx)^2+(Dy)^2+(Dz)^2)
*sqrt((0.9458)^2+(-0.3073)^2+(0.1045)^2)))*180/PI,21.5587
,if(5.500-acos((Dx*0.8613+Dy*-0.4973+Dz*0.1045)/(sqrt((Dx)^2+(Dy)^2+(Dz)^2)
*sqrt((0.8613)^2+(-0.4973)^2+(0.1045)^2)))*180/PI,21.2997
,if(5.500-acos((Dx*0.7391+Dy*-0.6655+Dz*0.1045)/(sqrt((Dx)^2+(Dy)^2+(Dz)^2)
*sqrt((0.7391)^2+(-0.6655)^2+(0.1045)^2)))*180/PI,19.6118
,if(5.500-acos((Dx*0.5846+Dy*-0.8046+Dz*0.1045)/(sqrt((Dx)^2+(Dy)^2+(Dz)^2)
*sqrt((0.5846)^2+(-0.8046)^2+(0.1045)^2)))*180/PI,16.7361
,if(5.500-acos((Dx*0.4045+Dy*-0.9085+Dz*0.1045)/(sqrt((Dx)^2+(Dy)^2+(Dz)^2)
*sqrt((0.4045)^2+(-0.9085)^2+(0.1045)^2)))*180/PI,16.3431
,if(5.500-acos((Dx*0.2068+Dy*-0.9728+Dz*0.1045)/(sqrt((Dx)^2+(Dy)^2+(Dz)^2)
*sqrt((0.2068)^2+(-0.9728)^2+(0.1045)^2)))*180/PI,15.9323
,if(5.500-acos((Dx*0.1977+Dy*-0.9303+Dz*0.3090)/(sqrt((Dx)^2+(Dy)^2+(Dz)^2)
*sqrt((0.1977)^2+(-0.9303)^2+(0.3090)^2)))*180/PI,11.6188
,if(5.500-acos((Dx*0.3868+Dy*-0.8688+Dz*0.3090)/(sqrt((Dx)^2+(Dy)^2+(Dz)^2)
*sqrt((0.3868)^2+(-0.8688)^2+(0.3090)^2)))*180/PI,12.3243
,if(5.500-acos((Dx*0.5590+Dy*-0.7694+Dz*0.3090)/(sqrt((Dx)^2+(Dy)^2+(Dz)^2)
*sqrt((0.5590)^2+(-0.7694)^2+(0.3090)^2)))*180/PI,13.1370
,if(5.500-acos((Dx*0.7068+Dy*-0.6364+Dz*0.3090)/(sqrt((Dx)^2+(Dy)^2+(Dz)^2)
*sqrt((0.7068)^2+(-0.6364)^2+(0.3090)^2)))*180/PI,13.7711
,if(5.500-acos((Dx*0.8236+Dy*-0.4755+Dz*0.3090)/(sqrt((Dx)^2+(Dy)^2+(Dz)^2)
*sqrt((0.8236)^2+(-0.4755)^2+(0.3090)^2)))*180/PI,14.0569
```



```
, if(5.500-acos((Dx*0.9045+Dy*-0.2939+Dz*0.3090)/(sqrt((Dx)^2+(Dy)^2+(Dz)^2)
*sqrt((0.9045)^2+(-0.2939)^2+(0.3090)^2))) *180/PI, 14.0658
, if(5.500-acos((Dx*0.9458+Dy*-0.0994+Dz*0.3090)/(sqrt((Dx)^2+(Dy)^2+(Dz)^2)
*sqrt((0.9458)^2+(-0.0994)^2+(0.3090)^2))) *180/PI, 13.5657
, if(5.500-acos((Dx*0.9458+Dy*0.0994+Dz*0.3090)/(sqrt((Dx)^2+(Dy)^2+(Dz)^2)
*sqrt((0.9458)^2+(0.0994)^2+(0.3090)^2))) *180/PI, 12.8691
, if(5.500-acos((Dx*0.9045+Dy*0.2939+Dz*0.3090)/(sqrt((Dx)^2+(Dy)^2+(Dz)^2)
*sqrt((0.9045)^2+(0.2939)^2+(0.3090)^2))) *180/PI, 12.1011
, if(5.500-acos((Dx*0.8236+Dy*0.4755+Dz*0.3090)/(sqrt((Dx)^2+(Dy)^2+(Dz)^2)
*sqrt((0.8236)^2+(0.4755)^2+(0.3090)^2))) *180/PI, 11.6188
, if(5.500-acos((Dx*0.7068+Dy*0.6364+Dz*0.3090)/(sqrt((Dx)^2+(Dy)^2+(Dz)^2)
*sqrt((0.7068)^2+(0.6364)^2+(0.3090)^2))) *180/PI, 11.1366
, if(5.500-acos((Dx*0.5590+Dy*0.7694+Dz*0.3090)/(sqrt((Dx)^2+(Dy)^2+(Dz)^2)
*sqrt((0.5590)^2+(0.7694)^2+(0.3090)^2))) *180/PI, 11.1366
, if(5.500-acos((Dx*0.3868+Dy*0.8688+Dz*0.3090)/(sqrt((Dx)^2+(Dy)^2+(Dz)^2)
*sqrt((0.3868)^2+(0.8688)^2+(0.3090)^2))) *180/PI, 12.0921
, if(5.500-acos((Dx*0.1977+Dy*0.9303+Dz*0.3090)/(sqrt((Dx)^2+(Dy)^2+(Dz)^2)
*sqrt((0.1977)^2+(0.9303)^2+(0.3090)^2))) *180/PI, 14.0658
, if(5.500-acos((Dx*-0.0000+Dy*0.9511+Dz*0.3090)/(sqrt((Dx)^2+(Dy)^2+(Dz)^2)
*sqrt((-0.0000)^2+(0.9511)^2+(0.3090)^2))) *180/PI, 17.2541
, if(5.500-acos((Dx*-0.1977+Dy*0.9303+Dz*0.3090)/(sqrt((Dx)^2+(Dy)^2+(Dz)^2)
*sqrt((-0.1977)^2+(0.9303)^2+(0.3090)^2))) *180/PI, 21.9069
, if(5.500-acos((Dx*-0.3868+Dy*0.8688+Dz*0.3090)/(sqrt((Dx)^2+(Dy)^2+(Dz)^2)
*sqrt((-0.3868)^2+(0.8688)^2+(0.3090)^2))) *180/PI, 28.1674
, if(5.500-acos((Dx*-0.5590+Dy*0.7694+Dz*0.3090)/(sqrt((Dx)^2+(Dy)^2+(Dz)^2)
*sqrt((-0.5590)^2+(0.7694)^2+(0.3090)^2))) *180/PI, 34.1956
, if(5.500-acos((Dx*-0.7068+Dy*0.6364+Dz*0.3090)/(sqrt((Dx)^2+(Dy)^2+(Dz)^2)
*sqrt((-0.7068)^2+(0.6364)^2+(0.3090)^2))) *180/PI, 53.7180
, if(5.500-acos((Dx*-0.8236+Dy*0.4755+Dz*0.3090)/(sqrt((Dx)^2+(Dy)^2+(Dz)^2)
*sqrt((-0.8236)^2+(0.4755)^2+(0.3090)^2))) *180/PI, 135.1658
, if(5.500-acos((Dx*-0.9045+Dy*0.2939+Dz*0.3090)/(sqrt((Dx)^2+(Dy)^2+(Dz)^2)
*sqrt((-0.9045)^2+(0.2939)^2+(0.3090)^2))) *180/PI, 77.9469
, if(5.500-acos((Dx*-0.9458+Dy*0.0994+Dz*0.3090)/(sqrt((Dx)^2+(Dy)^2+(Dz)^2)
*sqrt((-0.9458)^2+(0.0994)^2+(0.3090)^2))) *180/PI, 43.9300
, if(5.500-acos((Dx*-0.9458+Dy*-0.0994+Dz*0.3090)/(sqrt((Dx)^2+(Dy)^2+(Dz)^2)
*sqrt((-0.9458)^2+(-0.0994)^2+(0.3090)^2))) *180/PI, 31.1859
, if(5.500-acos((Dx*-0.9045+Dy*-0.2939+Dz*0.3090)/(sqrt((Dx)^2+(Dy)^2+(Dz)^2)
*sqrt((-0.9045)^2+(-0.2939)^2+(0.3090)^2))) *180/PI, 23.4698
, if(5.500-acos((Dx*-0.8236+Dy*-0.4755+Dz*0.3090)/(sqrt((Dx)^2+(Dy)^2+(Dz)^2)
*sqrt((-0.8236)^2+(-0.4755)^2+(0.3090)^2))) *180/PI, 18.3168
, if(5.500-acos((Dx*-0.7068+Dy*-0.6364+Dz*0.3090)/(sqrt((Dx)^2+(Dy)^2+(Dz)^2)
*sqrt((-0.7068)^2+(-0.6364)^2+(0.3090)^2))) *180/PI, 14.6910
, if(5.500-acos((Dx*-0.5590+Dy*-0.7694+Dz*0.3090)/(sqrt((Dx)^2+(Dy)^2+(Dz)^2)
*sqrt((-0.5590)^2+(-0.7694)^2+(0.3090)^2))) *180/PI, 12.3779
```

```
,if(5.500-acos((Dx*-0.3868+Dy*-0.8688+Dz*0.3090)/(sqrt((Dx)^2+(Dy)^2+(Dz)^2)
*sqrt((-0.3868)^2+(-0.8688)^2+(0.3090)^2)))*180/PI,11.2169
,if(5.500-acos((Dx*-0.1977+Dy*-0.9303+Dz*0.3090)/(sqrt((Dx)^2+(Dy)^2+(Dz)^2)
*sqrt((-0.1977)^2+(-0.9303)^2+(0.3090)^2)))*180/PI,10.9311
,if(5.500-acos((Dx*-0.0000+Dy*-0.9511+Dz*0.3090)/(sqrt((Dx)^2+(Dy)^2+(Dz)^2)
*sqrt((-0.0000)^2+(-0.9511)^2+(0.3090)^2)))*180/PI,12.0118
,if(5.500-acos((Dx*-0.0000+Dy*-0.8660+Dz*0.5000)/(sqrt((Dx)^2+(Dy)^2+(Dz)^2)
*sqrt((-0.0000)^2+(-0.8660)^2+(0.5000)^2)))*180/PI,8.7610
,if(5.500-acos((Dx*-0.2241+Dy*-0.8365+Dz*0.5000)/(sqrt((Dx)^2+(Dy)^2+(Dz)^2)
*sqrt((-0.2241)^2+(-0.8365)^2+(0.5000)^2)))*180/PI,8.5645
,if(5.500-acos((Dx*-0.4330+Dy*-0.7500+Dz*0.5000)/(sqrt((Dx)^2+(Dy)^2+(Dz)^2)
*sqrt((-0.4330)^2+(-0.7500)^2+(0.5000)^2)))*180/PI,9.1004
,if(5.500-acos((Dx*-0.6124+Dy*-0.6124+Dz*0.5000)/(sqrt((Dx)^2+(Dy)^2+(Dz)^2)
*sqrt((-0.6124)^2+(-0.6124)^2+(0.5000)^2)))*180/PI,10.6275
,if(5.500-acos((Dx*-0.7500+Dy*-0.4330+Dz*0.5000)/(sqrt((Dx)^2+(Dy)^2+(Dz)^2)
*sqrt((-0.7500)^2+(-0.4330)^2+(0.5000)^2)))*180/PI,13.6461
,if(5.500-acos((Dx*-0.8365+Dy*-0.2241+Dz*0.5000)/(sqrt((Dx)^2+(Dy)^2+(Dz)^2)
*sqrt((-0.8365)^2+(-0.2241)^2+(0.5000)^2)))*180/PI,18.0132
,if(5.500-acos((Dx*-0.8660+Dy*0.0000+Dz*0.5000)/(sqrt((Dx)^2+(Dy)^2+(Dz)^2)
*sqrt((-0.8660)^2+(0.0000)^2+(0.5000)^2)))*180/PI,23.5055
,if(5.500-acos((Dx*-0.8365+Dy*0.2241+Dz*0.5000)/(sqrt((Dx)^2+(Dy)^2+(Dz)^2)
*sqrt((-0.8365)^2+(0.2241)^2+(0.5000)^2)))*180/PI,31.4717
,if(5.500-acos((Dx*-0.7500+Dy*0.4330+Dz*0.5000)/(sqrt((Dx)^2+(Dy)^2+(Dz)^2)
*sqrt((-0.7500)^2+(0.4330)^2+(0.5000)^2)))*180/PI,35.4459
,if(5.500-acos((Dx*-0.6124+Dy*0.6124+Dz*0.5000)/(sqrt((Dx)^2+(Dy)^2+(Dz)^2)
*sqrt((-0.6124)^2+(0.6124)^2+(0.5000)^2)))*180/PI,29.4802
,if(5.500-acos((Dx*-0.4330+Dy*0.7500+Dz*0.5000)/(sqrt((Dx)^2+(Dy)^2+(Dz)^2)
*sqrt((-0.4330)^2+(0.7500)^2+(0.5000)^2)))*180/PI,16.5307
,if(5.500-acos((Dx*-0.2241+Dy*0.8365+Dz*0.5000)/(sqrt((Dx)^2+(Dy)^2+(Dz)^2)
*sqrt((-0.2241)^2+(0.8365)^2+(0.5000)^2)))*180/PI,16.1288
,if(5.500-acos((Dx*-0.0000+Dy*0.8660+Dz*0.5000)/(sqrt((Dx)^2+(Dy)^2+(Dz)^2)
*sqrt((-0.0000)^2+(0.8660)^2+(0.5000)^2)))*180/PI,12.5476
,if(5.500-acos((Dx*0.2241+Dy*0.8365+Dz*0.5000)/(sqrt((Dx)^2+(Dy)^2+(Dz)^2)
*sqrt((0.2241)^2+(0.8365)^2+(0.5000)^2)))*180/PI,10.2613
,if(5.500-acos((Dx*0.4330+Dy*0.7500+Dz*0.5000)/(sqrt((Dx)^2+(Dy)^2+(Dz)^2)
*sqrt((0.4330)^2+(0.7500)^2+(0.5000)^2)))*180/PI,8.8950
,if(5.500-acos((Dx*0.6124+Dy*0.6124+Dz*0.5000)/(sqrt((Dx)^2+(Dy)^2+(Dz)^2)
*sqrt((0.6124)^2+(0.6124)^2+(0.5000)^2)))*180/PI,8.6895
,if(5.500-acos((Dx*0.7500+Dy*0.4330+Dz*0.5000)/(sqrt((Dx)^2+(Dy)^2+(Dz)^2)
*sqrt((0.7500)^2+(0.4330)^2+(0.5000)^2)))*180/PI,8.9664
,if(5.500-acos((Dx*0.8365+Dy*0.2241+Dz*0.5000)/(sqrt((Dx)^2+(Dy)^2+(Dz)^2)
*sqrt((0.8365)^2+(0.2241)^2+(0.5000)^2)))*180/PI,9.3861
,if(5.500-acos((Dx*0.8660+Dy*-0.0000+Dz*0.5000)/(sqrt((Dx)^2+(Dy)^2+(Dz)^2)
*sqrt((0.8660)^2+(-0.0000)^2+(0.5000)^2)))*180/PI,9.9220
```

```
,if(5.500-acos((Dx*0.8365+Dy*-0.2241+Dz*0.5000)/(sqrt((Dx)^2+(Dy)^2+(Dz)^2)
*sqrt((0.8365)^2+(-0.2241)^2+(0.5000)^2)))*180/PI,10.3774
,if(5.500-acos((Dx*0.7500+Dy*-0.4330+Dz*0.5000)/(sqrt((Dx)^2+(Dy)^2+(Dz)^2)
*sqrt((0.7500)^2+(-0.4330)^2+(0.5000)^2)))*180/PI,10.4042
,if(5.500-acos((Dx*0.6124+Dy*-0.6124+Dz*0.5000)/(sqrt((Dx)^2+(Dy)^2+(Dz)^2)
*sqrt((0.6124)^2+(-0.6124)^2+(0.5000)^2)))*180/PI,10.1363
,if(5.500-acos((Dx*0.4330+Dy*-0.7500+Dz*0.5000)/(sqrt((Dx)^2+(Dy)^2+(Dz)^2)
*sqrt((0.4330)^2+(-0.7500)^2+(0.5000)^2)))*180/PI,9.7255
,if(5.500-acos((Dx*0.2241+Dy*-0.8365+Dz*0.5000)/(sqrt((Dx)^2+(Dy)^2+(Dz)^2)
*sqrt((0.2241)^2+(-0.8365)^2+(0.5000)^2)))*180/PI,9.0825
,if(5.500-acos((Dx*0.1923+Dy*-0.7178+Dz*0.6691)/(sqrt((Dx)^2+(Dy)^2+(Dz)^2)
*sqrt((0.1923)^2+(-0.7178)^2+(0.6691)^2)))*180/PI,7.3946
,if(5.500-acos((Dx*0.3716+Dy*-0.6436+Dz*0.6691)/(sqrt((Dx)^2+(Dy)^2+(Dz)^2)
*sqrt((0.3716)^2+(-0.6436)^2+(0.6691)^2)))*180/PI,7.7965
,if(5.500-acos((Dx*0.5255+Dy*-0.5255+Dz*0.6691)/(sqrt((Dx)^2+(Dy)^2+(Dz)^2)
*sqrt((0.5255)^2+(-0.5255)^2+(0.6691)^2)))*180/PI,8.0376
,if(5.500-acos((Dx*0.6436+Dy*-0.3716+Dz*0.6691)/(sqrt((Dx)^2+(Dy)^2+(Dz)^2)
*sqrt((0.6436)^2+(-0.3716)^2+(0.6691)^2)))*180/PI,8.1001
,if(5.500-acos((Dx*0.7178+Dy*-0.1923+Dz*0.6691)/(sqrt((Dx)^2+(Dy)^2+(Dz)^2)
*sqrt((0.7178)^2+(-0.1923)^2+(0.6691)^2)))*180/PI,8.0912
,if(5.500-acos((Dx*0.7431+Dy*-0.0000+Dz*0.6691)/(sqrt((Dx)^2+(Dy)^2+(Dz)^2)
*sqrt((0.7431)^2+(-0.0000)^2+(0.6691)^2)))*180/PI,7.9840
,if(5.500-acos((Dx*0.7178+Dy*0.1923+Dz*0.6691)/(sqrt((Dx)^2+(Dy)^2+(Dz)^2)
*sqrt((0.7178)^2+(0.1923)^2+(0.6691)^2)))*180/PI,7.8143
,if(5.500-acos((Dx*0.6436+Dy*0.3716+Dz*0.6691)/(sqrt((Dx)^2+(Dy)^2+(Dz)^2)
*sqrt((0.6436)^2+(0.3716)^2+(0.6691)^2)))*180/PI,7.5732
,if(5.500-acos((Dx*0.5255+Dy*0.5255+Dz*0.6691)/(sqrt((Dx)^2+(Dy)^2+(Dz)^2)
*sqrt((0.5255)^2+(0.5255)^2+(0.6691)^2)))*180/PI,7.5554
,if(5.500-acos((Dx*0.3716+Dy*0.6436+Dz*0.6691)/(sqrt((Dx)^2+(Dy)^2+(Dz)^2)
*sqrt((0.3716)^2+(0.6436)^2+(0.6691)^2)))*180/PI,7.8233
,if(5.500-acos((Dx*0.1923+Dy*0.7178+Dz*0.6691)/(sqrt((Dx)^2+(Dy)^2+(Dz)^2)
*sqrt((0.1923)^2+(0.7178)^2+(0.6691)^2)))*180/PI,8.7699
,if(5.500-acos((Dx*-0.0000+Dy*0.7431+Dz*0.6691)/(sqrt((Dx)^2+(Dy)^2+(Dz)^2)
*sqrt((-0.0000)^2+(0.7431)^2+(0.6691)^2)))*180/PI,10.2167
,if(5.500-acos((Dx*-0.1923+Dy*0.7178+Dz*0.6691)/(sqrt((Dx)^2+(Dy)^2+(Dz)^2)
*sqrt((-0.1923)^2+(0.7178)^2+(0.6691)^2)))*180/PI,11.9671
,if(5.500-acos((Dx*-0.3716+Dy*0.6436+Dz*0.6691)/(sqrt((Dx)^2+(Dy)^2+(Dz)^2)
*sqrt((-0.3716)^2+(0.6436)^2+(0.6691)^2)))*180/PI,13.9229
,if(5.500-acos((Dx*-0.5255+Dy*0.5255+Dz*0.6691)/(sqrt((Dx)^2+(Dy)^2+(Dz)^2)
*sqrt((-0.5255)^2+(0.5255)^2+(0.6691)^2)))*180/PI,16.7807
,if(5.500-acos((Dx*-0.6436+Dy*0.3716+Dz*0.6691)/(sqrt((Dx)^2+(Dy)^2+(Dz)^2)
*sqrt((-0.6436)^2+(0.3716)^2+(0.6691)^2)))*180/PI,18.3436
,if(5.500-acos((Dx*-0.7178+Dy*0.1923+Dz*0.6691)/(sqrt((Dx)^2+(Dy)^2+(Dz)^2)
*sqrt((-0.7178)^2+(0.1923)^2+(0.6691)^2)))*180/PI,18.1471
```

```
,if(5.500-acos((Dx*-0.7431+Dy*0.0000+Dz*0.6691)/(sqrt((Dx)^2+(Dy)^2+(Dz)^2)
*sqrt((-0.7431)^2+(0.0000)^2+(0.6691)^2)))*180/PI,15.7716
,if(5.500-acos((Dx*-0.7178+Dy*-0.1923+Dz*0.6691)/(sqrt((Dx)^2+(Dy)^2+(Dz)^2)
*sqrt((-0.7178)^2+(-0.1923)^2+(0.6691)^2)))*180/PI,13.3246
,if(5.500-acos((Dx*-0.6436+Dy*-0.3716+Dz*0.6691)/(sqrt((Dx)^2+(Dy)^2+(Dz)^2)
*sqrt((-0.6436)^2+(-0.3716)^2+(0.6691)^2)))*180/PI,11.0026
,if(5.500-acos((Dx*-0.5255+Dy*-0.5255+Dz*0.6691)/(sqrt((Dx)^2+(Dy)^2+(Dz)^2)
*sqrt((-0.5255)^2+(-0.5255)^2+(0.6691)^2)))*180/PI,9.2968
,if(5.500-acos((Dx*-0.3716+Dy*-0.6436+Dz*0.6691)/(sqrt((Dx)^2+(Dy)^2+(Dz)^2)
*sqrt((-0.3716)^2+(-0.6436)^2+(0.6691)^2)))*180/PI,8.2162
,if(5.500-acos((Dx*-0.1923+Dy*-0.7178+Dz*0.6691)/(sqrt((Dx)^2+(Dy)^2+(Dz)^2)
*sqrt((-0.1923)^2+(-0.7178)^2+(0.6691)^2)))*180/PI,7.7250
,if(5.500-acos((Dx*-0.0000+Dy*-0.7431+Dz*0.6691)/(sqrt((Dx)^2+(Dy)^2+(Dz)^2)
*sqrt((-0.0000)^2+(-0.7431)^2+(0.6691)^2)))*180/PI,7.6357
,if(5.500-acos((Dx*-0.0000+Dy*-0.5878+Dz*0.8090)/(sqrt((Dx)^2+(Dy)^2+(Dz)^2)
*sqrt((-0.0000)^2+(-0.5878)^2+(0.8090)^2)))*180/PI,6.8498
,if(5.500-acos((Dx*-0.2010+Dy*-0.5523+Dz*0.8090)/(sqrt((Dx)^2+(Dy)^2+(Dz)^2)
*sqrt((-0.2010)^2+(-0.5523)^2+(0.8090)^2)))*180/PI,7.1981
,if(5.500-acos((Dx*-0.3778+Dy*-0.4503+Dz*0.8090)/(sqrt((Dx)^2+(Dy)^2+(Dz)^2)
*sqrt((-0.3778)^2+(-0.4503)^2+(0.8090)^2)))*180/PI,7.8769
,if(5.500-acos((Dx*-0.5090+Dy*-0.2939+Dz*0.8090)/(sqrt((Dx)^2+(Dy)^2+(Dz)^2)
*sqrt((-0.5090)^2+(-0.2939)^2+(0.8090)^2)))*180/PI,9.0914
,if(5.500-acos((Dx*-0.5789+Dy*-0.1021+Dz*0.8090)/(sqrt((Dx)^2+(Dy)^2+(Dz)^2)
*sqrt((-0.5789)^2+(-0.1021)^2+(0.8090)^2)))*180/PI,10.7347
,if(5.500-acos((Dx*-0.5789+Dy*0.1021+Dz*0.8090)/(sqrt((Dx)^2+(Dy)^2+(Dz)^2)
*sqrt((-0.5789)^2+(0.1021)^2+(0.8090)^2)))*180/PI,11.9492
,if(5.500-acos((Dx*-0.5090+Dy*0.2939+Dz*0.8090)/(sqrt((Dx)^2+(Dy)^2+(Dz)^2)
*sqrt((-0.5090)^2+(0.2939)^2+(0.8090)^2)))*180/PI,12.1725
,if(5.500-acos((Dx*-0.3778+Dy*0.4503+Dz*0.8090)/(sqrt((Dx)^2+(Dy)^2+(Dz)^2)
*sqrt((-0.3778)^2+(0.4503)^2+(0.8090)^2)))*180/PI,11.4491
,if(5.500-acos((Dx*-0.2010+Dy*0.5523+Dz*0.8090)/(sqrt((Dx)^2+(Dy)^2+(Dz)^2)
*sqrt((-0.2010)^2+(0.5523)^2+(0.8090)^2)))*180/PI,10.1274
,if(5.500-acos((Dx*-0.0000+Dy*0.5878+Dz*0.8090)/(sqrt((Dx)^2+(Dy)^2+(Dz)^2)
*sqrt((-0.0000)^2+(0.5878)^2+(0.8090)^2)))*180/PI,8.6806
,if(5.500-acos((Dx*0.2010+Dy*0.5523+Dz*0.8090)/(sqrt((Dx)^2+(Dy)^2+(Dz)^2)
*sqrt((0.2010)^2+(0.5523)^2+(0.8090)^2)))*180/PI,7.6804
,if(5.500-acos((Dx*0.3778+Dy*0.4503+Dz*0.8090)/(sqrt((Dx)^2+(Dy)^2+(Dz)^2)
*sqrt((0.3778)^2+(0.4503)^2+(0.8090)^2)))*180/PI,7.1713
,if(5.500-acos((Dx*0.5090+Dy*0.2939+Dz*0.8090)/(sqrt((Dx)^2+(Dy)^2+(Dz)^2)
*sqrt((0.5090)^2+(0.2939)^2+(0.8090)^2)))*180/PI,7.0463
,if(5.500-acos((Dx*0.5789+Dy*0.1021+Dz*0.8090)/(sqrt((Dx)^2+(Dy)^2+(Dz)^2)
*sqrt((0.5789)^2+(0.1021)^2+(0.8090)^2)))*180/PI,7.0106
,if(5.500-acos((Dx*0.5789+Dy*-0.1021+Dz*0.8090)/(sqrt((Dx)^2+(Dy)^2+(Dz)^2)
*sqrt((0.5789)^2+(-0.1021)^2+(0.8090)^2)))*180/PI,7.1535
```

```
, if(5.500-acos((Dx*0.5090+Dy*-0.2939+Dz*0.8090)/(sqrt((Dx)^2+(Dy)^2+(Dz)^2)
*sqrt((0.5090)^2+(-0.2939)^2+(0.8090)^2)))*180/PI, 7.1267
, if(5.500-acos((Dx*0.3778+Dy*-0.4503+Dz*0.8090)/(sqrt((Dx)^2+(Dy)^2+(Dz)^2)
*sqrt((0.3778)^2+(-0.4503)^2+(0.8090)^2)))*180/PI, 7.0731
, if(5.500-acos((Dx*0.2010+Dy*-0.5523+Dz*0.8090)/(sqrt((Dx)^2+(Dy)^2+(Dz)^2)
*sqrt((0.2010)^2+(-0.5523)^2+(0.8090)^2)))*180/PI, 6.9659
, if(5.500-acos((Dx*0.2034+Dy*-0.3522+Dz*0.9135)/(sqrt((Dx)^2+(Dy)^2+(Dz)^2)
*sqrt((0.2034)^2+(-0.3522)^2+(0.9135)^2)))*180/PI, 6.5194
, if(5.500-acos((Dx*0.3522+Dy*-0.2034+Dz*0.9135)/(sqrt((Dx)^2+(Dy)^2+(Dz)^2)
*sqrt((0.3522)^2+(-0.2034)^2+(0.9135)^2)))*180/PI, 6.5819
, if(5.500-acos((Dx*0.4067+Dy*-0.0000+Dz*0.9135)/(sqrt((Dx)^2+(Dy)^2+(Dz)^2)
*sqrt((0.4067)^2+(-0.0000)^2+(0.9135)^2)))*180/PI, 6.4033
, if(5.500-acos((Dx*0.3522+Dy*0.2034+Dz*0.9135)/(sqrt((Dx)^2+(Dy)^2+(Dz)^2)
*sqrt((0.3522)^2+(0.2034)^2+(0.9135)^2)))*180/PI, 6.6891
, if(5.500-acos((Dx*0.2034+Dy*0.3522+Dz*0.9135)/(sqrt((Dx)^2+(Dy)^2+(Dz)^2)
*sqrt((0.2034)^2+(0.3522)^2+(0.9135)^2)))*180/PI, 7.2517
, if(5.500-acos((Dx*-0.0000+Dy*0.4067+Dz*0.9135)/(sqrt((Dx)^2+(Dy)^2+(Dz)^2)
*sqrt((-0.0000)^2+(0.4067)^2+(0.9135)^2)))*180/PI, 7.9572
, if(5.500-acos((Dx*-0.2034+Dy*0.3522+Dz*0.9135)/(sqrt((Dx)^2+(Dy)^2+(Dz)^2)
*sqrt((-0.2034)^2+(0.3522)^2+(0.9135)^2)))*180/PI, 8.8860
, if(5.500-acos((Dx*-0.3522+Dy*0.2034+Dz*0.9135)/(sqrt((Dx)^2+(Dy)^2+(Dz)^2)
*sqrt((-0.3522)^2+(0.2034)^2+(0.9135)^2)))*180/PI, 9.5290
, if(5.500-acos((Dx*-0.4067+Dy*0.0000+Dz*0.9135)/(sqrt((Dx)^2+(Dy)^2+(Dz)^2)
*sqrt((-0.4067)^2+(0.0000)^2+(0.9135)^2)))*180/PI, 9.1807
, if(5.500-acos((Dx*-0.3522+Dy*-0.2034+Dz*0.9135)/(sqrt((Dx)^2+(Dy)^2+(Dz)^2)
*sqrt((-0.3522)^2+(-0.2034)^2+(0.9135)^2)))*180/PI, 8.2966
, if(5.500-acos((Dx*-0.2034+Dy*-0.3522+Dz*0.9135)/(sqrt((Dx)^2+(Dy)^2+(Dz)^2)
*sqrt((-0.2034)^2+(-0.3522)^2+(0.9135)^2)))*180/PI, 7.3589
, if(5.500-acos((Dx*-0.0000+Dy*-0.4067+Dz*0.9135)/(sqrt((Dx)^2+(Dy)^2+(Dz)^2)
*sqrt((-0.0000)^2+(-0.4067)^2+(0.9135)^2)))*180/PI, 6.8856
, if(5.500-acos((Dx*-0.0000+Dy*-0.2079+Dz*0.9781)/(sqrt((Dx)^2+(Dy)^2+(Dz)^2)
*sqrt((-0.0000)^2+(-0.2079)^2+(0.9781)^2)))*180/PI, 6.6355
, if(5.500-acos((Dx*-0.1801+Dy*-0.1040+Dz*0.9781)/(sqrt((Dx)^2+(Dy)^2+(Dz)^2)
*sqrt((-0.1801)^2+(-0.1040)^2+(0.9781)^2)))*180/PI, 7.4750
, if(5.500-acos((Dx*-0.1801+Dy*0.1040+Dz*0.9781)/(sqrt((Dx)^2+(Dy)^2+(Dz)^2)
*sqrt((-0.1801)^2+(0.1040)^2+(0.9781)^2)))*180/PI, 7.8054
, if(5.500-acos((Dx*-0.0000+Dy*0.2079+Dz*0.9781)/(sqrt((Dx)^2+(Dy)^2+(Dz)^2)
*sqrt((-0.0000)^2+(0.2079)^2+(0.9781)^2)))*180/PI, 7.4214
, if(5.500-acos((Dx*0.1801+Dy*0.1040+Dz*0.9781)/(sqrt((Dx)^2+(Dy)^2+(Dz)^2)
*sqrt((0.1801)^2+(0.1040)^2+(0.9781)^2)))*180/PI, 6.5998
, if(5.500-acos((Dx*0.1801+Dy*-0.1040+Dz*0.9781)/(sqrt((Dx)^2+(Dy)^2+(Dz)^2)
*sqrt((0.1801)^2+(-0.1040)^2+(0.9781)^2)))*180/PI, 6.2604
, if(5.500-acos((Dx*-0.0000+Dy*-0.0000+Dz*1.0000)/(sqrt((Dx)^2+(Dy)^2+(Dz)^2)
```


Curriculum Vitae

Ehsan Mahmoudzadehvazifeh

Professional Background:

2015 – Present	Lead of Innovation, Qi-Leap Analytics Inc., Vancouver, Canada
2014 – Present	Univ. Ass., Department of Building Physics and Building Ecology, TU Wien, Austria
2012 – 2014	Project Assistant, Department of Building Physics and Building Ecology, TU Wien, Austria
2007 – 2012	Various Civil Engineering projects, Iran

Educational Background:

2012 – 2014	Master of Science, Building Science and Technology, TU Wien, Vienna, Austria
2005 – 2011	Bachelor of Science, Civil Engineering, Amirkabir University of Technology, Tehran, Iran

Research Area:

Solar radiation, Sky models, Predictive Control, Big Data, Machine learning, Recommender Systems, Building Automation

Linkedin: <https://www.linkedin.com/in/emvazifeh>